INAUGURAL - DISSERTATION

zur
Erlangung der Doktorwürde
der
Naturwissenschaftlich-Mathematischen Gesamtfakultät
der
Ruprecht-Karls-Universität
Heidelberg

vorgelegt von
Dipl.-Math. Frank Strauß
aus Nürnberg

Tag der mündlichen Prüfung: 17.11.2005

Design optimization of rotating bodies

Gutachter: Prof. Dr. Dr. h.c. mult. Willi Jäger
Prof. Dr. Dr. h.c. Hans Georg Bock

Zusammenfassung

Die vorliegende Arbeit befaßt sich mit Designoptimierungsproblemen in der Rotordynamik. Bei der Rotation von starren Körpern treten Schwingungen auf, die zu unerwünschten Geräuschen, sowie im Resonanzfall zu einer Beschädigung des Rotors führen können. Das Optimierungsziel ist deshalb, das Design des Rotors so zu verändern, daß bestimmte Resonanzgeschwindigkeiten vermieden werden und die Amplitude im Resonanzfall reduziert werden kann. Der Ansatz wird dabei so formuliert, daß er auf eine allgemeine Klasse rotierender Körper mit verschiedenen Arten von Lagern angewendet werden kann.
An erster Stelle im Designoptimierungsprozeß steht die Auswahl eines geeigneten physikalischen Modells, das die für unseren Fall wichtigen Effekte der Rotationsträgheit und der gyroskopischen Momente beinhaltet. Dann kann die Bewegungsgleichung für den stetigen Rotor aufgestellt werden. Die Lösung der Gleichung führt auf ein verallgemeinertes Eigenwertproblem. Die resultierenden Eigenfrequenzen und Eigenmoden sind Zielgrößen unserer Optimierung. Die dazugehörigen Operatoren sind aufgrund der gyroskopischen Terme nichtsymmetrisch. Unter geeigneten Randbedingungen kann die Kompaktheit des Operators gezeigt werden, womit die Lösbarkeit des Eigenwertproblems bewiesen wird. Es folgt die Existenz von Lösungen für das Optimierungsproblem. Die Untersuchungen für diese Art von Optimierungsproblemen sind eine Erweiterung bekannter Ergebnisse aus der Literatur.
Für die numerische Lösung des Problems ist eine Diskretisierung, basierend auf einer Variationsformulierung, erforderlich. Zunächst beweisen wir dabei, daß die Lösungen des diskretisierten Optimierungsproblems gegen die Lösungen des stetigen Optimierungsproblems konvergieren. Dann erfolgt die algebraische Formulierung der Diskretisierung und die numerische Lösung der diskretisierten Bewegungsgleichung wird angegeben. Im Anschluß werden geeignete Designvariablen ausgewählt und die Strategie zur Lösung des Optimierungsproblems vorgestellt. Diese basiert auf einem iterativen Optimierungsprozeß und der Anwendung von Algorithmen, die Gradienteninformationen nutzen. Die dafür benötigten Ableitungen werden bestimmt und ein Verfahren zum Verfolgen einzelner Moden wird betrachtet. Außerdem werden Ideen aufgezeigt, wie eine nichtleere Lösungsmenge mit Ansätzen der Mehrzieloptimierung erreicht werden kann. Im weiteren werden die verwendeten Algorithmen vorgestellt, die der Klasse der sequentiellen konvexen Programmierung angehören.
Im letzten Teil der Arbeit werden die numerischen Ergebnisse für zwei Turboladermodelle präsentiert, deren Lager sowohl durch lineare Feder-Dämpfer-Modelle als auch nichtlineare Flüssigkeitslager realisiert werden. Es zeigt sich, daß eine bedeutende Reduktion der Masse des Rotors sowie der Amplitude der Zielmoden in den betrachteten Fällen möglich ist. Weitere Verbesserungen ergeben sich durch Änderungen der Lagerkonfiguration. Insgesamt führt dies zu einer Reduktion des Geräuschpegels, einer geringeren Materialermüdung und einer größeren Effizienz.

Abstract

The presented work focuses on design optimization problems in rotordynamics. The rotation of rigid bodies causes vibrations which can lead to undesired noise, and in the resonance case, to a damage of the rotor. Therefore, the target of the optimization is to change the design of the rotor such that certain resonance frequencies are avoided in the operating speed range and the amplitude in the resonance case is reduced. The formulated approach can be applied to a general class of rotating bodies with different kinds of support.

At the beginning of the design optimization process a suitable physical model is chosen, which includes the important effects of rotary inertia and gyroscopic moments. Then the equation of motion for the continuous rotor is obtained. The solution of this equation leads to a generalized eigenvalue problem. The resulting natural frequencies and eigenmodes are target values of our optimization. The corresponding operators are non-symmetric due to the presence of the gyroscopic terms. Using suitable boundary conditions the compactness of the operator can be shown which is used to prove the solvability of the eigenvalue problem. The existence of solutions of the optimization problem follows. The research for this kind of design optimization problems extends known results of the literature.

For the numerical solution of the problem a discretization, based on a variational formulation, is necessary. We prove that the solutions of the discretized optimization problem converge towards the solution of the continuous optimization problem if the discretization parameter tends to zero. Then the algebraic formulation of the discretization and the numerical solution of the discretized equation of motion is given. Suitable design variables are chosen subsequently and the strategy for the solution of the optimization problem is presented. It is based on an iterative optimization process and the application of algorithms which use gradient information. The necessary sensitivities are determined and a mode tracking procedure is considered. Moreover, ideas are presented, how a nonempty set of solutions can be achieved by multiobjective optimization approaches. Algorithms from the class of sequential convex programming are applied to solve the numerical problems. Finally, computational results for two different turbocharger models are shown which are supported either by linear spring and damper or nonlinear fluid-film bearings. A significant reduction of mass of the rotor and of the amplitudes of the target modes is achieved in the considered cases. Further improvements are obtained by changes in the bearing configuration. All in all, the design optimization process for the rotating bodies leads to a reduction of noise and fatigue of material and an increase of efficiency.

Acknowledgements

First of all I want to express my gratitude to Professor Willi Jäger for giving me the opportunity to work in his group and for supporting me through all stages of the thesis.

In addition to that, I would like to thank Dr. Jens Starke for initiating the interesting project with Toyota Central R&D Labs., Inc. (TCRDL) and for arranging research stays in Japan and Denmark. Furthermore, I am grateful for useful advice and help.

This Ph.D. study has been financially supported by TCRDL which I wish to acknowledge. My special thank goes to Dr. Nobuyuki Mori, Mizuho Inagaki as well as all other members of the Structural Dynamics Lab. and the Design Engineering Lab. for a pleasant collaboration research. During two research stays in Nagakute I had many stimulating conversations on rotordynamics and learnt a lot about the engineering background.

Moreover, I gratefully acknowledge the opportunity of a six-week research stay at the Technical University of Denmark (DTU). A thank goes to Prof. Wolfhard Kliem for the excellent organization, to Prof. Martin P. Bendsøe and Prof. Pauli Pedersen for very fruitful discussions and to Dr. Atsushi Kawamoto for helpful remarks. I really enjoyed the inspriring atmosphere at DTU. This stay was supported by the European Research Training Network, Homogenization and Multiple Scales (HMS 2000).

Furthermore, I am very obliged to Prof. Ben Schweizer, Prof. Vincent Heuveline and Priv.-Doz. Christian Zillober for valuable discussions concerning subjects presented in the thesis. In addition, I would like to thank Prof. Krister Svanberg for the permission to use his MMA code.

I would like to express my special gratitude to Jan Rübel, my colleague on the joint project with TCRDL, for a good cooperation and for many interesting scientific and non-scientific discussions. It has been great to spend the time with him, in particular during our joint research stays in Japan and Denmark.

Finally, I would like to thank my parents and Silvia Harmsen for their kind support.

Contents

Chapter 1

Introduction

The research presented in this thesis deals with design optimization of rotating bodies. The work has been motivated by a joint project between the University of Heidelberg and the Toyota Central Research and Development Labs, Inc. (TCRDL) in Japan which focused on modelling and optimization of a turbocharger. In this context, the design optimization concept is formulated for a general class of rotating bodies and the turbocharger is considered as an example for such a rotating body in our numerical calculations.

Motivation

Rotating bodies play an important role in many industrial branches and one of them is automotive design. In the construction of cars and in particular their engines many such parts exist, e.g. crankshaft, gear-train and turbocharger. The rotation of these parts causes vibrations which lead to different kinds of oscillations. The most important ones are unbalance oscillations caused by unbalance forces and self-excited oscillations due to influence of lubricant films in fluid-film bearings. These vibrations cause unfavourable noise and may result in fatigue of material and early mechanical failure of engine parts. Therefore, a thorough analysis of rotor vibrations is necessary and techniques how to reduce them are desired. Our research focuses on the development of a design optimization technique to deal with these vibration problems. Having found a suitable optimization approach the cost of production could be drastically reduced. The desired shape of rotating bodies fulfilling all necessary constraints could be developed first on the computer such that less prototypes have to be built in practice. Our studies use a given mathematical model for the description of the rotating body. Extensive studies focusing on an improvement of the mathematical model in the special case of a fluid-film supported turbocharger were done in another part of the joint project with TCRDL. This includes in particular a prediction of the amplitudes of the vibrations. Results of this work can be found in [51].

Each rotating rigid body has an infinite number of natural frequencies and corresponding eigenmodes. Problems arise for the resonance case, when the rotational speed coincides with a certain natural frequency. Then the amplitude of the rotor vibration becomes large and failure may occur. In the operational speed range of interest only a small number of these modes is excited. We distinguish between rigid modes and bending modes. Rigid modes leave the rotor undeformed but a whirl around the rotational axis in the static position takes place. The most important ones are called conical modes since they describe a conical motion. Bending modes are modes describing a bending of the shaft (see Figure 1.1) and a deformation of the shaft occurs. Large displacements from the static position accelerate the fatigue of material and can lead to severe damage of the rotor. For more background about vibration modes in rotordynamics we refer to [63].

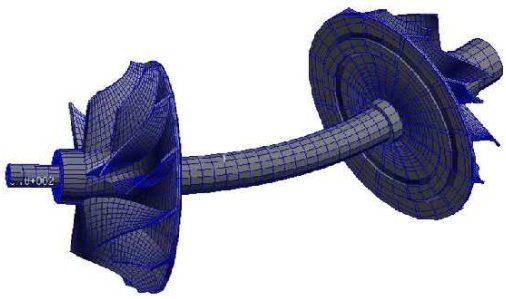

Figure 1.1. Strongly amplified bending of rotor (Figure by TCRDL).

Our research focuses on the amplitude of conical and bending modes in the resonance case excited by unbalance forces. The major source of the unbalance forces is the geometric eccentricity of the center of gravity of a rotor from the centerline of the shaft due to manufacturing error and material inhomogeneity. The general procedure to overcome this problem is to cut out certain pieces of the shaft or attached blades by trial and error procedures. However, this balancing of the rotor only leads to a limited reduction of the unbalance response and appropriate tools are desired to optimize the shape of the rotor in order to further decrease the vibrations.

Design optimization means to improve the design of the object in a way that a given cost functional representing certain properties of the object is maximized or minimized subject to constraints. Therefore, a parameter-dependent model for the description of the object has to be formulated and some of the parameters are allowed to vary. These are our design variables. The most important optimization targets in our case are

- the increase of the efficiency and
- the reduction of noise.

However, these targets are abstract targets and for the practical treatment of the problem we need to focus on values which can be influenced directly and which lead to the desired change of our abstract targets.

This can be achieved as follows.

- A higher efficiency would be obtained if the total mass was reduced and the operating speed range was increased. This is possible if certain resonance frequencies can be raised such that they are not excited when running the rotor. The lighter weight and the higher maximum rotating speed lead to a better response and higher aerodynamic efficiency of the rotor.
- A reduction of noise and increase of reliability could be achieved by reducing the vibration level of the rotor. The vibration level is measured by a quantity called unbalance response which is a measure for the amplitude of a certain mode at its resonance rotational speed, called critical speed.

This strategy is summarized in Figure 1.2.

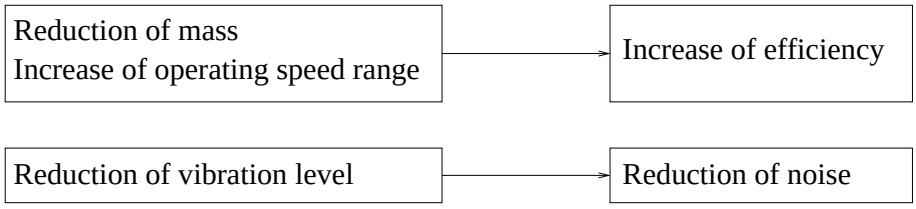

Figure 1.2. Considered optimization objectives and computational targets.

For the computational part we then proceed as shown in Figure 1.3. At first the critical speed ω of the mode whose unbalance response is of interest has to be determined. The upper diagram of Figure 1.3 shows that the natural frequency of the mode rises with increasing rotational speed. The intersection of this curve with the bisecting line yields the critical speed. The system is then excited with this critical speed to determine the amplitude of the unbalance response. This is shown by the blue curve in the lower diagram. The arrows indicate the optimization target which is to reduce the amplitude and raise the critical speed. The yellow curve represents the desired behaviour after the optimization process.

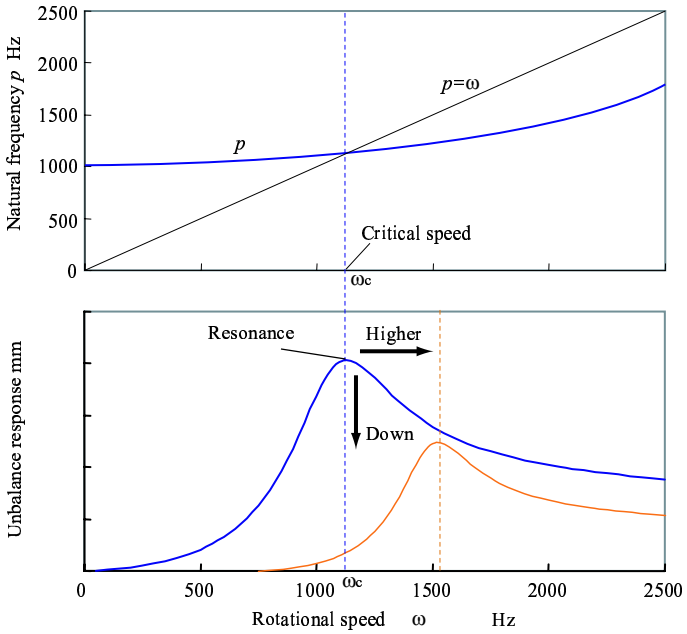

Figure 1.3. Concept of vibration level optimization –
Determination of critical speed (top),
Optimization targets: decrease of unbalance response, increase of critical speed (bottom).

Design optimization problems

The design optimization, focusing on the above mentioned targets, is essentially treated by two optimization problems. The model problems are formulated with a suitable objective function J and constraints on the natural frequencies and unbalance response. Other formulations are also possible and discussed in the thesis.

(i) The first optimization problem considers only natural frequency constraints and is given by

$$\begin{aligned} &\min J \\ &\text{subject to} \\ &\lambda_{\mathrm{m1}} \geq \lambda^*_{\mathrm{m1}}, \\ &\lambda_{\mathrm{m2}} \geq \lambda^*_{\mathrm{m2}}. \end{aligned}$$

The natural frequencies of certain modes λ_{m1} and λ_{m2} are increased above given target values λ^*_{m1} and λ^*_{m2}. In this case the rotational speed is fixed. We refer to this problem as **natural frequency optimization problem** and it serves as kind of preparation for the following optimization problem.

(ii) In the second optimization problem the critical speed ω is determined first and then for this fixed critical speed natural frequencies and eigenmodes are computed yielding the expression of the unbalance response a. The corresponding optimization problem looks like

$$\begin{aligned} &\min J \\ &\text{subject to} \\ &\omega_{\mathrm{m1}} \geq \omega^*_{\mathrm{m1}}, \\ &a(\omega_{\mathrm{m2}}) \leq a^*_{\mathrm{m2}}. \end{aligned}$$

where ω_{m1} is the critical speed of a certain mode m1 and a the unbalance response at the critical speed of a mode m2. The two modes may coincide. The critical speed and the unbalance response are bounded from below and above, respectively, by externally given target values ω^*_{m1} and a^*_{m2}. This problem is called **vibration level optimization problem**.

Further details of the problem formulations are given in Chapter 5. At this point they serve as motivation for the following work.

Purpose of research

Various design optimization problems concerning vibrating structures have been treated in the literature [7, 39, 40]. However, work therein focuses on static vibration problems and even if rotations are considered, effects of rotary inertia and gyroscopic moments are neglected (see e.g. [6, 50]). But these effects are essential for the class of rotating bodies to be studied here. Such systems are called gyroscopic systems. They lack some nice mathematical properties because the underlying operator is non-symmetric due to the influence of the gyroscopic term. This changes the corresponding theory since we can no longer assume the natural frequencies and eigenmodes to have real values but instead we have to work with complex values.

One central aim of the thesis is to prove theorems about the existence of solutions for the given optimization problems based on a physical model including effects of rotary inertia and gyroscopic moments. A Rayleigh beam model [44] is used to describe the rotor and a second-order equation of motion is obtained [20, 63]. Transformation of it into a first-order system and separation of variables lead to a generalized eigenvalue problem. The solution of this eigenvalue problem gives natural frequencies and eigenmodes which are target of the optimization. Since the governing operator is non-symmetric we cannot use results from the literature (e.g. [27]) for the solution of the problem. But we are able to show that the operator of the eigenvalue problem is compact. Then the solvability of the eigenvalue problem can be shown and the spectrum is described. From these results the existence of solutions of the optimization problem can also be derived. The theorems are proven for the case of a continuous rotor.

The second major target is to establish a method for the numerical solution of given design optimization problems for gyroscopic systems. For this, a suitable finite element discretization based on a variational formulation is introduced. Using results on spectral approximation of linear operators (see e.g. [4, 10, 34]) it can be shown that the solution of the discretized optimization problem converges towards the solution of the continuous problem if the discretization parameter tends to zero. The discretized equation of motion leads to a generalized matrix eigenvalue problem. The solution of this matrix eigenvalue problem gives the critical speeds and the eigenmodes of the vibrating body. For the optimization suitable design variables have to be chosen and the necessary sensitivity analysis has to be performed. Results on sensitivity analysis can be found in [25, 28, 45]. An iterative optimization process is applied using algorithms from the class of sequential convex programming to solve the optimization problem. Such algorithms are presented e.g. in [9, 25, 46, 54]. Certain modifications guarantee the convergence of the algorithm towards a Karush-Kuhn-Tucker point of the discretized problem as shown in [56, 66]. Since the optimization process focuses on certain modes, some extensions to the algorithms have to be made. This comprises e.g. the inclusion of a procedure which guarantees to follow the correct mode (see e.g. [33]). The target values for the constraints are often set heuristically according to engineering demands, where existence of solutions cannot be guaranteed. Studies were performed how to choose them to guarantee a non-empty set of solutions to the optimization problem. Indeed, threshold values, which can serve as bounds for the set of feasible solutions, can be determined numerically, by reformulations of the problem into a multiobjective optimization problem. Books on this subject include [27, 42].

For the numerical calculations a turbocharger in the engine of a passenger car is studied as an example of a rotating body. It has to be mentioned that the presented approach is applicable for general rotating bodies. This concrete rotor is only used as an example for our numerical results. Nevertheless, we want to introduce it already at this early stage since it serves as main motivation for our research and can be kept in mind when studying the more general theory.

Example turbocharger

The efficiency of a combustion engine in a passenger car is limited by the amount of air that can be used for combustion, i.e. the cylinder capacity. To increase efficiency it is either possible to increase cylinder capacity or to compress the air which flows into the cylinder. A turbocharger is a supercharging device to increase efficiency and reduce fuel consumption based on the latter principle. It consists of a shaft to which two blades are attached, impeller and turbine, and is supported by bearings. The whole turbocharger is in a casing which is attached to the motorblock. A prototype of a turbocharger of TCRDL can be seen in Figure 1.4.

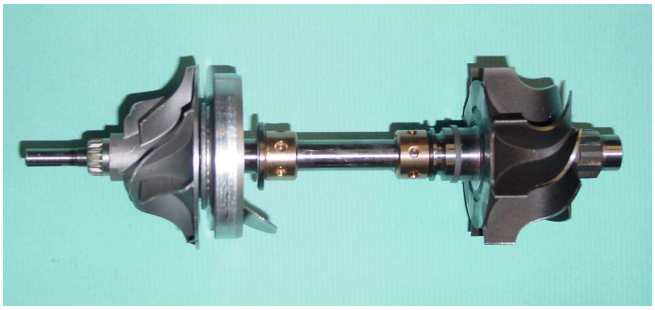

Figure 1.4. Prototype of turbocharger.

This turbocharger works as follows. Exhaust gas coming out of the cylinder drives the turbine which is the right blade in Figure 1.4. Then shaft and disks start to rotate and the impeller, the left blade, compresses air which is flowing into the cylinder. Hence, the air is compressed higher as usual leading to a more efficient combustion. Turbochargers rotate very fast with rotational speeds up to 210 000 revolutions per minute. More background about turbochargers can be found in [5].

Turbochargers are widespread for diesel engines to increase the torque and efficiency of the engine system as well as the maximum power. Knocking phenomena do not occur due to high pressure supercharging. This is why it can be used for a wide range of vehicles, from small passenger cars to heavy trucks. For the gasoline engine, the turbocharger has also gained more importance to downsize the engine cylinder volume which leads eventually to lower fuel consumption, even though the supercharging of gasoline engines has some difficulties to avoid knocking phenomena.

Description of the contents

This thesis is organized as follows.

In Chapter 2 the rotordynamical background including all necessary mechanics is explained. A Rayleigh beam model is introduced as the model of our choice. Then the equation of motion for a continuous rotor is derived which is the basis for the forthcoming studies.

In Chapter 3 the equation of motion is considered in a functional analytical framework. This is done under the assumption of mild boundary conditions. The equation of motion for free vibrations is solved by the separation of variables and an approach with an exponential function for the time dependence which results in a non-symmetric generalized eigenvalue problem. The operator of the generalized eigenvalue problem is shown to be compact. The application of the Riesz-Schauder spectral theorem yields the solvability of the equation of motion. Continuity of a finite subset of eigenvalues and eigenvectors guarantees the existence of solutions

for the natural frequency optimization problem and the vibration level optimization problem.

In the first section of Chapter 4 the convergence of eigenvalues and eigenvectors of a discretized problem towards those of the continuous problem is shown if the discretization parameter tends to zero. These results are used to show the convergence of the solutions of the corresponding optimization problems. Then an algebraic formulation for the discretized model is introduced. Moreover, the finite element discretization scheme and the resulting structural matrices for the numerical treatment of our problems are given. It is shown how the relevant expressions, such as critical speed and unbalance response, are determined. An extension of the model including nonlinear bearing forces is introduced in the last section of this chapter.

In Chapter 5 the strategy for the solution of the discretized design optimization problems is presented. Furthermore, the sensitivity analysis and crucial differentiability questions are discussed which are necessary for the application of gradient-based optimization algorithms. The technique of mode tracking is introduced which guarantees the consideration of the correct mode throughout the optimization process. In the last section different formulations of the optimization problems using the idea of multicriteria optimization are discussed. It is shown how this can be used to ensure a non-empty solution set for the initial optimization problems.

Chapter 6 gives an overview about suitable algorithms for our design optimization problems. Essentially, the class of sequential convex programming algorithms is regarded and the method of moving asymptotes is presented in detail. Extensions that lead to a convergence of the algorithm towards a stationary point of the discretized system are shown.

The numerical results are summarized in Chapter 7. It shows that the engineering application problems can be solved satisfactorily. An increase of critical speeds as well as a substantial reduction of mass and unbalance response are obtained. Moreover, additional calculations yield bounds for the target values such that the feasible domain is non-empty. These results hold for both the model with linear spring and damper support and the model including nonlinear fluid-film forces of the bearings.

Chapter 2

Physical model of rotating bodies

In this chapter a physical model is presented to describe the motion of our rotating bodies. It captures the important effects of rotary inertia and gyroscopic moments and is therefore also called gyroscopic system. Here we consider a rotor model with distributed mass, stiffness and damping and to which rigid disks can be attached. Such a model is called continuous rotor. In Section 2.1 the description of the rotor by a beam model is introduced. This model serves also as basis for the finite element model in Chapter 4. The equation of motion for the rotor based on this beam model is derived in Section 2.2. It is obtained by using Hamilton's principle of extremal action and the Lagrange equations.

2.1 Beam model

Our rotor is a three-dimensional body which we want to describe by an one-dimensional model based on theories of lateral beam vibrations. This approach is sufficient to study all effects we are interested in and can be solved in moderate computational time. Of course, this requires some form of approximation to the underlying physics.

There exist various beam theories to describe the motion of the rotor. A good overview about different models can be found in [26] and we adopt the classification stated there. The classical theory for the analysis of a transversely vibrating beam is the Euler-Bernoulli beam which goes back to Jacob and Daniel Bernoulli as well as Leonhard Euler. This model includes the strain energy and the kinetic energy due to the lateral displacement. However, this beam model does not consider effects of rotary inertia which are important in our case since we are dealing with rotating bodies. These effects and the notion of gyroscopic moments are captured by an extended model called Rayleigh beam upon which our research is based. A further development which includes also shear deformation is the Timoshenko beam but is not necessary for the scope of this research.

We can summarize some general assumptions which hold for all mentioned models (see e.g. [15] and [26]).

- One dimension (axial direction) is considerably larger than the other two.
- The material is linear elastic.
- The cross-sectional area is symmetric and is either constant or varies smoothly.
- Planes perpendicular to the centerline of the shaft remain perpendicular after deformation.
- The angle of rotation is small so that the small angle assumption can be used.

We now want to derive the equation of motion for a rotating Rayleigh beam. We use a static XYZ-coordinate system whose Z-axis coincides in the static position with the centerline of the shaft. We consider a shaft of length l and the spatial variable along the Z-axis is denoted by s. The motion of the rotor is described by the lateral deflections and inclinations in each point along the Z-axis (see Figures 2.1 and 2.2).

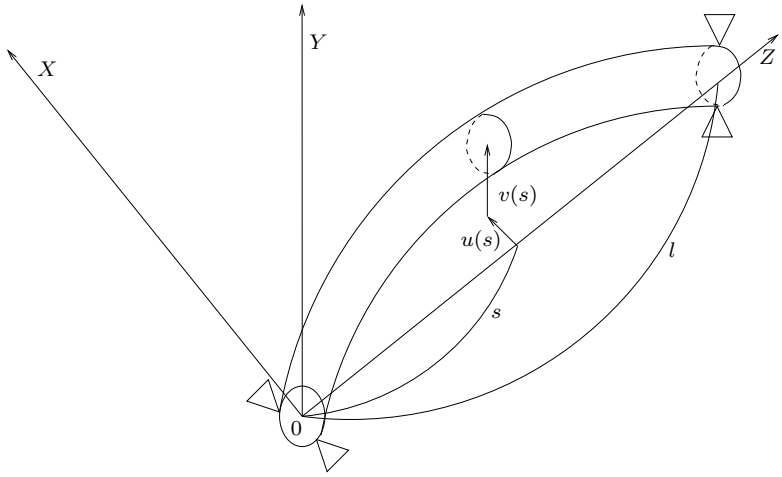

Figure 2.1. Model of rotor in XYZ-coordinate system.

The lateral deflections in X- and Y-direction are denoted by u and v, respectively. The inclination angle θ of the tangent to the rotor deflection curve can be decomposed into two components θ_x and θ_y which are the projections of θ onto the XZ- and YZ-plane, respectively. The deflections and inclinations also depend on the time variable t. For the sake of simplicity this is not mentioned explicitly in each equation.

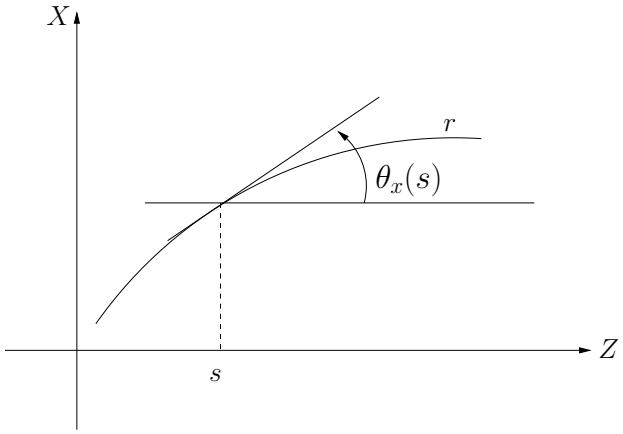

Figure 2.2. Inclination angle in XZ-plane.

Since we assume the inclination angles to be small we have

$$\theta_x(s) = u'(s) \quad \text{and} \quad \theta_y(s) = v'(s), \tag{2.1}$$

where a prime denotes a differentiation by s. The consideration of the inclination motion leads to the gyroscopic moment in this system which is essential for our further studies.

The shape of the rotor is described by a continuous function $r \in C(I)$, where $I = [0, l]$ and $r(s)$ is the radius of the shaft at position s. It is bounded from below and above by fixed functions $\underline{r}$ and $\bar{r}$ respectively and $\underline{r}, \bar{r} \in L^\infty(I)$.

2.2 Formulation of equation of motion

The derivation of the equation of motion is based upon the principle of extremal action, also called *Hamilton's principle* [20]. It is generally formulated for a system of mass points. It says that the variation of the functional of action vanishes

$$\delta S(q) = 0, \tag{2.2}$$

where the functional S is the integral over the Lagrange function $\mathcal{L}$ which is describing the mechanical system,

$$S = \int_{t_1}^{t_2} \mathcal{L}(q, \dot{q}, t)\, dt,$$

and q is a vector of generalized coordinates. A dot indicates differentiation by t.

It can be shown [20, 36] that (2.2) is equivalent to the *Lagrange equations*

$$\frac{d}{dt}\frac{\partial \mathcal{L}}{\partial \dot{q}_i} = \frac{\partial \mathcal{L}}{\partial q_i}. \tag{2.3}$$

The Lagrange function $\mathcal{L}$ is given by the difference between kinetic energy T and the potential energy U

$$\mathcal{L} = T - U. \tag{2.4}$$

If external forces are acting upon the rotor, an additional potential energy term U_f appears in the system [20]. Then forced vibrations occur in contrast to the previous case of free vibrations and we have

$$\mathcal{L} = T - U - U_f. \tag{2.5}$$

Moreover, we distinguish between damped and undamped systems. If the system is damped a Rayleigh dissipation function is defined by

$$F(\dot{u}, \dot{v}) = \frac{1}{2}c(\dot{u}^2 + \dot{v}^2),$$

where c is a distributed damping parameter (see e.g. [63]). The Lagrange equations are then extended as follows

$$\frac{d}{dt}\frac{\partial \mathcal{L}}{\partial \dot{q}_i} - \frac{\partial \mathcal{L}}{\partial q_i} + \frac{\partial F}{\partial \dot{q}_i} = 0, \tag{2.6}$$

where the Lagrange function $\mathcal{L}$ is given by (2.4) or (2.5). In the case of external forces (i.e. Lagrange function (2.5)) we always consider damped systems.

Remark. In our case of a continuous rotor, which is the limit of a system of mass points, the Lagrange equations also hold (see [20]).

Equation of motion for free vibrations

In the case of free vibrations the Lagrange function (2.4) is relevant and the expressions for the kinetic energy T and the potential energy U for our system have to be determined. The formulation of the energy terms T and U follows [63]. Then the equation of motion is derived by determining the expressions of the Lagrange equations (2.6).

The kinetic energy T can be decomposed into a term for translational energy T_{trans} and a term for rotational energy T_{rot},

$$T = T_{\text{trans}} + T_{\text{rot}}.$$

The translational term is given by

$$T_{\text{trans}} = \int_0^l \frac{\mu(s)}{2}(\dot{u}^2(s) + \dot{v}^2(s))\, ds,$$

where $\mu(s) = r^2(s)\pi\rho$ is the mass per unit length and ρ the density of the shaft material. The motion in Z-direction is neglected. The rotational term T_{rot} is a quadratic form of the angular velocity Ω. In our case the axes of the coordinate system coincide with the principal axes of the moments of inertia and then we obtain the following expression,

$$T_{\text{rot}} = \frac{1}{2}\int_0^l \left(I_d(s)\Omega_X^2(s) + I_d(s)\Omega_Y^2(s) + I_p(s)\Omega_Z^2(s)\right)\, ds,$$

where the moments of inertia I_d about the X- and Y-axes are called the diametral moments of inertia and are given by $I_d(s) = r^4(s)\pi\rho/4$. The moment of inertia I_p about the Z-axis is called the polar moment of inertia and is $I_p(s) = r^4(s)\pi\rho/2$.

The components $(\Omega_X, \Omega_Y, \Omega_Z)$ of the angular velocity Ω can be expressed by means of Eulerian angles. To avoid the introduction of too much notation, which we do not need later, we do not go into details of this technique and refer to [20] or [36]. Instead, we immediately want to state the result which is obtained under the assumption of small shaft inclination angles θ_x and θ_y. The rotational energy can then be written as

$$T_{\text{rot}} = \int_0^l \left(\frac{1}{2}I_d(s)(\dot{\phi}_x^2(s) + \dot{\phi}_y^2(s)) + \frac{1}{2}I_p(s)(\omega^2 + \omega(\dot{\phi}_x(s)\phi_y(s) - \phi_x(s)\dot{\phi}_y(s)))\right)\, ds,$$

where ω is the constant rotational speed of the shaft. In our gyroscopic setting a slight modification has been made in the notation and the variables

$$\phi_x = -\theta_y \quad \text{and} \quad \phi_y = \theta_x \tag{2.7}$$

were introduced. The angles ϕ_x and ϕ_y are now rotation angles in the YZ- and XZ-plane and the rotation is about the X- and Y-axis, respectively.

The total potential energy of a beam is the difference of internal and external energies. In the Rayleigh beam model the internal strain energy accounts only for bending moment deformations. All other effects, notably transverse shear and axial forces, are ignored [15]. They are captured in the Timoshenko beam theory, but this concept is not needed in our analysis. The external energy accounts for the applied forces and is neglected initially. The internal potential energy U is then given by

$$U = \frac{1}{2}\int_0^l U(s)\, ds = \frac{1}{2}\int_0^l \left(M_{XZ}(s)u''(s) + M_{YZ}(s)v''(s)\right)\, ds,$$

where the bending moments working in the XZ- and YZ-plane are given by

$$M_{XZ}(s) = Eu''(s) \int_A r^2(s) dA = EI_a(s)u''(s) \tag{2.8}$$

and

$$M_{YZ}(s) = Ev''(s) \int_A r^2(s) dA = EI_a(s)v''(s), \tag{2.9}$$

where I_a denotes the moment of inertia of the cross-section A with respect to the Z-axis and is given by $I_a(s) = \pi r^4(s)/16$. The material parameter E denotes Young's modulus. The product EI_a is called the bending rigidity of the beam. The deformed beam axis curvature is to first order given by u'' and v'', respectively.

To apply the Lagrange equations we now have to find suitable generalized coordinates. It is obvious to take the above introduced lateral deflections and inclinations.

Then the generalized coordinates in each point along the Z-axis are fixed as

$$q_1 = u, \quad q_2 = v, \quad q_3 = \phi_x, \quad q_4 = \phi_y$$

and we refer to $q = (q_1, q_2, q_3, q_4)$ as displacement vector. The values of the generalized coordinates depend on s and t which is suppressed to shorten notation.

With these generalized coordinates the kinetic and potential energy can be written as

$$T = \int_0^l \left(\frac{\mu(s)}{2}(\dot{q}_1^2 + \dot{q}_2^2) + \frac{1}{4} I_p(s)(\dot{q}_3^2 + \dot{q}_4^2) + \frac{1}{2} I_p(s)(\omega^2 + \omega(\dot{q}_3 q_4 - q_3 \dot{q}_4)) \right) ds$$

and

$$U = \frac{1}{2} \int_0^l U(s)\, ds = \frac{1}{2} \int_0^l \left(EI_a(s)(q_1'')^2 + EI_a(s)(q_2'')^2 \right) ds.$$

The functional of action S is now [20]

$$S = \int_{t_1}^{t_2} \int_0^l L(q, \dot{q}, q'', s, t)\, ds\, dt, \tag{2.10}$$

and the integral density L is given by

$$\begin{aligned} L &= \frac{\mu}{2}(\dot{q}_1^2 + \dot{q}_2^2) + \frac{1}{4} I_p(\dot{q}_3^2 + \dot{q}_4^2) \\ &\quad + \frac{1}{2} I_p(\omega^2 + \omega(\dot{q}_3 q_4 - q_3 \dot{q}_4)) - \frac{1}{2}(EI_a(q_1'')^2 + EI_a(q_2'')^2). \end{aligned} \tag{2.11}$$

The Lagrange equations at one certain point read as [20]

$$\frac{\partial L}{\partial q} = \frac{d}{dt}\frac{\partial L}{\partial \dot{q}} - \frac{d^2}{ds^2}\frac{\partial L}{\partial q''}. \tag{2.12}$$

Then the derivative after each of the four generalized coordinates can be determined, yielding

$$\begin{array}{rlll} (I) & q_1 = u: & \mu\ddot{u} + (EI_a u'')'' &= 0, \\ (II) & q_2 = v: & \mu\ddot{v} + (EI_a v'')'' &= 0, \\ (III) & q_3 = \phi_x: & \frac{1}{2}\ddot{\phi}_x I_p + I_p\omega\dot{\phi}_y &= 0, \\ (IV) & q_4 = \phi_y: & \frac{1}{2}\ddot{\phi}_y I_p - I_p\omega\dot{\phi}_x &= 0. \end{array}$$

With $\phi_x = -v'$ and $\phi_y = u'$ as given by (2.1) and (2.7) we obtain

$$\begin{array}{rlll} (III') & -\frac{1}{2}\ddot{v}' I_p + I_p\omega\dot{u}' &= 0, \\ (IV') & \frac{1}{2}\ddot{u}' I_p + I_p\omega\dot{v}' &= 0. \end{array}$$

The units in equation (I) and (II) are [kg/s^2] whereas for (III') and (IV') we have [kg m/s^2]. Therefore, we differentiate the latter two equations again by s to obtain the same units as in the first two equations,

$$\begin{array}{rlll} (III'') & \left(-\frac{1}{2}\ddot{v}' I_p\right)' + (I_p\omega\dot{u}')' &= 0, \\ (IV'') & \left(\frac{1}{2}\ddot{u}' I_p\right)' + (I_p\omega\dot{v}')' &= 0. \end{array}$$

The aim is to have one equation of motion in the end. A first step is done by reducing the system to a system of two equations. This can be achieved by subtracting equations (I) and (IV''),

$$\mu\ddot{u} - \left(\frac{1}{2}\ddot{u}' I_p\right)' - (I_p\omega\dot{v}')' + (EI_a u'')'' = 0, \tag{2.13}$$

and adding (II) and (III''),

$$\mu\ddot{v} - \left(\frac{1}{2}\ddot{v}' I_p\right)' + (I_p\omega\dot{u}')' + (EI_a v'')'' = 0. \tag{2.14}$$

Finally, we introduce a complex-valued notation by setting $z = u + iv$ and obtain one single equation of motion.

The **equation of motion governing free vibrations of a continuous rotor without damping** is given by

$$\mu\ddot{z} - \frac{1}{2}\left(I_p\ddot{z}'\right)' + i\left(I_p\omega\dot{z}'\right)' + \left(EI_a z''\right)'' = 0. \tag{2.15}$$

The next step is to add damping to the system. By differentiating the Rayleigh dissipation function $F = c(\dot{u}^2 + \dot{v}^2)/2$ we obtain

$$\frac{\partial F}{\partial \dot{u}} = c\dot{u} \quad \text{and} \quad \frac{\partial F}{\partial \dot{v}} = c\dot{v}.$$

The damping terms can be added immediately to the Lagrange equation (2.6).

The **equation of motion governing free vibrations of a continuous rotor with damping** is given by

$$\mu\ddot{z} - \frac{1}{2}\left(I_p\ddot{z}'\right)' + i\left(I_p\omega\dot{z}'\right)' + c\dot{z} + \left(EI_a z''\right)'' = 0. \tag{2.16}$$

For a complete description of the system initial values and boundary conditions due to rotor support have to be formulated.

Rotor support and boundary conditions

In our case, simple support and linear spring and damper support are of relevance. We want to state the boundary conditions for both cases. Conditions of order zero and one are called essential boundary conditions whereas those of higher order are natural boundary conditions since they are fulfilled implicitly (see e.g. [14] or [16]).

(a) Simple support at both ends.

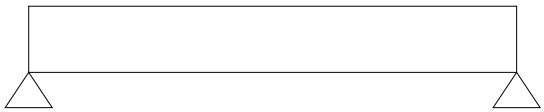

Figure 2.3. Beam with simple support.

In this case transverse displacements are not possible, but end rotations are permitted. The boundary conditions can be written as

$$z(0,t) = 0,\ z(l,t) = 0,\ z''(0,t) = 0,\ z''(l,t) = 0.$$

(b) Linear spring support in the center part of the rotor yields free-free boundary conditions at the end.

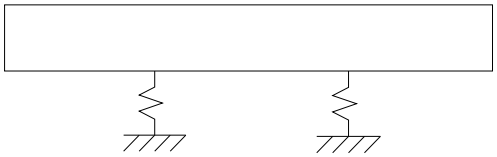

Figure 2.4. Beam with spring support.

This implies that the moments and shearing forces vanish at the end points (see also [37]). The moments M_{XZ} and M_{YZ} are given by (2.8) and (2.9). The

shearing forces in our system including rotary inertia and gyroscopic moments are [63]

$$F_x = \frac{1}{2} I_p \ddot{u}' + I_p \omega \dot{v}' - (E I_a u'')',$$

$$F_y = \frac{1}{2} I_p \ddot{v}' - I_p \omega \dot{u}' - (E I_a v'')'.$$

The boundary conditions are then as follows

$$M_{XZ}(s) = M_{YZ}(s) = F_x(s) = F_y(s) = 0 \quad \text{for} \quad s = 0,\, s = l.$$

In the complex formulation $z = u + iv$ this reduces to

$$M = E I_a z'' \quad \text{and} \quad F = \frac{1}{2} I_p \ddot{z}' - i I_p \omega \dot{z}' - (E I_a z'')'$$

and

$$M(s) = F(s) = 0 \quad \text{for} \quad s = 0,\, s = l.$$

The case of support by fluid-film bearings is discussed later in Section 4.5.

Equation of motion for forced vibration

In practice, unbalance forces cannot be avoided. They appear due to the eccentricity of the center of gravity from the centerline of the shaft. In this case the additional potential energy term U_f in (2.5) has to be specified. We assume a description of the unbalance forces by a force density $f_{\text{unb}}(s)$ to obtain

$$U_f = -\int_0^l \left(u(s) f_{\text{unb}}(s) + v(s) f_{\text{unb}}(s)\right) ds. \tag{2.17}$$

In general, unbalance forces are periodically excited and depend on mass m, eccentricity e and rotational speed ω of the rotor. They are expressed as (see e.g. [63] and [23])

$$f_{\text{unb}}(s) = m e(s) \omega^2 e^{i\omega t}.$$

The integrand of (2.17) is added to the integral density of the action functional given by (2.11). Inserting into the Lagrange equations (2.12) and proceeding as above, an extended equation of motion is obtained.

The **equation of motion governing forced vibrations of a continuous rotor** is given by

$$\mu \ddot{z} - \frac{1}{2} \left(I_p \ddot{z}'\right)' + i \left(I_p \omega \dot{z}'\right)' + c \dot{z} + \left(E I_a z''\right)'' = f_{\text{unb}}. \tag{2.18}$$

Using a suitable solution technique for the introduced equations of motion these can be transformed into an eigenvalue problem giving the natural frequencies and mode

shapes which are the target objects of our optimization problems. This is done by the separation of variables and a solution approach by an exponential function for the time dependence. The physical motivation behind this approach is that the gyroscopic moment working in the rotor leads to a deflection curve and that the shaft whirls with a frequency keeping the mode shape constant in each mode [63].

The solution of the equation of motion for the continuous and a discretized rotor as well as some statements about the existence of solutions are shown in Chapters 3 and 4.

Chapter 3

Existence theorems

In this chapter we prove the existence of solutions for the two optimization problems mentioned in Chapter 1, i.e. the natural frequency optimization problem and the vibration level optimization problem. In a first step the equation of motion for the rotor, which is derived in Chapter 2, is solved in Section 3.1. This is achieved by the separation of variables which leads to an eigenvalue problem and which is giving the natural frequencies and eigenmodes. The operator in the eigenvalue problem is shown to be compact and the spectrum is described by the theorem of Riesz-Schauder. This result is then used to show the existence of solutions for the optimization problem in Section 3.2. An overview about the theorems of functional analysis which are applied can be found in Appendix A.

Similar results for the non-rotating case can e.g. be found in Haslinger and Mäkinen [27] and Fichera [16]. The inclusion of the gyroscopic term, however, yields a non-symmetric system and the theory of compact operators is used. Hence our approach is an extension of existing results in the literature.

3.1 Solvability of equation of motion

Let us first consider the equation of motion for undamped free oscillations which was deduced in the previous chapter

$$\mu\ddot{z} - \frac{1}{2}(I_p\ddot{z}')' + i(I_p\omega\dot{z}')' + (EI_a z'')'' = 0, \tag{3.1}$$

where μ, I_p and I_a are given in Section 2.2. These parameters depend on the rotor shape function r and hence on the spatial variable s. The function r belongs to the set of admissible functions U which is given by

$$U = \{r \in C(I), \quad \underline{r} \leq r \leq \bar{r}, \quad |r(x) - r(y)| \leq L_0|x - y|, \quad \forall x, y \in I\}, \tag{3.2}$$

where $I = [0, l]$ as in Chapter 2. The additional Lipschitz condition with constant L_0 makes U a compact subset of $C(I)$ which follows from the theorem of Arzelà-Ascoli. Equation (3.1) is now transformed into an eigenvalue problem by the separation of variables and an exponential function approach for the time variable. Every solution of the eigenvalue problem leads to a solution of the original equation of motion and we just focus on these special solutions.

For the theoretical studies of this chapter simple support boundary conditions at both ends of the rotating body are used, i.e.

$$z(0,t) = 0,\ z(l,t) = 0,\ z''(0,t) = 0,\ z''(l,t) = 0.$$

The separation of variables is now written as

$$z(s,t) = \varphi(s)\psi(t),$$

where φ and ψ only depend on one of the variables. The original equation of motion (3.1) becomes

$$\mu\varphi\ddot{\psi} - \frac{1}{2}\left(I_p\varphi'\right)'\ddot{\psi} + i\left(I_p\omega\varphi'\right)'\dot{\psi} + \left(EI_a\varphi''\right)''\psi = 0 \tag{3.3}$$

and the boundary conditions are satisfied if

$$\varphi(0) = 0,\ \varphi(l) = 0,\ \varphi''(0) = 0,\ \varphi''(l) = 0. \tag{3.4}$$

Equation (3.3) can immediately be transformed into the desired eigenvalue problem. However, before doing this, to avoid a quadratic eigenvalue problem, the second-order-equation (3.3) is transformed into a first-order-system by writing

$$\begin{pmatrix} \mu\varphi - \frac{1}{2}(I_p\varphi')' & 0 \\ 0 & \mu\varphi - \frac{1}{2}(I_p\varphi')' \end{pmatrix}\begin{pmatrix} \ddot{\psi} \\ \dot{\psi} \end{pmatrix} = \begin{pmatrix} -i(I_p\omega\varphi')' & -(EI_a\varphi'')'' \\ \mu\varphi - \frac{1}{2}(I_p\varphi')' & 0 \end{pmatrix}\begin{pmatrix} \dot{\psi} \\ \psi \end{pmatrix}.$$

Setting $\psi(t) = e^{\lambda t}$ we want to solve for $\Phi = (\phi_1, \phi_2)$ the equation

$$\lambda A(\phi_1, \phi_2) = B(\phi_1, \phi_2), \tag{3.5}$$

where

$$A(\phi_1,\phi_2) = \begin{pmatrix} \mu\phi_1 - \frac{1}{2}(I_p\phi_1')' \\ \mu\phi_2 - \frac{1}{2}(I_p\phi_2')' \end{pmatrix} \quad \text{and} \quad B(\phi_1,\phi_2) = \begin{pmatrix} -i(I_p\omega\phi_1')' - (EI_a\phi_2'')'' \\ \mu\phi_1 - \frac{1}{2}(I_p\phi_1')' \end{pmatrix}.$$

Once (3.5) is solved we may set $\varphi = \phi_2$ and obtain $\phi_1 = \lambda\phi_2 = \lambda\varphi$ from the second line and the solution property for the first line.

Proposition 3.1. *Let φ satisfy the boundary conditions (3.4). The function $\varphi(s)e^{\lambda t}$ is a solution of equation (3.1) if and only if $(\lambda\varphi, \varphi)^T$ is a solution of system (3.5).*

Proof. We assume that $\varphi(s)e^{\lambda t}$ solves (3.1). Then it is obvious that $\varphi(s)e^{\lambda t}$ solves (3.3) where we set $\psi(t) = e^{\lambda t}$. This equation can be transformed into a first order system as shown above. If we then set $\phi_1 = \lambda\varphi$ and $\phi_2 = \varphi$ the eigenvalue problem (3.5) is satisfied.

For the other direction we assume that $(\lambda\varphi, \varphi)^T$ is a solution of (3.5). Then the first line of (3.5) yields that φ and $\psi(t) = e^{\lambda t}$ solve the first-order system (3.3). Then $z(s,t) = \varphi(s)e^{\lambda t}$ is a solution of (3.1). □

To prove the existence of solutions of eigenvalue problem (3.5) and thus for the equation of motion (3.1) a suitable analytical framework has to be introduced. We define the two Sobolev spaces V_1 and V_2 on $I = [0, l]$ by

$$V_1 = \{v \in H^1(I) |\ v(0) = 0,\ v(l) = 0\} = H_0^1(I),$$

$$\|v\|_{V_1} = \left(\int_I |v(s)|^2\, ds + \int_I |v'(s)|^2\, ds \right)^{1/2}$$

and

$$V_2 = \{v \in H^2(I) |\ v(0) = 0,\ v(l) = 0\},$$

$$\|v\|_{V_2} = \left(\int_I |v(s)|^2\, ds + \int_I |v'(s)|^2\, ds + \int_I |v''(s)|^2\, ds \right)^{1/2}$$

and their dual spaces are denoted by $V_1' = H^{-1}(I)$ and V_2', respectively. The conditions on the second derivatives are not imposed but turn out to be satisfied as the natural boundary conditions.

The formulas (3.1) and (3.5) are the **classical formulation** of the equation of motion and the eigenvalue problem. This is sufficient for the existence theorems of this chapter. For the convergence analysis of a discretized model which is done in Chapter 4 the weak formulation is also needed and is therefore introduced now.

The **weak formulation** of the equation of motion is obtained by multiplying equation (3.1) by test functions $\eta \in V_2$ and integrating the whole equation over the interval I. Partial integration and the use of boundary conditions (3.4) yields

$$\left(\int_I \mu\varphi\bar{\eta}\, ds + \frac{1}{2} \int_I I_p \varphi'\bar{\eta}'\, ds \right) \ddot{\psi} - \left(i \int_I I_p \omega \varphi'\bar{\eta}'\, ds \right) \dot{\psi} + \left(\int_I E I_a \varphi''\bar{\eta}''\, ds \right) \psi = 0.$$

Setting $\psi(t) = e^{\lambda t}$ and $\Phi = (\phi_1, \phi_2)$ the weak formulation of the eigenvalue problem (3.5) is

$$\lambda a(\Phi, \eta) = b(\Phi, \eta) \quad \text{for } \eta \in V_2, \tag{3.6}$$

where

$$a(\Phi,\eta) = a(\phi_1,\phi_2,\eta) = \begin{pmatrix} \int \mu\phi_1\bar{\eta}\,ds + \frac{1}{2}\int I_p\phi_1'\bar{\eta}'\,ds \\ \int \mu\phi_2\bar{\eta}\,ds + \frac{1}{2}\int I_p\phi_2'\bar{\eta}'\,ds \end{pmatrix}$$

and

$$b(\Phi,\eta) = b(\phi_1,\phi_2,\eta) = \begin{pmatrix} -i\int I_p\omega\phi_1'\bar{\eta}'\,ds - \int EI_a\phi_2''\bar{\eta}''\,ds \\ \int \mu\phi_1\bar{\eta}\,ds + \frac{1}{2}\int I_p\phi_1'\bar{\eta}'\,ds \end{pmatrix}.$$

Remark. All lemmas and theorems formulated for the classical case then obviously hold for the weak case as well.

The crucial point now is to transform the generalized eigenvalue problem given by (3.5) into a standard one by inverting one of the operators A or B, then to show the compactness of the resulting operator which allows the application of the Riesz-Schauder spectral theorem (see Appendix A).

We consider the operator $M : V_1 \to V_1'$ formally written as

$$M(u) = \mu u - \frac{1}{2}(I_p u')' \tag{3.7}$$

and for any $v \in V_1$ defined by

$$M(u)(v) = \int \left(\mu(s)u(s)\bar{v}(s) + \frac{1}{2}I_p(s)u'(s)\bar{v}'(s)\right) ds,$$

and the operator $L : V_1 \times V_2 \to V_2'$ formally written as

$$L(u_1,u_2) = -i(I_p\omega u_1')' - (EI_a u_2'')''$$

and for any $v \in V_2$ defined by

$$L(u_1,u_2)(v) = i\int \omega I_p(s)u_1'(s)\bar{v}'(s)\,ds - \int EI_a(s)u_2''(s)\bar{v}''(s)\,ds.$$

Then eigenvalue problem (3.5) reads as

$$\lambda \underbrace{\begin{pmatrix} M(\phi_1) \\ M(\phi_2) \end{pmatrix}}_{=A(\phi_1,\phi_2)} = \underbrace{\begin{pmatrix} L(\phi_1,\phi_2) \\ M(\phi_1) \end{pmatrix}}_{=B(\phi_1,\phi_2)}, \tag{3.8}$$

where $A : V_1 \times V_1 \to V_1' \times V_1'$ and $B : V_1 \times V_2 \to V_2' \times V_1'$. Note that A and B map into different spaces. However, if we can find an inverse operator to B we can

construct an operator $B^{-1}A$ which then is well-defined since $V_1' \subset V_2'$ and we have to solve

$$B^{-1}A\Phi = \zeta\Phi, \tag{3.9}$$

where $\zeta = 1/\lambda$.

Now the goal is to show that such an operator B^{-1} exists.

We first want to prove two lemmas giving us the invertibility of the operator M as introduced above and the operator $K : V_2 \to V_2'$ which is the second term of the operator L and is given formally by

$$K(u) = (EI_a u'')'' \tag{3.10}$$

and for any $v \in V_2$

$$K(u)(v) = \int EI_a(s)u''(s)\bar{v}''(s)\,ds,$$

respectively. As usual in such cases the theorem of Lax-Milgram is used (see Appendix A).

CONVENTION: In this chapter the letter C stands for a generic positive constant attaining different values at different places

Lemma 3.1. *The operator $M : V_1 \to V_1'$ given by (3.7) is invertible.*

Proof. To apply the theorem of Lax-Milgram we have to show that the associated sesquilinear form $m : V_1 \times V_1 \to \mathbb{C}$ given by

$$m(u,v) = \int_I \mu(s)u(s)\bar{v}(s)\,ds + \frac{1}{2}\int_I I_p(s)u'(s)\bar{v}'(s)\,ds$$

is continuous and coercive.

The continuity and coercivity follow from the boundedness of μ and I_p. Indeed, we have

$$\begin{aligned}|m(u,v)| &= \left|\int \mu(s)u(s)\bar{v}(s)\,ds + \frac{1}{2}\int I_p(s)u'(s)\bar{v}'(s)\,ds\right| \\ &\le C\left|\int u(s)\bar{v}(s)\,ds + \int u'(s)\bar{v}'(s)\,ds\right| = C|\langle u,v\rangle_{V_1}| \le C\|u\|_{V_1}\|v\|_{V_1}.\end{aligned}$$

and

$$\begin{aligned}m(u,u) &= \int \mu|u(s)|^2ds + \frac{1}{2}\int I_p|u'(s)|^2ds \\ &\ge C\left(\int |u(s)|^2ds + \int |u'(s)|^2ds\right) = C\|u\|^2_{V_1}.\end{aligned}$$

Then the application of Lax-Milgram yields

$$m(u,v) = M(u)(v)$$

and the operator $M : V_1 \to V_1^{'}$ is invertible. □

Lemma 3.2. *The operator $K : V_2 \to V_2'$ given by (3.10) is invertible.*

Proof. The proof is as above. The associated sesquilinear form $k : V_2 \times V_2 \to \mathbb{C}$ given by

$$k(u,v) = \int EI_a u''(s)\bar{v}''(s)ds$$

is shown to be continuous and coercive.

The continuity is obvious again due to the boundedness of I_a.
For the coercivity we have to apply the standard Poincaré inequality (Theorem A.3) as well as a generalized form of it (Theorem A.4) since we have no boundary conditions for the first derivatives. The set S in Theorem A.4 is chosen to be

$$S = \left\{ v \in H^1(I) | \int_0^l v = 0 \right\}$$

and having in mind that $v = u'$ and $u \in V_2$. This set is a subspace of $H^1(I)$ and hence a cone with apex 0. Then condition (1) of Theorem A.4 is fulfilled with $C_0 = 0$, since for any $u_0 \in S$ and $\xi \neq 0$, we have $u_0 + \xi \notin S$. Then the estimate

$$\int |u'(s)|^2 \, ds \leq C \int |u''(s)|^2 \, ds \quad \forall u' \in S$$

is obtained.
The coercivity follows immediately

$$\begin{aligned} \|u\|_{V_2}^2 &= \left(\int |u(s)|^2 \, ds + \int |u'(s)|^2 \, ds + \int |u''(s)|^2 \, ds \right) \\ &\leq C \int |u'(s)|^2 \, ds + \int |u''(s)|^2 \, ds \\ &\leq C \int |u''(s)|^2 \, ds \\ &\leq C \int EI_a(s) u''(s) \bar{u}''(s) \, ds = C \, k(u,u). \end{aligned}$$

The first inequality holds due to the standard Poincaré inequality and the second one due to the generalized Poincaré inequality. The remaining expression can again be estimated due to the boundedness of I_a leading to the last inequality.

Then, by applying Lax-Milgram,

$$k(u, v) = K(u)(v)$$

and K is invertible. □

Knowing the invertibility of M and K we can construct an inverse operator to the operator B given in (3.8).

Lemma 3.3. *To the operator B given in (3.8) there exists an inverse operator $B^{-1} : V_2' \times V_1' \to V_1 \times V_2$.*

Proof. We consider an arbitrary right-hand-side $(f_1, f_2) \in V_2' \times V_1'$ and look at the system $B(\phi_1, \phi_2) = (f_1, f_2)^T$, i.e.

$$L(\phi_1, \phi_2) = -i(I_p\omega\phi_1')' - (EI_a\phi_2'')'' = f_1 \quad \in V_2', \tag{3.11}$$

$$M(\phi_1) = \mu\phi_1 - \frac{1}{2}(I_p\phi_1')' = f_2 \quad \in V_1'. \tag{3.12}$$

From Lemma 3.1 we know that M is invertible. Hence we can write

$$\phi_1 = M^{-1}f_2 \quad \in V_1.$$

Then the equation (3.11) can be written as

$$-(EI_a\phi_2'')'' = i(I_p\omega(M^{-1}f_2)')' + f_1 \quad \in V_2'.$$

Lemma 3.2 shows that the operator on the left-hand-side is invertible and we have

$$\phi_2 = -K^{-1}(i(I_p\omega(M^{-1}f_2)')' + f_1) \in V_2.$$

Thus we have found a preimage $(\phi_1, \phi_2) \in V_1 \times V_2$. □

The next step is to show that the operator $B^{-1}A$ is compact. The notion of compactness requires a mapping from a certain space onto itself. We notice that the space $V_1 \times V_2$ is the correct space for which the operator $B^{-1}A$ compact.

Lemma 3.4. *The operator $B^{-1}A : V_1 \times V_2 \to V_1 \times V_2$ is compact.*

Proof. We apply the operator on an arbitrary pair $(\phi_1, \phi_2) \in V_1 \times V_2$. Note that we restrict the second component to be in V_2 whereas A also allows V_1-functions. Then we have

$$\begin{aligned} B^{-1}A(\phi_1, \phi_2) &= B^{-1}(M(\phi_1), M(\phi_2)) \\ &= (M^{-1}(M(\phi_2)), -K^{-1}(i(I_p\omega(M^{-1}(M(\phi_2)))')' + M(\phi_1))) \\ &= (\phi_2, -K^{-1}(i(I_p\omega\phi_2')' + M(\phi_1))). \end{aligned}$$

We show that the mapping is compact in each component.
For the first component we have

$$\begin{array}{cccccc} (\phi_1,\phi_2) & \overset{B^{-1}A}{\mapsto} & \phi_2 & \overset{id}{\mapsto} & \phi_2, \\ V_1 \times V_2 & \to & V_2 & \overset{cpt}{\hookrightarrow} & V_1, \end{array}$$

and for the second component

$$\begin{array}{ccccccc} (\phi_1,\phi_2) & \mapsto & i(I_p\omega\phi_2')' + M(\phi_1) & \overset{id}{\mapsto} & \dots & \overset{K^{-1}}{\mapsto} & -K^{-1}(i(I_p\omega\phi_2')' + M(\phi_1)), \\ V_1 \times V_2 & \to & V_1' & \overset{cpt}{\hookrightarrow} & V_2' & \to & V_2. \end{array}$$

All operators are linear and continuous and the composition with a compact embedding yields a compact operator. Hence, the operator $B^{-1}A : V_1 \times V_2 \to V_1 \times V_2$ is compact. □

Theorem 3.1. *Let $T := B^{-1}A$. The spectrum $\sigma(T)$ is an at most countable set with no accumulation point different from zero. Let $\sigma'(T)$ be a finite system of eigenvalues, which is separated from the rest $\sigma''(T)$ of $\sigma(T)$ by a closed Jordan curve. All eigenvalues λ of $\sigma'(T)$ depend continuously on the shape function r. The same holds for the set of corresponding eigenvectors Φ.*

Proof. Since the operator $B^{-1}A$ is compact the spectral theorem of Riesz-Schauder can be applied and the eigenvalue problem (3.9) has a solution with eigenvalues ζ_i with at most one accumulation point at zero. This means that the values $\lambda_i = 1/\zeta_i$ tend to infinity. It also implies that the spectrum can be separated into two parts by a closed Jordan curve with the part inside the curve consisting of a finite number of eigenvalues and not containing zero. Then from Kato [31, IV.3.5], it follows that the eigenvalues and eigenvectors depend continuously on the closed operator $B^{-1}A$ and hence also on the shape function r. □

Remark. Our focus lies only on eigenvalues belonging to modes which are excited in the respective operating speed range. Their number is limited and can be included in a finite system of eigenvalues and can be separated from the accumulation point zero. Then the continuity argument of Theorem 3.1 holds for this case.

3.2 Solvability of optimization problems

(I) Natural frequency optimization problem

As pointed out in Chapter 1, the design optimization problem we want to study for a continuous rotor is the following: Find a thickness distribution which minimizes a given continuous cost functional J subject to natural frequency and unbalance

response constraints as given in the introduction. The rotor shape function r is bounded from below and above. More precisely, r belongs to the class of admissible functions U as in (3.2).

The first optimization problem deals with a continuous objective function J and a constraint on the natural frequency λ_{m} of a certain mode m and is written as

$$\begin{array}{l} \min_r J(r) \\ \text{subject to} \\ \lambda_{\mathrm{m}}(r) \geq \lambda_{\mathrm{m}}^*, \\ r \in U. \end{array} \tag{P1}$$

In our applications the function of the total mass of the rotor is often chosen as cost functional J. For the natural frequency λ_{m} a lower bound λ_{m}^* is given. The constraint on the natural frequencies can be put into U as defined in (3.2) giving the (new) class of admissible functions for this problem

$$U_c = \{r \in U |\, \lambda_{\mathrm{m}}(r) \geq \lambda_{\mathrm{m}}^*\}.$$

The theory of the last section enables us to show the existence of solutions for problem (P1).

Theorem 3.2. *Let $U_c \neq \emptyset$. Then the optimization problem (P1) has a solution.*

Proof. Due to Theorem 3.1 and the subsequent remark λ_{m} is a continuous function in r. Hence U_c is a compact subset of $C(I)$. Moreover, the objective function is assumed to be continuous in r. Since a continuous function on a compact set possesses a minimum the existence of solutions is proven. □

(II) Vibration level optimization problem

The second optimization problem deals with constraints on the vibration level. The relevant terms are critical speed and unbalance response. In contrast to the previous problem where the natural frequency for a given rotational speed is considered, we focus here directly on the critical speed of the mode of interest. The system is excited for this certain frequency and the unbalance response is calculated.

For this problem damped systems have to be studied since otherwise the amplitudes in the resonance case are unbounded. In contrast to (3.1) the equation of motion then contains a damping term $c\dot{z}$ and the force term f on the right-hand-side.

$$\mu\ddot{z} - \frac{1}{2}(I_p\ddot{z}')' + i(I_p\omega\dot{z}')' + (EI_a z'')'' + c\dot{z} = f, \tag{3.13}$$

where c is a (viscous) damping coefficient and $f(s,t) = \tilde{f}(s)e^{i\omega t}$ is an unbalance force acting periodically on the rotor. The spatial force density $\tilde{f}$ is assumed to be a continuous function, i.e. $\tilde{f} \in C(I)$.

We now want to show how critical speed and unbalance response are determined analytically and then prove the solvability of the vibration level optimization problem. The critical speed is denoted by ω since it is identical to a certain rotational speed. Natural frequencies for the critical speed or another rotational speed are further denoted by λ.

Critical speed

To determine the critical speeds analytically, the homogeneous equation is studied

$$\mu\ddot{z} - \frac{1}{2}(I_p\ddot{z}')' + i(I_p\omega\dot{z}')' + c\dot{z} + (EI_a z'')'' = 0. \tag{3.14}$$

Similar to the development in Section 3.1 this system can be transformed into an eigenvalue problem by the separation of variables $z(s,t) = \varphi(s)\psi(t)$. In this case the natural frequency λ is equated with the rotational speed ω, such that $\psi(t) = e^{i\lambda t} = e^{i\omega t}$. We obtain

$$i\omega\tilde{A}(\phi_1,\phi_2) = \tilde{B}(\phi_1,\phi_2), \tag{3.15}$$

where

$$\tilde{A}(\phi_1,\phi_2) = \begin{pmatrix} \mu\phi_1 + \frac{1}{2}(I_p\phi_1')' \\ \mu\phi_2 - \frac{1}{2}(I_p\phi_2')' \end{pmatrix} \quad \text{and} \quad \tilde{B}(\phi_1,\phi_2) = \begin{pmatrix} -c\phi_1 - (EI_a\phi_2'')'' \\ \mu\phi_1 - \frac{1}{2}(I_p\phi_1')' \end{pmatrix}.$$

Again $\phi_2 = \varphi$ and $\phi_1 = i\omega\phi_2$. Continuity and coercivity also holds for the operator $\mu\phi_1 + \frac{1}{2}(I_p\phi_1')'$. Then all lemmas and theorems of Section 3.1 can be copied resulting in the following theorem for this case.

Theorem 3.3. *The spectrum $\sigma(\tilde{T})$ of the operator $\tilde{T} = \tilde{B}^{-1}\tilde{A}$ is an at most countable set with no accumulation point different from zero. Every finite subset $\sigma'(\tilde{T})$ which is separated from $\sigma(\tilde{T}) \setminus \sigma'(\tilde{T})$ by a closed Jordan curve depends continuously on the shape function r.*

Remark. The solution of eigenvalue problem (3.15) gives all critical speeds for a given rotor shape function r. For the further unbalance response analysis a certain critical speed belonging to a mode of interest is selected and taken as fixed rotational speed. The set $\sigma'(\tilde{T})$ can be chosen to include this particular critical speed and hence continuity of the critical speed function holds.

Unbalance response

A solution of the inhomogeneous equation of motion (3.13) describes the shape of the running mode of the forced system by its lateral displacements. As unbalance response the displacement at a certain point or an average displacement is considered. Hence the unbalance response can be regarded as a measure for the amplitude of the

running mode of the forced system. The solution of the inhomogeneous equation (3.13) is determined by first solving the homogeneous system for the given critical speed resulting in a set of natural frequencies λ and eigenmodes Φ. The proceeding is similar as in Section 3.1 with the only difference in the additional damping term. This includes the reduction of the system (3.14), the separation of variables $z(s,t) = \varphi(s)\psi(t)$ and setting $\psi(t) = e^{\lambda t}$. The eigenvalue problem is then written as

$$\lambda \hat{A}(\phi_1, \phi_2) = \hat{B}(\phi_1, \phi_2), \tag{3.16}$$

where

$$\hat{A}(\phi_1, \phi_2) = \begin{pmatrix} \mu\phi_1 - \frac{1}{2}(I_p\phi_1')' \\ \mu\phi_2 - \frac{1}{2}(I_p\phi_2')' \end{pmatrix}$$

and

$$\hat{B}(\phi_1, \phi_2) = \begin{pmatrix} -\omega(iI_p\phi_1')' - c\phi_1 - (EI_a\phi_2'')'' \\ \mu\phi_1 - \frac{1}{2}(I_p\phi_1')' \end{pmatrix}.$$

Again we have $\Phi = (\phi_1, \phi_2)$, where $\phi_2 = \varphi$.

We also consider the adjoint system to system (3.16)

$$\bar{\lambda}\hat{A}^*(\xi) = \hat{B}^*(\xi) \tag{3.17}$$

with (left) eigenmode ξ to the eigenvalue $\bar{\lambda}$. The solution of eigenvalue problem (3.16) and its adjoint system (3.17) gives countably many eigenvectors Φ_i and ξ_i which are assumed to form a normalized biorthogonal system of the vector space V_2 with respect to operator $\hat{A}$, i.e.

$$\langle \xi_i, \hat{A}(\Phi_j)\rangle_{V_1 \times V_2} = \delta_{ij} \quad \forall i, j = 1, \ldots, \infty. \tag{3.18}$$

To calculate the general inhomogeneous solution of equation (3.13) a particular solution has to be determined. Therefore, the mode shape φ is written as a linear combination of functions φ_j which are solutions of system (3.16). For our definition of an unbalance response term it is sufficient to consider an approximation of the solution of the inhomogeneous equation of motion. Hence only finitely many functions $\varphi_j, j = 1, \ldots, N$ are taken in the linear combination, such that $z = (\sum_{j=1}^{N} z_j\varphi_j(s))\psi(t)$ and N is the number of considered modes. Furthermore, in this case we set $\psi = e^{i\omega t}$ with ω being the critical speed of the relevant mode. Again we have $\phi_2 = \varphi = \sum_{j=1}^{N} z_j\varphi_j$ and $\phi_1 = i\omega\phi_2$ and we write $\Phi = \sum_{j=1}^{N} z_j\Phi_j$ with $\Phi_j = (i\omega\varphi_j, \varphi_j)^T$. To guarantee a solution the part of the force density $\tilde{f}$ spanned by the vectors $\varphi_1, \ldots, \varphi_N$ is considered, having now $\tilde{f} = \sum_{j=1}^{N} \tilde{f}_j\varphi_j$ with suitable coefficients $\tilde{f}_j$. The problem becomes

$$i\omega\hat{A}(\Phi) = \hat{B}(\Phi) + \hat{f}$$

with $\hat{f} = (\tilde{f}, 0)^T$ and can be written as

$$\sum_{j=1}^{N} i\omega z_j \hat{A}(\Phi_j) = \sum_{j=1}^{N} z_j \hat{B}(\Phi_j) + \hat{f}. \tag{3.19}$$

If we now multiply (3.19) successively from left by the eigenfunctions ξ_l of the adjoint system we obtain N equations

$$\sum_{j=1}^{N} i\omega z_j \langle \xi_l, \hat{A}(\Phi_j)\rangle = \sum_{j=1}^{N} z_j \langle \xi_l, \hat{B}(\Phi_j)\rangle + \langle \xi_l, \hat{f}\rangle, \quad l = 1, \ldots, N.$$

Due to relation (3.18) these equations can be simplified significantly

$$i\omega z_l = \lambda_l z_l + \langle \xi_l, \hat{f}\rangle, \quad l = 1, \ldots, N$$

with λ_l being the eigenvalues of the homogeneous system. The z_l can be determined by

$$z_l = \frac{\langle \xi_l, \hat{f}\rangle}{i\omega - \lambda_l}.$$

For $\phi_2 = \varphi = \sum_{l=1}^{N} z_l \varphi_l$ we can write

$$\varphi = \sum_{l=1}^{N} \frac{\langle \xi_l, \hat{f}\rangle}{i\omega - \lambda_l} \varphi_l. \tag{3.20}$$

An (approximate) solution of the inhomogeneous equation of motion (3.13) is then given by $z = \varphi\psi$, where $\psi(t) = e^{i\omega t}$.

Remark.
(i) If the equation of motion contains a damping term the critical speed $i\omega$ is not equal to an eigenvalue λ_l of the homogenous equation which is then no longer purely imaginary. Hence the denominator in (3.20) is not equal to 0 for all l.

(ii) For the definition of the unbalance response expression only the approximation of the particular solution of the inhomogeneous equation of motion as given in (3.20) is considered. The solutions of the homogeneous equation of motion can be neglected since they vanish with increasing time due to the damping [23].

Definition 3.1. *Based on the expression for φ given by (3.20) we consider as unbalance response a either*

- *the value of φ at a certain point*

$$a = \varphi(s)$$

- *or a norm of φ*

$$a = \left(\int |\varphi(s)|^p \, ds \right)^{1/p}, \quad p \in \mathbb{N}.$$

For these choices of unbalance response we can state the following important lemma.

Lemma 3.5. *The unbalance response a depends continuously on the rotor shape function r.*

Proof. The expression for the unbalance response is a composition of functions which depend continuously on the rotor shape function r as shown in Theorem 3.3. Hence the composition is also continuous. □

Remark. In the preceding development we used $\psi(t) = e^{\lambda t}$ and $\psi(t) = e^{i\omega t}$, respectively, depending on the equation we want to solve. The explanation for the different choice is as follows. If we study the case of forced vibrations we have an unbalance force which is given by an expression $f = \tilde{f} e^{i\omega t}$ with real-valued rotational speed ω. Then to determine a particular solution we set $\psi(t) = e^{i\omega t}$ such that the term of the exponential function cancels out in the inhomogeneous equation. Another case is the determination of the critical speed, where the real-valued rotational speed is equated with the natural frequencies, yielding the critical speed in the real part of the obtained eigenvalues. However, if we want to calculate natural frequencies for given rotational speed, we always consider $\psi(t) = e^{\lambda t}$ giving the frequencies in the imaginary part of the eigenvalues λ.

Optimization problem

Having obtained the terms of critical speed and unbalance response the main optimization problem is formulated for a continuous objective function J and given target values ω^*_{m1} and a^*_{m2}. The modes m1 and m2 are modes in the operating speed range and may coincide,

$$\begin{aligned} &\min_r J(r) \\ &\text{subject to} \\ &\omega_{\mathrm{m1}}(r) \geq \omega^*_{\mathrm{m1}}, \\ &a_{\mathrm{m2}}(r) \leq a^*_{\mathrm{m2}}, \\ &r \in U. \end{aligned} \tag{P2}$$

The set of admissible functions $U_{\tilde{c}}$ is then

$$U_{\tilde{c}} = \{ r \in U \,|\, \omega_{\mathrm{m1}}(r) \geq \omega^*_{\mathrm{m1}},\ a_{\mathrm{m2}}(r) \leq a^*_{\mathrm{m2}} \}.$$

Finally, the existence of solutions for this vibration level optimization problem can be proven.

Theorem 3.4. *Let $U_{\tilde{c}} \neq \emptyset$. Then optimization problem (P2) has a solution.*

Proof. From Theorem 3.3 and Lemma 3.5 it follows that the functions of the critical speed ω and the unbalance response a depend continuously on the shape function r. Then the set $U_{\tilde{c}}$ is a compact subset of $C(I)$. Since we have a continuous objective function J the optimization problem (P2) has a solution. □

We obtained a result for the existence of solutions for our chosen design optimization problems for a continuous rotor. However, to determine solutions in practice we have to formulate a finite element model. This is done in the next section and we can show the convergence of the solutions of the discretized problem towards those of the continuous problem.

Chapter 4

Finite element model

For the numerical solution of the equation of motion for our continuous rotor a discretization procedure is necessary to describe the system by a finite number of parameters. The continuous model is regarded as assemblage of finite elements connected by nodes. Equations of motion for each single element are formulated and later assembled to form the equation of motion of the whole discretized model. Then suitable solution techniques are applied to solve the finite-dimensional problem. This concept is known as finite element method.
A good overview about the method of finite elements in mechanics can be found in the books of Kikuchi [32], Ishida [63] and Meirovitch [41] as well as in the paper of Nelson & McVaugh [44]. For the mathematical background we refer to the book of Strang & Fix [53].

In the Sections 4.1 and 4.2 of this chapter we take up the abstract setting of the previous chapter. The infinite-dimensional operators are approximated by finite dimensional operators which are related to a suitable discretization of the design space. Convergence of the solutions of the approximating subproblem towards the solution of the continuous problem is shown.

In Section 4.3 an algebraic formulation for the finite element model is presented. This is first done for a general approximation space. Then the choice for our numerical calculations is shown. Following the concept introduced in Chapter 2 we want to work with one-dimensional finite beam elements. We divide our rotor shaft in several piecewise constant finite elements bounded by nodes with the lateral displacements and inclinations being the degrees of freedom. Every element is assumed to have a constant cross-section and diameter and uniform material properties. This implies that each time the diameter in the rotor changes we have to take a new element. A formulation of the corresponding matrices for an individual beam element can be found in Appendix B. From an engineering point of view the number of finite elements is governed by the number of modes under consideration. It should not be

too large to avoid heavy computations.

In Section 4.4 the numerical solution for the discretized model is done yielding natural frequencies and eigenmodes which are the targets of our optimization problem. Section 4.5 considers an extension of the model about fluid-film-bearings. Some theoretical background and the way how this type of bearings are integrated into our finite element model is shown.

4.1 Convergence of eigenvalues of discretized problem

In a first step, the convergence of the eigenvalues and eigenvectors of discretized generalized eigenvalue problems has to be shown. These functions appear in the constraints of our optimization problem. Important results in spectral approximation can be found in Babuška & Osborn [4], Chatelin [10] and Kolata [34] and can be applied to our case.

The approximation of the operators and the optimization problems is based on the partition of the interval $I = [0, l]$,

$$0 = a_0 < a_1 < \ldots < a_n = l,$$

where $h = \max_{i=1,\ldots,n} |a_i - a_{i-1}|$ is the discretization parameter. We assume a partition such that $h \to 0$ if $n \to \infty$. Moreover, let $P_k([a_{i-1}, a_i])$ denote the space of polynomials of degree $\leq k$ on the interval $[a_{i-1}, a_i]$.

The rotor shape function $r \in U$, where U is given by (3.2), is then assumed to be approximated by piecewise constant functions r_h belonging to the set

$$\begin{aligned} U_h \;=\; \{r \in L^\infty(I) |\, r^i = r|_{[a_{i-1},a_i]} \in P_0([a_{i-1}, a_i]),\ i = 1, \ldots, n,\ \underline{r} \leq r \leq \bar{r}, \\ |r^{i+1} - r^i| \leq L_0 h, \quad L_0 > 0, \quad i = 1, \ldots, n-1\}. \end{aligned}$$

The spaces V_1 and V_2 defined in Chapter 3 are replaced by finite dimensional approximations V_1^h and V_2^h. The exact choice of these approximations depends on the degrees of freedom under consideration. Moreover, we set $V^h = V_1^h \times V_2^h$ and we assume a partition such that $\cup_{h>0} V^h$ is dense in the space $V = V_1 \times V_2$.

The discretized eigenvalue problem is now obtained by replacing the continuous rotor shape function $r \in U$ by a function $r_h \in U_h$. This is written as follows. At first, the notation of the eigenvalue problem of Chapter 3 is extended about a subscript r indicating the dependence on the continuous function r, i.e.

$$\lambda A_r(\Phi) = B_r(\Phi), \qquad \Phi = (\phi_1, \phi_2) \in V_1 \times V_2$$

and

$$\lambda a_r(\Phi, \eta) = b_r(\Phi, \eta), \qquad \eta \in V_2,$$

respectively. Furthermore, we write

$$T_r = B_r^{-1} A_r, \qquad V_1 \times V_2 \to V_1 \times V_2$$

for the operator which was shown to be compact in Lemma 3.4.

The discretized subproblem for $r_h \in U_h$ is then

$$\lambda_h A_{r_h}(\Phi_h) = B_{r_h}(\Phi_h), \qquad \Phi_h \in V^h \tag{4.1}$$

with eigenvalues λ_h and eigenvectors Φ_h in V^h.
The corresponding weak formulation is then

$$\lambda_h a_{r_h}(\Phi_h, \eta_h) = b_{r_h}(\Phi_h, \eta_h), \qquad \eta_h \in V_2^h. \tag{4.2}$$

Following Kolata [34] we now define a projection of the space $V = V_1 \times V_2$ on the space V^h. This is done by using the weak formulation.

Definition 4.1. *We define a linear operator $P_h : V \to V^h$ by*

$$b_{r_h}(P_h\Phi, \eta_h) = b_r(\Phi, \eta_h), \quad \forall \eta_h \in V_2^h.$$

Furthermore, let $T_{r_h} : V \to V^h$ be given by

$$T_{r_h} = P_h \circ T_r$$

and $T_{r_h} = B_{r_h}^{-1} A_{r_h}$.

The convergence of eigenvalues λ_h and eigenvectors Φ_h of the discretized problem to those of the continuous problem is shown by applying the concept of strongly stable convergence (see Chatelin [10]).

Theorem 4.1. *Let $r_h \to r$ as $h \to 0$ in $L^\infty(I)$. Moreover, let S be a set bounded by a closed Jordan curve which encloses exactly one eigenvalue λ of T_r with multiplicity m. Then $\sigma(T_{r_h}) \cap S$ consists for h small enough of exactly m eigenvalues, counting their multiplicities.*

Proof. Since $\cup_{h\to 0} V^h$ is dense in V the projection operator converges pointwise towards the identity operator, $P_h \to I$. The convergence is uniform on any sequentially compact set. Since we know that T_r is compact it follows

$$\|T_r - T_{r_h}\| = \|(I - P_h)T_r\| \to 0 \quad \text{as} \quad h \to 0.$$

This implies strongly stable convergence of the sequence T_{r_h} (see Chatelin [10, Example 5.14]). For a definition of strongly stable convergence see [10, Chapter 5.2]. Let now λ be an eigenvalue of T_r with multiplicity m. Then the strongly stable convergence property of T_{r_h} guarantees that $\sigma(T_{r_h}) \cap S$ consists for h small enough of exactly m eigenvalues, counting their multiplicities [10, Proposition 5.6]. □

The convergence of eigenvectors then also follows immediately by [10, Theorem 5.10].

Theorem 4.2. *Let T_{r_h} be an approximation of T_r, converging strongly stable in S. Then for any sequence of eigenvalues λ_h converging to λ and for any sequence of associated eigenvectors Φ_h there exists a subsequence converging to an eigenvector Φ associated with λ.*

4.2 Convergence of solutions of optimization problem

Having established the convergence of the constraint functions in Section 4.1 we now want to show the convergence of the solutions of the natural frequency and vibration level optimization problems for rotating bodies. Similar results for problems for the non-rotating case can be found in [27].

For the formulation of the discretized natural frequency optimization problem the set of admissible functions U_h is restricted about the constraint on the eigenvalues and is

$$U_{h,c} \;=\; \{r \in U_h |\, \lambda_h(r) \geq \lambda^*\}.$$

In practice the eigenvalue constraint is only set for few specific modes. Similar to Chapter 3 we consider only one constraint function for the analysis. Other constraints can be included in the same way.

Then the natural frequency optimization problem with a continuous objective function J writes as

$$\begin{array}{l} \min_{r_h} J(r_h) \\ \text{subject to} \\ r_h \in U_{h,c}. \end{array} \qquad (P_h1)$$

We now show that a sequence of optimal solutions of (P_h1) converges towards an optimal solution of (P1).

Theorem 4.3. *Let r_h^* be a sequence of optimal solutions of (P_h1), $h \to 0$. Then one can pass to a subsequence such that there exists a function $r^* \in U$ and*

$$r_h^* \to r^* \quad in \quad L^\infty(I)$$

and r^* is an optimal solution of (P1). In addition, any accumulation point of r_h^* possesses this property.

Proof. Let $r_h \in U_h, h \to 0$ be an arbitrary sequence. With any r_h a continuous piecewise linear function $\hat{r}_h$ is defined on the partition $\{b_i\}_{i=0,\ldots,n+1}$, where

$$0 = b_0 = a_0 < b_1 < a_1 < \ldots < a_{n-1} < b_n < a_n = b_{n+1}$$

and b_i is the midpoint of the interval $[a_{i-1}, a_i]$,

$$b_i = \frac{a_i + a_{i-1}}{2}, \quad i = 1, \ldots, n.$$

The function $\hat{r}_h$ is given by

$$\hat{r}_h(b_i) = r_h(b_i), \quad i = 0, \ldots, n \quad \text{and} \quad \hat{r}_h(b_{n+1}) = r_h(a_n)$$

and

$$\hat{r}_h|_{[b_{i-1},b_i]} \in P_1([b_{i-1}, b_i]), \quad i = 1, \ldots, n+1.$$

This definition implies that

$$\underline{r} \leq \hat{r}_h \leq \bar{r} \quad \text{in } I$$

and

$$|\hat{r}_h'| \leq L_0 \quad \text{in } I.$$

We have that $\hat{r}_h \in U$. Since U is compact there exists a subsequence $\hat{r}_h$ and a function $\hat{r} \in U$ such that

$$\|\hat{r}_h - \hat{r}\|_{L^\infty(I)} \to 0 \quad \text{as} \quad h \to 0.$$

The function r_h can be viewed as piecewise constant interpolant of $\hat{r}_h$ implying that

$$\|r_h - \hat{r}_h\|_{L^\infty(I)} \leq L_0 h.$$

Using the triangle inequality we can now show that r_h converges towards the function $\hat{r}$

$$\|r_h - \hat{r}\|_{L^\infty(I)} \leq \|r_h - \hat{r}_h\|_{L^\infty(I)} + \|\hat{r}_h - \hat{r}\|_{L^\infty(I)} \to 0.$$

So far, we only have $\hat{r} \in U$. But of course, the constraint on the eigenvalue should also be fulfilled for the limit function. This follows straightforwardly from the continuous dependence of λ on r, i.e $\lambda_h(r_h) \overset{h\to 0}{\to} \lambda(r)$ which was shown in Theorem 3.1. Hence we have $\hat{r} \in U_c$.

The density of $\cup_{h\to 0} U_h$ in U in the L^∞-norm can be shown as follows.
Let $r \in U$ and define r_h as

$$r_h = \sum_{i=1}^{n} \left(\frac{1}{|a_i - a_{i-1}|} \int_{a_{i-1}}^{a_i} r(s)\, ds \right) \chi_i,$$

where χ_i is the characteristic function of $[a_{i-1}, a_i]$, $i = 1, \ldots, n$. We have $r_h \in U_h$ and $r_h \to r$ in $L^\infty(I)$ if $h \to 0$. Restricting both spaces about the eigenvalue constraint the density result also holds for the spaces $\cup_{h\to 0} U_{h,c}$ in U_c.

We now consider a sequence of optimal solutions r_h^* to problems (P_h1) and denote its limit function by r^*. It remains to show that r^* is an optimal solution of (P1). Therefore we consider an arbitrary $\tilde{r} \in U_c$. A sequence $\tilde{r}_h \in U_{h,c}$ can be found such that

$$\|\tilde{r}_h - \tilde{r}\|_{L^\infty(I)} \to 0.$$

Since r_h^* is an optimal solution of problem (P_h1) we have

$$J(r_h^*) \leq J(\tilde{r}_h).$$

Since $\|r_h^* - r^*\|_{L^\infty(I)} \to 0$ and $\|\tilde{r}_h - \tilde{r}\|_{L^\infty(I)} \to 0$ and J is continuous in r for suitable functions we obtain in the limit

$$J(r^*) \leq J(\tilde{r})$$

for any $\tilde{r} \in U$. This shows that r^* is an optimal solution of (P1). □

Theorem 4.3 for the natural frequency optimization problem can be transformed analogously to the vibration level optimization problem,

$$\begin{array}{l} \min_{r_h} J(r_h) \\ \text{subject to} \\ r_h \in U_{h,\tilde{c}}, \end{array} \qquad (P_h2)$$

where

$$U_{h,\tilde{c}} = \{r \in U_h |\ \omega_h(r) \geq \omega^*,\ a_h(r) \leq a^*\}.$$

Theorem 4.4. *Let r_h^* be a sequence of optimal solutions of (P_h2), $h \to 0$. Then one can pass to a subsequence such that there exists a function $r^* \in U$ and*

$$r_h^* \to r^* \quad in \quad L^\infty(I)$$

and r^* is an optimal solution of (P2).

4.3 Algebraic formulation of discretized model

For the numerical calculations we develop an algebraic formulation of the discretized problem. Then an equation of motion consisting of the structural matrices and a vector consisting of all degrees of freedom contained in the discretized formulation

is obtained. To achieve this we work with the two equations of motion (2.13) and (2.14) for the real variables u and v which were introduced in Chapter 2

$$\mu\ddot{u} - \left(\frac{1}{2}\ddot{u}'I_p\right)' - (I_p\omega\dot{v}')' + (EI_a u'')'' = 0,$$

$$\mu\ddot{v} - \left(\frac{1}{2}\ddot{v}'I_p\right)' + (I_p\omega\dot{u}')' + (EI_a v'')'' = 0.$$

By using the two equations with real variables complex matrix entries are avoided. Due to the coupling we have to consider both equations simultaneously.

The matrices of the system are determined by using the weak formulation of the equations of motion. It is formulated with respect to the spatial variable only. This implies that the separation of variables is performed again, writing $u = \varphi_u(s)\psi(t)$ and $v = \varphi_v(s)\psi(t)$. We have

$$\mu\varphi_u\ddot{\psi} - \frac{1}{2}(\varphi_u' I_p)'\ddot{\psi} - (I_p\omega\varphi_v')'\dot{\psi} + (EI_a\varphi_u'')''\psi = 0,$$

$$\mu\varphi_v\ddot{\psi} - \frac{1}{2}(\varphi_v' I_p)'\ddot{\psi} + (I_p\omega\varphi_u')'\dot{\psi} + (EI_a\varphi_v'')''\psi = 0.$$

Since the two equations are considered separately, the approximation space V_2^h is decomposed into two spaces $V_{2,u}^h$ and $V_{2,v}^h$ describing the interpolation in each direction. In our case, we can assume that $V_{2,u}^h = V_{2,v}^h$ and have $\varphi_u, \varphi_v \in V_{2,u}^h$. Using test functions $\eta \in V_{2,u}^h$ the weak formulation is obtained as

$$\left(\int \mu\varphi_u\bar{\eta}\,ds + \frac{1}{2}\int I_p\varphi_u'\bar{\eta}'\,ds\right)\ddot{\psi} + \left(\omega\int I_p\varphi_v'\bar{\eta}'\,ds\right)\dot{\psi} + \left(\int EI_a\varphi_u''\bar{\eta}''\,ds\right)\psi = 0,$$

$$\left(\int \mu\varphi_v\bar{\eta}\,ds + \frac{1}{2}\int I_p\varphi_v'\bar{\eta}'\,ds\right)\ddot{\psi} - \left(\omega\int I_p\varphi_u'\bar{\eta}'\,ds\right)\dot{\psi} + \left(\int EI_a\varphi_v''\bar{\eta}''\,ds\right)\psi = 0.$$

Each of these two equations can be decomposed into three components, namely the mass component m, the gyroscopic component g and the stiffness component k. For $\varphi, \eta \in V_{2,u}^h$ they are given by

$$m(\varphi,\eta) = \int\left(\mu\varphi\bar{\eta} + \frac{1}{2}I_p\varphi'\bar{\eta}'\right)ds,$$

$$g(\varphi,\eta) = \int I_p\varphi'\bar{\eta}'\,ds,$$

$$k(\varphi,\eta) = \int EI_a\varphi''\bar{\eta}''\,ds.$$

These expressions are now used to define our structural matrices. The function φ_u is written as a linear combination of the basis vectors of $V_{2,u}^h$. This basis is given by vectors $\{\tilde{b}_i\}_{i=1}^m$, where $m = \dim(V_{2,u}^h)$ is indicating the number of degrees of freedom in one direction. Then we have

$$\varphi_u = \sum_{i=1}^{m} c_i \tilde{b}_i$$

and

$$\varphi_v = \sum_{i=m+1}^{2m} c_i \tilde{b}_{i-m}$$

with a constant coefficient vector $c = (c_1, \ldots, c_{2m})^T \in \mathbb{R}^{2m}$. Since the equations cross-couple we have to consider them simultaneously. A basis for the space V_2^h is given by

$$\begin{pmatrix} \{\tilde{b}_i\}_{i=1}^m \\ 0 \end{pmatrix} \quad \text{and} \quad \begin{pmatrix} 0 \\ \{\tilde{b}_i\}_{i=1}^m \end{pmatrix}$$

and we denote these basis vectors of V_2^h by $\{b_i\}_{i=1}^{2m}$. They are assembled in a $2 \times 2m$-matrix B,

$$B = (b_1, \ldots, b_{2m}) = \begin{pmatrix} \tilde{b}_1 & \ldots & \tilde{b}_m & 0 & \ldots & 0 \\ 0 & \ldots & 0 & \tilde{b}_1 & \ldots & \tilde{b}_m \end{pmatrix}.$$

Then $\varphi = (\varphi_u, \varphi_v)^T$ can be written in matrix notation giving

$$\varphi = Bc.$$

The structural matrices M, G and K are determined straightforwardly. The i-th column of each matrix is determined by taking the i-th basis function b_i as test function η. This yields for the mass component,

$$\begin{aligned} m(\varphi, b_i) &= \int \left(\mu (Bc)^T b_i + \frac{1}{2} I_p (B'c)^T b_i' \right) ds = c^T \left(\int \left(\mu B^T b_i + \frac{1}{2} I_p B'^T b_i' \right) ds \right) \\ &= c^T M_i = M_i^T c, \quad i = 1, \ldots, 2m, \end{aligned}$$

where M_i is the i-th column of the mass matrix M. The elements of M are given by

$$M_{i,j} = \int \left(\mu b_i^T b_j + \frac{1}{2} I_p b_i'^T b_j' \right) ds, \quad i, j = 1, \ldots, 2m. \tag{4.3}$$

For the stiffness component holds

$$\begin{aligned} k(\varphi, b_i) &= \int E I_a (B''c)^T b_i'' \, ds = c^T \left(\int E I_a B''^T b_i'' \, ds \right) \\ &= c^T K_i = K_i^T c, \quad i = 1, \ldots, 2m, \end{aligned}$$

with K_i being the i-th column of the stiffness matrix K and

$$K_{i,j} = \int EI_a b_i''^T b_j'' \, ds. \quad i,j = 1,\ldots,2m. \tag{4.4}$$

The most interesting term is the gyroscopic term since here the cross-coupling occurs. Therefore, the two rows of the matrix B are divided into B_u and B_v and for one single basis vector b_i into $b_{i,u}$ and $b_{i,v}$. This gives

$$\begin{aligned} g(\varphi, b_i) &= \int I_p \left(\begin{pmatrix} B_v' \\ -B_u' \end{pmatrix} c \right)^T \begin{pmatrix} b_{i,u}' \\ b_{i,v}' \end{pmatrix} ds = c^T \left(\int I_p ({B_v'}^T b_{i,u}' - {B_u'}^T b_{i,v}') \, ds \right) \\ &= -c^T G_i = G_i^T c, \quad i = 1,\ldots,2m, \end{aligned}$$

where G_i is the i-th column of the gyroscopic matrix. This matrix is skew-symmetric and all its elements are given by

$$G_{i,j} = \int I_p ({b_{i,u}'}^T b_{j,v}' - {b_{i,v}'}^T b_{j,u}') \, ds, \quad i,j = 1,\ldots,2m. \tag{4.5}$$

Assembling all columns, the mass, gyroscopic and stiffness matrices M, G and K of the discretized system are obtained. The **algebraic formulation of the equation of motion** is then given by

$$Mc\ddot{\psi} + \omega G c\dot{\psi} + Kc\psi = 0. \tag{4.6}$$

Matrices in our model

For the explicit formulation of the matrices the space V_2^h has to be defined and the basis functions for it have to be determined. The development in our case is based on the beam model from Chapter 2. We first do this for one beam element and later assemble over all beam elements. The choice of space depends on the information which we have and on which the approximation is based. Here, the behaviour of each element is described by the lateral displacement and inclination in the nodes which were introduced in Chapter 2. Then the displacement and inclination for any part within a beam element is determined by certain interpolation functions which are the same for each element. It is assumed that cross section, diameter and material properties are uniform in each element. Our choice of space and basis functions follows [63] and [44].

Let us consider beam element k bounded by nodes a_k and a_{k+1} as shown in Figure 4.1. The length of this element is l_k.

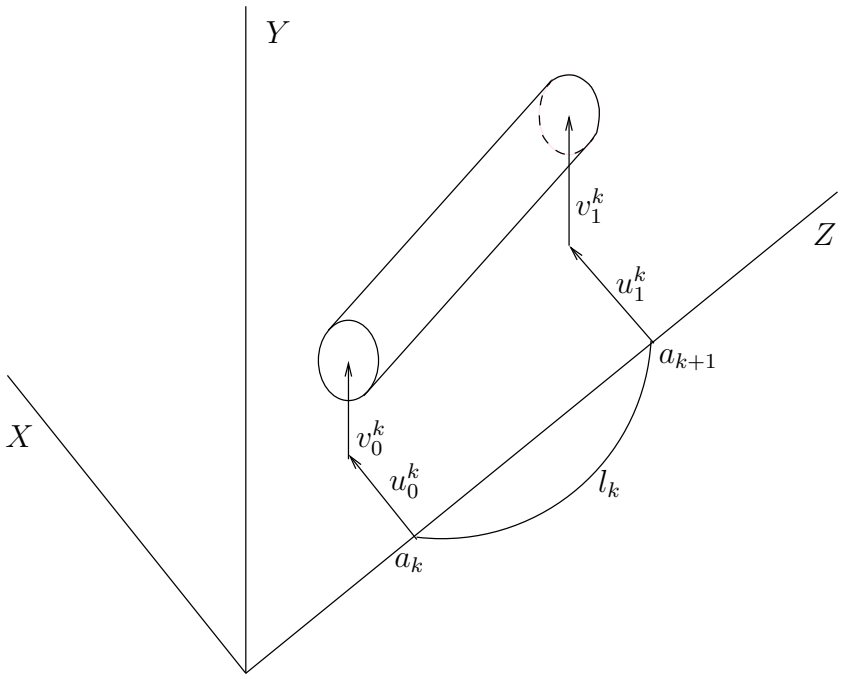

Figure 4.1. One beam element.

For this arbitrary element we denote the displacements in X-direction in the nodes a_k and a_{k+1} for simplification of notation by u_0^k and u_1^k and due to our first-order analysis the derivatives of the displacements in the nodes are the rotation angles ϕ_{y0}^k and ϕ_{y1}^k. Knowing these four values the displacement function $u(s)$ depending on the spatial variable s can be approximated by a uniquely given cubic polynomial,

$$u(s) = as^3 + bs^2 + cs + d, \quad s \in [a_k, a_{k+1}].$$

The coefficients are determined by solving the corresponding linear system of equations. This is called Hermite interpolation. The approximation space for beam element k is then the space of cubic polynomials $P_3([a_k, a_{k+1}])$. We have $\dim(V_k) = 4$ and the Hermite polynomials L_i^k, $i = 1, \ldots, 4$, given by

$$L_1^k(s) = 1 - 3\left(\tfrac{s-a_k}{l_k}\right)^2 + 2\left(\tfrac{s-a_k}{l_k}\right)^3, \quad L_2^k(s) = (s-a_k)\left[1 - 2\left(\tfrac{s-a_k}{l_k}\right) + \left(\tfrac{s-a_k}{l_k}\right)^2\right],$$
$$L_3^k(s) = 3\left(\tfrac{s-a_k}{l_k}\right)^2 - 2\left(\tfrac{s-a_k}{l_k}\right)^3, \qquad L_4^k(s) = l_k\left[-\left(\tfrac{s-a_k}{l_k}\right)^2 + \left(\tfrac{s-a_k}{l_k}\right)^3\right]$$

are a basis of this space. The displacement function u_k can then be written as

$$u_k(s) = L_1^k(s)u_0^k + L_2^k(s)\phi_{y0}^k + L_3^k(s)u_1^k + L_4^k(s)\phi_{y1}^k.$$

The same approach can be done for the lateral displacements v_k in Y-direction resulting in

$$v_k(s) = L_1^k(s)v_0^k - L_2^k(s)\phi_{x0}^k + L_3^k(s)v_1^k - L_4^k(s)\phi_{x1}^k.$$

The vector consisting of all degrees of freedom for beam element k is given by $c^k = (u_0^k, v_0^k, \phi_{x0}^k, \phi_{y0}^k, u_1^k, v_1^k, \phi_{x1}^k, \phi_{y1}^k)^T$. Considering now both equations simultaneously the matrix notation can be used and is here

$$\begin{pmatrix} u_k \\ v_k \end{pmatrix} = B_k c^k,$$

with

$$B_k = \begin{pmatrix} L_1^k & 0 & 0 & L_2^k & L_3^k & 0 & 0 & L_4^k \\ 0 & L_1^k & -L_2^k & 0 & 0 & L_3^k & -L_4^k & 0 \end{pmatrix}.$$

Mass, gyroscopic and stiffness matrices can now be determined by the expressions (4.3), (4.4) and (4.5) and the formulation can be found in Appendix B. This yields the **equation of motion for one beam element based on Hermite interpolation**

$$M_k \ddot{x}_k + \omega G_k \dot{x}_k + K_k x_k = 0, \tag{4.7}$$

where $x_k = c^k \psi$. Since this is the equation for beam element k only, the element matrices M_k, G_k and K_k as well as the vector x_k are written with a subscript k.

Inclusion of rigid disks

Our model can be extended by rigid disks which are often part of rotating bodies (e.g. blades). In our finite element formulation these disks are attached to certain nodes. The corresponding matrices are derived by considering the kinetic energy of the disk which is given by

$$T_d = \frac{1}{2} m_d (\dot{u}^2 + \dot{v}^2) + \frac{1}{2} I_d (\dot{\phi}_x^2 + \dot{\phi}_y^2) + \frac{1}{2} I_p (\omega^2 + \omega(\dot{\phi}_x \phi_y - \phi_x \dot{\phi}_y)).$$

The only difference to the previous case is that we have the mass m_d of the rigid disks and the moments of inertia I_d and I_p instead of the corresponding terms per unit length and an integral over the length of the beam element. The displacements u, v, ϕ_x and ϕ_y are taken in the node to which the rigid disk is attached and are collected in the vector $x_d = (u, v, \phi_x, \phi_y)^T$. The values for m_d, I_d and I_p are in our case given by the engineer. As in Chapter 2 the technique of Lagrange equations is used to obtain the equations

$$m_d \ddot{u} + I_d \ddot{\phi}_x + \omega I_p \dot{\phi}_y = 0$$

and

$$m_d \ddot{v} + I_d \ddot{\phi}_y - \omega I_p \dot{\phi}_x = 0.$$

This is in matrix notation

$$M_d \ddot{x}_d + G_d \dot{x}_d = 0,$$

where M_d and G_d denote the mass and gyroscopic matrices of the rigid disk and are given by

$$M_d = \begin{pmatrix} m_d & 0 & 0 & 0 \\ 0 & m_d & 0 & 0 \\ 0 & 0 & I_d & 0 \\ 0 & 0 & 0 & I_d \end{pmatrix} \quad \text{and} \quad G_d = \omega \begin{pmatrix} 0 & 0 & 0 & 0 \\ 0 & 0 & 0 & 0 \\ 0 & 0 & 0 & I_p \\ 0 & 0 & -I_p & 0 \end{pmatrix}.$$

Assembly of matrices

After having determined all beam element and rigid disk matrices they have to be assembled to form the system matrices. This means we first have to write our 8×8-beam element matrices in an appropriate way into our $4n \times 4n$-matrix with n being the number of nodes in the beam model. This can be done via suitable $8 \times 4n$-matrices A_k given by

$$A_k = \begin{pmatrix} 0 & \cdots & 0 & 1 & 0 & \cdots & 0 & 0 & \cdots & 0 \\ 0 & \cdots & 0 & 0 & 1 & \cdots & 0 & 0 & \cdots & 0 \\ \vdots & & & & & \ddots & & & & \vdots \\ 0 & \cdots & 0 & 0 & 0 & \cdots & 1 & 0 & \cdots & 0 \end{pmatrix},$$

where the block of the 8×8 identity matrix starts in column $4(k-1)+1$ and which relates the element displacement vector x_k to the displacement vector x of the whole system by

$$x_k = A_k x.$$

The vector x of the whole system contains x_k at positions $(4(k-1)+l)_{l=1,\ldots,8}$. For the large system it is also written as

$$x = c \cdot \psi,$$

where $c = (u_1, v_1, \phi_{x1}, \phi_{y1}, \ldots, u_n, v_n, \phi_{xn}, \phi_{yn}) \in \mathbb{R}^{4n}$.

Assembling all beam elements the expressions for the mass, gyroscopic and stiffness matrices for the whole system are determined by

$$M = \sum_{k=1}^{n-1} (A_k)^T M_k A_k,$$

$$G = \sum_{k=1}^{n-1} (A_k)^T G_k A_k,$$

$$K = \sum_{k=1}^{n-1} (A_k)^T K_k A_k.$$

The rigid disk matrices M_d and G_d are assembled as follows.
Each 4×4-matrix is added blockwise into M and G respectively at positions $(4(a_d - 1) + i, 4(a_d - 1) + j)_{i,j=1,\ldots,4}$, where a_d is the number of the node to which the rigid disk is attached. To keep the notation simple, the structural matrices after the inclusion of the rigid disk part are still denoted by M, G and K.

We now obtain the **equation of motion for the complete system**

$$M\ddot{x} + \omega G\dot{x} + Kx = 0. \tag{4.8}$$

Finally, we can formulate the approximation space V_2^h on the whole interval I in our case. It consists of differentiable functions, which are piecewise cubic polynomials, i.e.

$$V_2^h = \{u \in C^1(I) |\, u|_{[a_k, a_{k+1}]} \in P_3([a_k, a_{k+1}])\}.$$

Remark. The space $\cup_{h \to 0} V_2^h$ is dense in V_2 and the convergence theorems of Sections 4.1 and 4.2 can be applied to this case.

Equation of motion with bearing and unbalance forces

For simplicity of the treatment the equation of motion was formulated without any forces so far. But of course, unbalance forces F_{unb} as well as forces F_b due to bearing support have to be included for the analysis of the vibrations

$$F = F_b + F_{\text{unb}}.$$

Here, F is a vector of length $4n$. In the case of the discretized model no distributed forces are considered but discrete (point) forces instead. Similar to the concept for the rigid disks the forces are assumed to act on certain nodes of the rotor and the force vectors have only entries at these nodes.

Concerning the bearings we initially limit our studies to orthotropic bearings such that the bearing forces obey the governing equations of the form (see e.g. [44])

$$F_b = -C\dot{x} - K_b x.$$

The damping and stiffness matrices C and K_b are $4n \times 4n$-matrices having only entries on the main diagonal at the positions corresponding to the lateral deflections

at the bearing nodes,

$$C = \begin{pmatrix} \ddots & & & & & \\ & c_u & & & & \\ & & c_v & & & \\ & & & \ddots & & \\ & & & & \ddots & \end{pmatrix} \quad \text{and} \quad K_b = \begin{pmatrix} \ddots & & & & & \\ & k_u & & & & \\ & & k_v & & & \\ & & & \ddots & & \\ & & & & \ddots & \end{pmatrix}.$$

The matrix elements c_u, c_v, k_u, k_v are called damping and stiffness coefficients. Multiplication of the matrices with x and $\dot{x}$ respectively gives a force vector having only entries at the relevant positions.

Later the influence of the oil film forces caused by fluid film journal bearings is integrated into the model. The entries of the damping and stiffness matrices are then 2×2-blocks at the positions corresponding to the lateral deflections since now a coupling occurs. This case is shown in detail in Section 4.5.

The unbalance forces F_{unb} are assumed to act on certain nodes k. Strictly, the unbalances of all nodes should be considered in the rotor finite element model since the unbalance is distributed in the direction of the rotor axis due to production error. However, the unbalance of rigid disks is much larger than that in the other part of the rotor. Therefore, only unbalances of the rigid disks are considered in this case and are concentrated on the nodes next to the rigid disk. The unbalance force is assumed to be excited harmonically such that in each node they are given by

$$F_{\text{unb},k} = \begin{pmatrix} F_{k,X} \\ F_{k,Y} \end{pmatrix} = \begin{pmatrix} \tilde{u}_k \omega^2 e^{i(\omega t + \Theta_k)} \\ \tilde{u}_k \omega^2 e^{i(\omega t + \Theta_k - \frac{\pi}{2})} \end{pmatrix} = \begin{pmatrix} f_{k,X} \\ f_{k,Y} \end{pmatrix} e^{i\omega t}.$$

The forces $f_{k,x}$ and $f_{k,y}$ in X- and Y-direction are

$$f_{k,x} = \omega^2 \tilde{u}_k e^{i\Theta_k}, \quad f_{k,y} = \omega^2 \tilde{u}_k e^{i(\Theta_k - \frac{\pi}{2})}.$$

The product of mass and eccentricity is denoted by $\tilde{u}$, the rotational speed again by ω and Θ is the angle between the X-axis and the direction of eccentricity and is called phase (see Figure 4.2). The eccentricity of the rigid disks can not be measured directly. In the real manufacturing process, the product of mass and eccentricity is measured by a balancing machine. Therefore, in our case values for $\tilde{u}_k$ and Θ_k are given by the engineer. The values for $f_{k,x}$ and $f_{k,y}$ are written into a vector $f \in \mathbb{C}^{4n}$, which then has exactly $2 \cdot n_f$ nonzero elements, where n_f is the number of discrete force components.

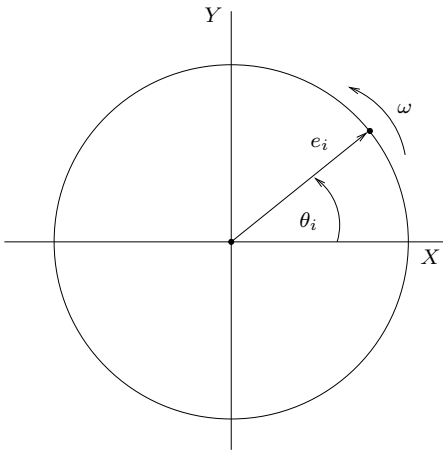

Figure 4.2. Unbalance of node i with eccentricity e_i and phase Θ_i.

The **equation of the system including bearing and unbalance forces** is then given by

$$M\ddot{x} + (\omega G + C)\dot{x} + (K + K_b)x = F_{\text{unb}}. \tag{4.9}$$

4.4 Numerical solution of equation of motion

The equation of motion is solved to obtain eigenvalues and eigenvectors which are the basis for our further calculations. All steps shown for the continuous model in Chapter 3 can be done in the same way for the discretized model. In this section we want to give the corresponding matrix formulations since these are used in the numerical part following in the next chapters.

Let us first study the equation of motion for free vibrations (4.8), i.e. $F_{\text{unb}} = 0$ and without any bearing forces. Then we again set $\psi(t) = e^{\lambda t}$ to obtain natural frequencies and eigenmodes of our system. The result is either a quadratic eigenvalue problem

$$\lambda^2 Mc + \lambda\omega Gc + Kc = 0$$

with $c \in \mathbb{C}^{N/2}$ or the generalized eigenvalue problem

$$\lambda A\phi = B\phi,$$

with $\phi \in \mathbb{C}^N$ which is obtained by a transformation of the equation of motion into a first-order system

$$\lambda \underbrace{\begin{pmatrix} M & 0 \\ 0 & M \end{pmatrix}}_{=A} \begin{pmatrix} \ddot{x} \\ \dot{x} \end{pmatrix} = \underbrace{\begin{pmatrix} -\omega G & -K \\ M & 0 \end{pmatrix}}_{=B} \begin{pmatrix} \dot{x} \\ x \end{pmatrix}$$

and setting

$$\phi = \begin{pmatrix} \lambda c \\ c \end{pmatrix}.$$

As above we have $x(t) = c\psi(t)$. Solving this eigenvalue problem, the natural frequencies λ and the eigenmodes ϕ are obtained.

The problem for one specific mode is then written as

$$(B - \lambda_i A)\phi_i = 0, \quad i = 1, \ldots, N,$$

with $N = 2 \cdot 4 \cdot n$ being the number of modes in the reduced system, where n is the number of nodes in the beam model.

Since the system is non-symmetric we have to calculate the left eigenvectors ξ_i separately by

$$\xi_i^T (B - \lambda_i A) = 0. \tag{4.10}$$

Normalization of eigenvectors

For the subsequent analysis a normalization of the eigenvectors is necessary. This is in particular relevant for the sensitivity analysis in Chapter 5. Two different normalizations are considered.

- In normalization (1) we want the eigenvectors to be normalized with respect to A, i.e.
$$\xi_j^T A \phi_i = \delta_{i,j}, \quad i, j = 1, \ldots, N. \tag{4.11}$$
- Normalization (2) sets one component equal to one
$$\tilde{\phi}_i = \frac{1}{\phi_i^{(l)}} \phi_i \quad \rightarrow \quad \tilde{\phi}_i^{(l)} = 1. \tag{4.12}$$
This can for example be the largest component of the absolute value, i.e. we choose l by setting
$$|\phi_i^{(l)}| = \max_k |\phi_i^{(k)}|.$$

Normalization (1) is sufficient when calculating the derivatives of the natural frequencies. For the unbalance oscillation, however, we need to determine the derivative of the eigenvectors. In this case we additionally need a normalization which renders the eigenvectors unique. This can be achieved by normalization (2).

Critical speed

The critical speeds are determined analytically by the equation of motion for free vibrations. In this case a damped system is studied. Setting $x = c\psi = ce^{i\lambda t}$ gives

$$-\lambda^2 Mc + (\omega G + C)i\lambda c + (K + K_b)c = 0.$$

and equating $\lambda = \omega$ yields

$$-\omega^2(M + iG)c + \omega iCc + (K + K_b)c = 0. \tag{4.13}$$

Solving this system gives us all critical speeds ω_j. Then the equation of motion with unbalance forces (4.9) is regarded for one certain critical speed.

Solution of inhomogeneous equation of motion

We proceed in the same way as in Chapter 3. The inhomogeneous equation of motion is solved by determining a fundamental system of the homogeneous equation and a particular solution of the inhomogeneous one. Then an appropriate expression for the unbalance response can be defined. The solutions of the homogeneous system are only used for the determination of the particular solution but can be neglected later since they vanish with increasing time (see [23]).

Firstly, we transform the second-order equation of motion (4.9) into a first-order-system,

$$\underbrace{\begin{pmatrix} M & 0 \\ 0 & M \end{pmatrix}}_{=A} \dot{y} = \underbrace{\begin{pmatrix} -(\omega G + C) & -(K + K_b) \\ M & 0 \end{pmatrix}}_{=B} y + \underbrace{\begin{pmatrix} \tilde{f} \\ 0 \end{pmatrix}}_{=\hat{f}} e^{i\omega t}, \tag{4.14}$$

where

$$y = \begin{pmatrix} \dot{x} \\ x \end{pmatrix}$$

and the expression of the unbalance forces $F_{\text{unb}} = \tilde{f}e^{i\omega t}$ was used. Then (4.14) reads as

$$A\dot{y} = By + \hat{f}e^{i\omega t}. \tag{4.15}$$

We first solve the homogeneous system

$$A\dot{y} = By.$$

With $y = \phi e^{\lambda t}$ we obtain the eigenvalue problem

$$\lambda A\phi = B\phi,$$

giving us the natural frequencies λ and eigenmodes ϕ for the system with given critical speed.

The particular solution is determined by a representation as linear combination of eigenvectors and we set $y = \Phi z$ in (4.15). Now Φ denotes the matrix with all eigenvectors ϕ. For the time dependent component z we set

$$z = \tilde{z}e^{i\omega t}$$

with a vector $\tilde{z} \in \mathbb{C}^N$. We obtain

$$A\Phi\dot{z} = B\Phi z + \hat{f}e^{i\omega t},$$

and

$$i\omega A\Phi\tilde{z} = B\Phi\tilde{z} + \hat{f},$$

respectively. The standard technique of multiplying the equation from the left with the left eigenvector matrix Ξ^T and using normalization (1) yields

$$i\omega \underbrace{\Xi^T A\Phi}_{=I}\tilde{z} = \underbrace{\Xi^T B\Phi}_{=\Lambda}\tilde{z} + \Xi^T\hat{f},$$

where I is the $N \times N$-identity matrix and Λ the $N \times N$- diagonal matrix containing the natural frequencies λ. We can solve

$$\tilde{z} = (i\omega I - \Lambda)^{-1}\Xi^T\hat{f}.$$

The solution of the inhomogenuous equation of motion is then

$$y = \Phi\tilde{z}e^{i\omega t} = \Phi(i\omega I - \Lambda)^{-1}\Xi^T\hat{f}e^{i\omega t}.$$

As in Chapter 3 the part y_s only depending on the space variable is relevant for the determination of the unbalance response,

$$y_s = \Phi\tilde{z} = \Phi(i\omega I - \Lambda)^{-1}\Xi^T\hat{f} = \sum_{j=1}^{n_f}\sum_{l=1}^{N}\frac{\xi_{\nu_j,l}\hat{f}_{\nu_j}}{i\omega - \lambda_l}\phi_l,$$

where n_f is the number of force components and N the number of modes. The lower part of this vector is identical to the previously introduced vector c, i.e. $c = (y_{N/2+1}, \ldots, y_N)$. For one certain component k the expression is

$$c_k = \sum_{j=1}^{n_f}\sum_{l=1}^{N}\frac{\xi_{\nu_j,l}\phi_{k,l}\hat{f}_{\nu_j}}{i\omega - \lambda_l}, \quad k = 1, \ldots, N/2$$

where ν_j are the indices of the nonzero components of $\hat{f}$. Usually, it is not necessary to consider all N modes. Indeed, we show later that it is sufficient just to consider one mode which saves a lot of computation time.

Within the vector c the components representing the lateral displacements are of special interest. The displacements in X- and Y-direction are coupled so it is sufficient to consider e.g. the lateral displacement in X-direction. These entries are collected in a new vector $\tilde{c}$.

As unbalance response target a we now have several options. The following objectives are most common.

- In some cases it makes sense to consider the displacements at a certain node k, e.g. to bound them to avoid contact with the casing. Then we want to control

$$a = |\tilde{c}_k|. \tag{4.16}$$

- More often a norm of the vector $\tilde{c}$ is considered. Then the objective value is

$$a = \left(\sum_i |\tilde{c}_i|^p \right)^{1/p} \tag{4.17}$$

  for a suitable p. Usually, one uses $p = 1$ or $p = 2$, in some cases also $p = \infty$, i.e. $a = \max_i |\tilde{c}_i|$.

4.5 Inclusion of nonlinear bearing forces

Often rotors, and in particular the turbochargers we look at, are supported by oil in fluid-film bearings. The lubricant film in the bearings generates forces that strongly influence the behaviour of the rotor. Therefore we want to extend our calculations on a model where the linear spring support is replaced by oil film bearings. If the forces are only in radial direction we speak of a journal bearing and this is our reference case. For our numerical studies the generated forces which act on the rotor have to be determined. The oil film forces are obtained by integration of the pressure field which is governed by Reynolds' equation. They are nonlinear functions of position and velocity of the journal center. The derivation is done under the assumption of an incompressible Newtonian fluid and a thickness of the oil film which is thin compared to the rotor diameter. If we additionally assume small displacements an approximation of the forces can be obtained by a linearization about their static equilibrium value. Then stiffness and damping matrices are obtained which are included into our equation of motion. More details about the background of fluid film lubrication can be found in Childs [11], Szeri [57] and Vance [59]. A detailed

study of a turbocharger with fluid-film bearings including a complex description of the occurring oil film forces is done in [51]. The latter work focuses in particular on self-excited vibrations of the rotor inherent to fluid-film bearings but which are not considered here.

A sketch of a cylindrical journal bearing is shown in Figure 4.3. The part of the rotor in the bearing is called journal and the cylinder supporting it is called bearing.

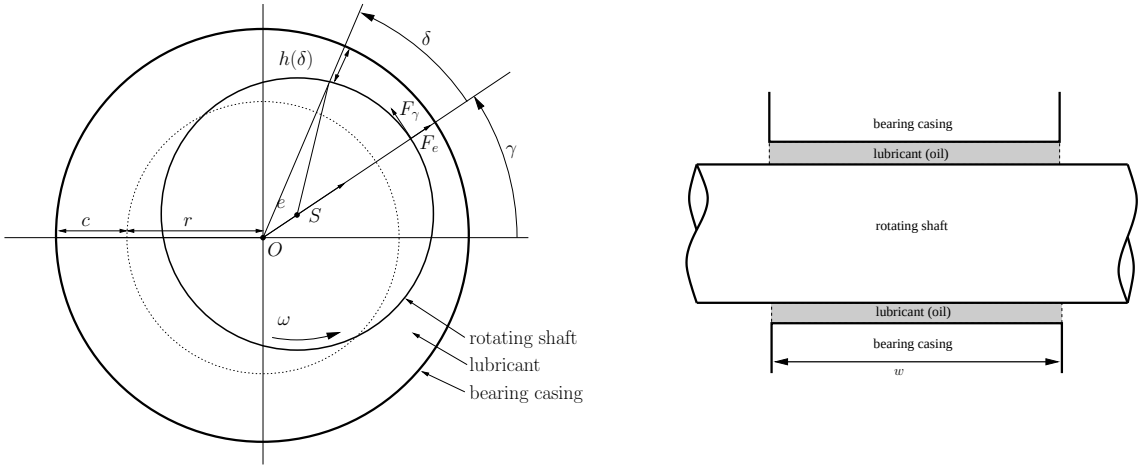

Figure 4.3. Sketch of journal bearing, cross-sectional (left) and lateral (right) view.

The rotor is whirling in the fluid with angular velocity ω. The journal center is displaced from the center of the bearing by the eccentricity e. The clearance c is the difference between bearing radius and journal radius r. The oil film generates the forces F_e and F_γ in the direction of the journal eccentricity and its normal direction, respectively, where γ is the azimuthal angle of the journal center with the X-axis.

Determination of oil film forces

To determine the forces the pressure distribution in the oil film has to be known. It is governed by Reynolds' equation [11]

$$\partial_\delta \left(\frac{h^3}{\eta} \partial_\delta p \right) + r^2 \partial_z \left(\frac{h^3}{\eta} \partial_z p \right) = \frac{6r^2}{c^2} ((\omega - 2\dot{\gamma})\varepsilon \sin\delta - 2\dot{\varepsilon}\cos\delta), \tag{4.18}$$

where $h = 1 - \varepsilon\cos\delta$ is the relative oil-film thickness, $\varepsilon = e/c$ is the eccentricity ratio, r the shaft radius and η the viscosity of the oil. Then F_e and F_γ are obtained by integrating the pressure field

$$F_e = -r \int_0^w \int_{p>0} p \cos\delta \, d\delta \, d\zeta \tag{4.19}$$

and

$$F_\gamma = -r \int_0^w \int_{p>0} p \sin\delta \, d\delta \, d\zeta, \tag{4.20}$$

where w is the bearing width. In our case we use Gümbel's boundary condition, implying that the pressure is set to zero where it is negative, to model cavitation and the inability of fluids to transmit drag forces (see [38]).

Since it is generally impossible to solve the Reynolds' equation (4.18) analytically, simplifications of the equation are necessary. One possibility is the short bearing approximation. In very short bearings the pressure variation in axial direction is larger than the circumferential pressure variation such that the first term on the left-hand side of equation (4.18) can be neglected. Using this short bearing assumption, it can be shown (see e.g. [51]) that the forces F_e and F_γ are as follows,

$$F_e = -\frac{\eta\omega r w^3}{2c^2}(GA_1 - EA_2)$$

and

$$F_\gamma = -\frac{\eta\omega r w^3}{2c^2}(GA_3 - EA_1).$$

The terms E and G are given by

$$E = \frac{2}{\omega}\dot{\varepsilon}, \quad \text{and} \quad G = \left(1 - \frac{2}{\omega}\dot{\gamma}\right)\varepsilon$$

and are introduced to obtain a non-dimensionalization of the whole approach.
The expressions A_1, A_2 and A_3 are depending on ε and on the time derivatives $\dot{\varepsilon}$ and $\dot{\gamma}$, but not on ω,

$$A_1 = A_1(\varepsilon, \dot{\varepsilon}, \dot{\gamma}), \quad A_2 = A_2(\varepsilon, \dot{\varepsilon}, \dot{\gamma}), \quad A_3 = A_3(\varepsilon, \dot{\varepsilon}, \dot{\gamma}).$$

To be able to include the oil film forces into the framework of the previously developed equation of motion (4.8) an expression depending directly on the displacement vector x is desired. Therefore we determine forces F_X and F_Y in X and Y-direction. This is done by a rotation about the azimuthal angle γ,

$$\begin{pmatrix} F_X \\ F_Y \end{pmatrix} = \begin{pmatrix} \cos\gamma & -\sin\gamma \\ \sin\gamma & \cos\gamma \end{pmatrix} \begin{pmatrix} F_e \\ F_\gamma \end{pmatrix}.$$

The forces depend on position and velocity of the journal center x, which are implicitly given via A_1, A_2, A_3, and we write

$$F_{\text{oil}}(x, \dot{x}) = (F_X, F_Y)^T.$$

The **equation of motion with unbalance and oil film forces** is then written as

$$M\ddot{x} + \omega G\dot{x} + Kx = F_{\text{unb}} + F_{\text{oil}}(x, \dot{x}),$$

where the previous damping and stiffness matrices of the spring and damper support are replaced by F_{oil}.

Linearization of oil film forces

A linearization of the displacements (u, v) and velocities $(\dot{u}, \dot{v})$ about their static equilibrium value $(u_0, v_0, \dot{u}_0, \dot{v}_0)$ in the bearing nodes gives the new damping and stiffness matrices C_{oil} and K_{oil} for one bearing node,

$$\begin{aligned} F_{\text{oil}}(u, v, \dot{u}, \dot{v}) = (F_X, F_Y)^T = \\ F_{\text{oil}}(u_0, v_0, \dot{u}_0, \dot{v}_0) + \underbrace{\begin{pmatrix} \frac{\partial F_X}{\partial u} & \frac{\partial F_X}{\partial v} \\ \frac{\partial F_Y}{\partial u} & \frac{\partial F_Y}{\partial v} \end{pmatrix}}_{=K_{\text{oil}}} \begin{pmatrix} u - u_0 \\ v - v_0 \end{pmatrix} + \underbrace{\begin{pmatrix} \frac{\partial F_X}{\partial \dot{u}} & \frac{\partial F_X}{\partial \dot{v}} \\ \frac{\partial F_Y}{\partial \dot{u}} & \frac{\partial F_Y}{\partial \dot{v}} \end{pmatrix}}_{=C_{\text{oil}}} \begin{pmatrix} \dot{u} - \dot{u}_0 \\ \dot{v} - \dot{v}_0 \end{pmatrix}. \end{aligned} \tag{4.21}$$

At first the static equilibrium value has to be calculated (see also [51]). Therefore we look at a rotor-bearing-system without unbalance forces, which is

$$M\ddot{x} + \omega G\dot{x} + Kx = F_{\text{oil}}(x, \dot{x}). \tag{4.22}$$

Moreover, gravity forces are neglected which simplifies the subsequent development. As before the system is transformed into a first-order system and we obtain

$$\begin{pmatrix} M & 0 \\ 0 & M \end{pmatrix} \begin{pmatrix} \ddot{x} \\ \dot{x} \end{pmatrix} = \begin{pmatrix} -\omega G & -K \\ M & 0 \end{pmatrix} \begin{pmatrix} \dot{x} \\ x \end{pmatrix} + \begin{pmatrix} F_{\text{oil}}(x, \dot{x}) \\ 0 \end{pmatrix}.$$

The static equilibrium value is characterized by $(\ddot{x}, \dot{x})^T = 0$ which results in

$$0 = -Kx + F_{\text{oil}}(x, \dot{x}).$$

The vector x can be decomposed in a part belonging to the rigid translation x_r and one belonging to the bending deflection x_b, i.e. $x = x_r + x_b$. The equation $Kx_r = 0$ holds for a rigid body motion since the second derivative of the mode shape function vanishes in this case and hence there is no contribution to the stiffness matrix defined by (4.4). Therefore, we obtain

$$F_{\text{oil}}(x, \dot{x}) = Kx_b.$$

For the bending deflection vector x_b we have zero deflection at the nodes of the bearings. The matrices and vectors are then rearranged so that we have the zero components of x_b in the first components [41],

$$\begin{pmatrix} F_{\text{oil}}(x,\dot{x}) \\ 0 \end{pmatrix} = \begin{pmatrix} K_1 & K_2 \\ K_3 & K_4 \end{pmatrix} \begin{pmatrix} 0 \\ \tilde{x}_b \end{pmatrix}.$$

Due to the second line, $\tilde{x}_b = 0$, since K_4 has full rank. Then we have $F_{\text{oil}}(x_0, \dot{x_0}) = 0$ which implies that $x_0 = 0$ since the pressure is nowhere positive and hence the integrals (4.19) and (4.20) vanish.

Knowing that the static equilibrium value $(u_0, v_0, \dot{u}_0, \dot{v}_0) = 0$ the oil film forces in equation (4.21) for one bearing node simplify to

$$\begin{aligned} F_{\text{oil}}(u,v,\dot{u},\dot{v}) = \begin{pmatrix} F_X \\ F_Y \end{pmatrix} &= \begin{pmatrix} \frac{\partial F_X}{\partial u} & \frac{\partial F_X}{\partial v} \\ \frac{\partial F_Y}{\partial u} & \frac{\partial F_Y}{\partial v} \end{pmatrix} \begin{pmatrix} u \\ v \end{pmatrix} + \begin{pmatrix} \frac{\partial F_X}{\partial \dot{u}} & \frac{\partial F_X}{\partial \dot{v}} \\ \frac{\partial F_Y}{\partial \dot{u}} & \frac{\partial F_Y}{\partial \dot{v}} \end{pmatrix} \begin{pmatrix} \dot{u} \\ \dot{v} \end{pmatrix} \\ &= \begin{pmatrix} k_{XX} & k_{XY} \\ k_{YX} & k_{YY} \end{pmatrix} \begin{pmatrix} u \\ v \end{pmatrix} + \begin{pmatrix} c_{XX} & c_{XY} \\ c_{YX} & c_{YY} \end{pmatrix} \begin{pmatrix} \dot{u} \\ \dot{v} \end{pmatrix}. \end{aligned}$$

Having now determined all terms needed for the calculation of the oil film forces F_X and F_Y we can calculate the damping and stiffness matrices C_{oil} and K_{oil} by the method of finite differences.

The **equation of motion for the system including linearized oil film forces** is given by

$$M\ddot{x} + (\omega G - C_{\text{oil}})\dot{x} + (K - K_{\text{oil}})x = F_{\text{unb}}. \tag{4.23}$$

In the case that the static equilibrium value is at $x_0 = 0$ we can make an important statement which leads to a simplification of the forthcoming analysis.

Proposition 4.1. *If the static equilibrium value is at $x_0 = 0$ we obtain in a neighborhood of the equilibrium for the linearized damping and stiffness matrices*

$$F_{\text{oil}}(x,\dot{x}) = C_{\text{oil}}\dot{x} + \omega K_{\text{oil}}x,$$

where the damping matrix C_{oil} and the stiffness matrix K_{oil} are independent of the rotational speed ω.

Proof. The stiffness coefficients are determined by a spatial perturbation of $x = 0$. Hence $x \neq 0$ and $\dot{x} = 0$. This implies $\varepsilon = \varepsilon(x) \neq 0$ and $\dot{\varepsilon}(x) = 0 = \dot{\gamma}(x)$. Then $E = 2\dot{\varepsilon}/\omega = 0$ and $G = (1 - 2\dot{\gamma}/\varepsilon)\varepsilon = \varepsilon \neq 0$. We obtain

$$F_e = \omega \cdot \frac{\eta r w^3}{2c^2}\varepsilon A_1 \quad \text{and} \quad F_\gamma = \omega \cdot \frac{\eta r w^3}{2c^2}\varepsilon A_3.$$

Since r, c, w, A_1, A_2 and A_3 are independent of ω the linear dependence of K_{oil} on ω is shown.

Similarly, the damping coefficients are obtained by a perturbation of $\dot{x} = 0$. This means $\dot{x} \neq 0$ and $x = 0$ implying $\dot{\varepsilon}(x) \neq 0$ and $\varepsilon(x) = 0$. This gives $E = 2\dot{\varepsilon}/\omega \neq 0$ and $G = 0$. We have

$$F_e = -\frac{\eta r w^3}{c^2}\dot{\varepsilon}A_2 \quad \text{and} \quad F_\gamma = -\frac{\eta r w^3}{c^2}\dot{\varepsilon}A_1$$

resulting in a constant damping matrix C_{oil}, independent of ω. □

The **equation of motion for the model with oil film forces** now looks as follows

$$M\ddot{x} + (\omega G - C_{\text{oil}})\dot{x} + (K - \omega K_{\text{oil}})x = F_{\text{unb}}. \tag{4.24}$$

The optimization problem with vibration level constraints is now solved based on this new equation of motion. The first step is again the calculation of the critical speeds which is done by setting $x = de^{i\omega t}$ with $d \in \mathbb{C}^{N/2}$ and solving the equation

$$\omega^2(-M + iG)d + \omega(-iC_{\text{oil}} - K_{\text{oil}})d + Kd = 0.$$

The unbalance response is obtained via equation

$$\begin{pmatrix} M & 0 \\ 0 & M \end{pmatrix}\dot{y} = \begin{pmatrix} -(\omega G - C_{\text{oil}}) & -(K - K_{\text{oil}}) \\ M & 0 \end{pmatrix} y,$$

where $y = (\dot{x}, x)^T$. Then the critical modes can be determined which are target of our optimization.

Remark. It has to be mentioned that in the case of nonlinear fluid-film bearings instability can occur. Then the solution of the homogenous system does not tend to 0 any longer [11]. This effect is not considered here.

We have now introduced a finite element model which serves as basis for our numerical calculations. Different support conditions such as linear spring and damper support as well as nonlinear fluid-film bearings can be included. A discretized equation of motion was presented as well as a numerical solution of it. This yields natural frequencies, critical speeds and the unbalance response which are our optimization objectives. We can now proceed with the development of a solution concept for our design optimization process. This is done in Chapter 5.

Chapter 5

Optimization of gyroscopic systems

In this chapter we present a concept to solve certain design optimization problems based on the described physical model and finite element discretization. This work extends research found in the literature, where mainly only non-rotating problems are treated [27] and if rotating bodies are considered, gyroscopic effects are neglected [6]. The aim of our research is to shift critical speeds of certain modes to avoid their excitation in the operating speed range and to decrease the unbalance response at certain critical speeds. We want to stress that frequencies and unbalance responses belonging to specific modes are studied. This is different to the consideration of the smallest natural frequency independent of the corresponding mode (see e.g. [47] or [35]).

Engineering design optimization problems are distinguished between size, shape and topology optimization problems depending on the geometrical design variables that are taken. An additional classification can be made between single and multiobjective optimization problems. Details on these topics are mentioned in Section 5.1. Due to the nonlinearity of the design optimization problem a direct solution is in general not possible. An iterative process is required to yield an approximating solution. A corresponding computational procedure is shown in Section 5.2. Since gradient-based algorithms are used to determine the approximating solution, sensitivities of the relevant expressions are needed. They are formulated in Section 5.3. When optimizing eigenvalues, multiple eigenvalues might occur and the derivatives can no longer be calculated as before. Techniques how to proceed in this case are shown in Section 5.4. The above mentioned focus on one certain mode requires mode tracking in every step of the optimization process. Possible methods to do this are demonstrated in Section 5.5. The inclusion of nonlinear bearing forces leads to modifications in the sensitivity analysis and a consideration of additional design

variables. The corresponding theory is presented in Section 5.6. Finally, in Section 5.7 the single objective optimization problem is reformulated into a multiobjective optimization problem. This is used to guarantee a non-empty feasible domain by determining suitable target values for the constraint functions since these are often set heuristically according to engineering demands.

5.1 Classification of optimization problems

As already mentioned in the introduction the design optimization of gyroscopic systems includes various targets such as maximizing natural frequencies or critical speeds, minimizing unbalance responses and all of this in combination with a reduction of mass. This can be formulated within a multiobjective optimization problem or as a single objective optimization problem taking one target as objective function and the others as constraints using suitable bounds for them. We opt for this latter approach and the objective function is usually the total mass of the rotor. Other functions are also possible such as e.g. the inertia of the rotor. This choice of objective function implies that requirements on frequencies and unbalance responses are regarded as constraints. Later, multiobjective approaches are used to determine suitable bounds for the constraint functions. This is explained in detail in Section 5.7.

Design optimization problems can be classified according to the geometric design variables which are chosen. The standard classification differentiates between size, shape and topology design variables (see e.g. [49]). Size design variables describe cross-sectional properties of structural components, like diameters, cross-sectional areas or moments of inertia. Shape design variables govern the shape of external boundaries and surfaces. Topology design variables describe the type of the structure such as the number of interior holes. Considering our finite element beam model as introduced in Chapter 4 our problem can be classified as a sizing optimization problem with the diameters or lengths of the beam elements taken as design variables. However, the difference to shape optimization problems is blurred since by optimizing the diameter we also modify the shape of the rotor. This holds in particular for a fine discretization. In addition to the size design variables, material and support design variables are considered, depending on the concrete problem.

The optimization problems introduced in Chapter 1 can then be written in dependence of a design variable vector $q = (q_1, \ldots, q_{n_{dv}})$, which can include diameters and lengths of certain design variables as well as certain material and bearing properties. The number of design variables is denoted by n_{dv}. We obtain the following *natural*

frequency optimization problem,

$$\begin{aligned} &\min_q \operatorname{mass}(q) \\ &\text{subject to} \\ &\lambda_{\mathrm{m1}}(q) \geq \lambda^*_{\mathrm{m1}}, \\ &\lambda_{\mathrm{m2}}(q) \geq \lambda^*_{\mathrm{m2}}, \\ &\underline{q} \leq q \leq \bar{q}. \end{aligned} \tag{5.1}$$

The total mass of the rotor is minimized subject to constraints on the natural frequency λ_{m1} and λ_{m2} of certain modes m1 and m2. The natural frequencies should be increased above given target values λ^*_{m1} and λ^*_{m2}. The lower and upper bounds $\underline{q}$ and $\bar{q}$ are set due to manufacturing constraints and to prevent critical stress.

The *vibration level optimization problem* is given by

$$\begin{aligned} &\min_q \operatorname{mass}(q) \\ &\text{subject to} \\ &\omega_{\mathrm{m1}}(q) \geq \omega^*_{\mathrm{m1}}, \\ &a(\omega_{\mathrm{m2}}(q)) \leq a^*_{\mathrm{m2}}, \\ &\underline{q} \leq q \leq \bar{q}. \end{aligned} \tag{5.2}$$

Here, constraints are set to increase the critical speed ω_{m1} above a target value ω_{m1} and to decrease the unbalance response $a(\omega_{\mathrm{m2}})$ below the target values a^*_{m2}.

Since our gyroscopic system is non-symmetric, in practical calculations care has to be taken because complex eigenvalues and eigenvectors appear. As mentioned in Chapter 3 it depends on the approach chosen for the time dependence, in our case $\psi(t) = e^{\lambda t}$ or $\psi(t) = e^{i\lambda t}$, whether the frequency appears in the real or in the imaginary part of the complex eigenvalue. If only free vibrations are considered the imaginary part of the eigenvalues represents the natural frequency. The natural frequency optimization problem (5.1) which is actually computed looks like,

$$\begin{aligned} &\min_q \operatorname{mass}(q) \\ &\text{subject to} \\ &\operatorname{Im}(\lambda_{\mathrm{m1}}(q)) \geq \operatorname{Im}(\lambda^*_{\mathrm{m1}}), \\ &\operatorname{Im}(\lambda_{\mathrm{m2}}(q)) \geq \operatorname{Im}(\lambda^*_{\mathrm{m2}}), \\ &\underline{q} \leq q \leq \bar{q}. \end{aligned}$$

For the sake of simplicity, however, we want to turn back to the previous notation, writing simply λ and meaning either real or imaginary part.

5.2 Solution strategy

The concept of our solution process is based on the procedure applied to general design optimization problems which can be found e.g. in [25] or [7]. We formulate it with focus on our optimization problem for gyroscopic systems.

To solve the nonlinear progamming problem, a sequence of subproblems is constructed which are solved successively. This is done as follows.

We start with a given initial design. This can be an existing prototype which should be optimized or a guess of a good model due to the intuition of the engineer. This might help preventing a mathematical programming algorithm to end up in a bad local optimum which may exist due to the nonlinearities of the functions. Then the desired finite element model is set up and the stiffness, gyroscopic and mass matrices describing the equation of motion are determined as presented in Chapter 4. The critical speed and unbalance response analysis is performed as in Section 4.4. This includes the determination of the critical modes for which the unbalance response is too high. These modes are chosen as target of our optimization. To be able to apply a gradient-based optimization algorithm the derivatives of objective and constraint functions are calculated. Then the approximation scheme of the original problem can be constructed and is solved numerically. We use certain convex approximating functions which are presented in detail in Chapter 6. At this stage a mode tracking procedure is needed to follow the critical mode. For the obtained new design a termination criterion is checked. If it is fulfilled the algorithm stops and yields the final design. If not, a finite element model for the new design with new mass, gyroscopic and stiffness matrices is calculated and a new iteration starts for the updated model. The flowchart in Figure 5.1 summarizes this procedure.

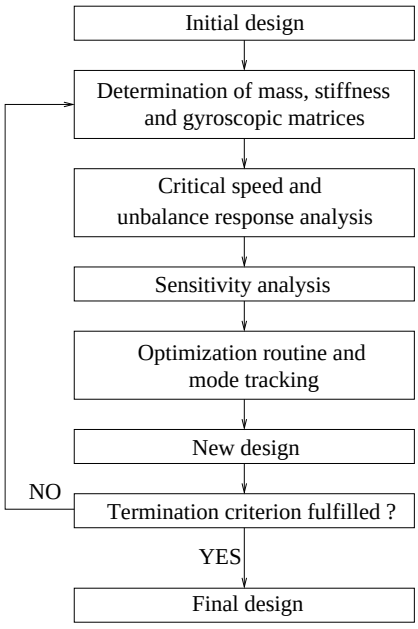

Figure 5.1. Computational algorithm to solve the introduced design optimization problems.

5.3 Sensitivity analysis

In order to apply gradient-based optimization algorithms, derivatives of the expressions appearing in our optimization problems have to be determined. In our case these are the functions of total mass, natural frequency, critical speed and unbalance response. In this section analytical expressions for the sensitivities are formulated based on a finite element discretization of the rotor model. They are determined by differentiating the defining equations for the respective expressions. For our terms this reduces to the determination of sensitivities of eigenvalues and eigenvectors. Whereas the calculation of the eigenvalue sensitivity is straightforward, the determination of the eigenvector sensitivity is much more sophisticated. For eigenvalues and eigenvectors results are known from the literature. Here we put particular emphasis on the sensitivities of critical speed and unbalance response which are related to eigenvalues and eigenvectors and the corresponding expressions are derived below. A detailed overview of design sensitivity analysis can e.g. be found in Haug et al. [28] which treats also the case of a continuous rotor model with distributed parameters.

If the calculation of the analytical expressions requires too heavy computations, which is often the case for eigenvector derivatives, the method of finite differences may be considered alternatively though then an additional function evaluation for each design variable is needed.

Let us now introduce the analytical expressions of the sensitivities.

Total mass

The function of the total mass of the discretized rotor is a polynomial function of diameter d_i, length l_i and density ρ_i of the beam elements,

$$\text{mass} = \sum_{i=1}^{n-1} \left(\frac{d_i}{2}\right)^2 \rho_i \pi l_i.$$

This expression is easily differentiated by the length l_i and the diameter d_i which are often taken as design variables. An important observation related to the formulation of the optimization problems is, that the mass function is convex in the design variables representing diameter and length.

Natural frequency

For the natural frequency λ_i of a certain mode ϕ_i the eigenvalue equation for this mode

$$\lambda_i A \phi_i = B \phi_i, \quad i = 1, \ldots, N,$$

is differentiated by the design parameter q_j for any $j = 1, \ldots, n_{dv}$ to obtain

$$\left(\frac{\partial B}{\partial q_j} - \lambda_i \frac{\partial A}{\partial q_j} - \frac{\partial \lambda_i}{\partial q_j} A\right) \phi_i + (B - \lambda_i A) \frac{\partial \phi_i}{\partial q_j} = 0. \tag{5.3}$$

Multiplying by the left eigenvector ξ_i^T we get

$$\xi_i^T \left(\frac{\partial B}{\partial q_j} - \lambda_i \frac{\partial A}{\partial q_j} - \frac{\partial \lambda_i}{\partial q_j} A\right) \phi_i + \underbrace{\xi_i^T (B - \lambda_i A)}_{=0} \frac{\partial \phi_i}{\partial q_j} = 0. \tag{5.4}$$

It should be noted that we deal with a non-symmetric system, so that we have to distinguish between left and right eigenvectors. Making use of the normalization of the eigenvectors with respect to A (see (4.11)) and the solution property of left eigenvectors we finally obtain

$$\frac{\partial \lambda_i}{\partial q_j} = \xi_i^T \left(\frac{\partial B}{\partial q_j} - \lambda_i \frac{\partial A}{\partial q_j}\right) \phi_i, \tag{5.5}$$

where

$$\frac{\partial A}{\partial q_j} = \begin{pmatrix} \frac{\partial M}{\partial q_j} & 0 \\ 0 & \frac{\partial M}{\partial q_j} \end{pmatrix} \quad \text{and} \quad \frac{\partial B}{\partial q_j} = \begin{pmatrix} -(\omega \frac{\partial G}{\partial q_j} + \frac{\partial C}{\partial q_j}) & -\frac{\partial K}{\partial q_j} \\ \frac{\partial M}{\partial q_j} & 0 \end{pmatrix}.$$

All entries of A and B are rational functions in each of the design variables.

It has to be mentioned that formula (5.5) only holds if the eigenvalue λ_i has multiplicity one. In case of multiple eigenvalues differentiability gets lost and special techniques have to be applied which are discussed in Section 5.4.

Critical speed

The sensitivity for the special case of the critical speed is determined in a similar way. The eigenvalue equation

$$\left((-M + iG)\omega^2 + iC\omega + K + K_b\right) c = 0$$

is differentiated with respect to a design variable q_j resulting in

$$\begin{aligned} &\left(2\omega \frac{\partial \omega}{\partial q_j}(-M + iG) + \omega^2 \left(-\frac{\partial M}{\partial q_j} + i\frac{\partial G}{\partial q_j}\right) + i\frac{\partial \omega}{\partial q_j} C + i\omega \frac{\partial C}{\partial q_j}\right) c \\ &+ \left(\frac{\partial K}{\partial q_j} + \frac{\partial K_b}{\partial q_j}\right) c + \left(\omega^2(-M + iG) + i\omega C + K + K_b\right) \frac{\partial c}{\partial q} = 0. \end{aligned}$$

Again we use the technique of premultiplying the equation by a left eigenvector d^T to obtain

$$\frac{\partial \omega}{\partial q_j} = \frac{d^T \left(\omega^2 \left(\frac{\partial M}{\partial q_j} - i\frac{\partial G}{\partial q_j}\right) - i\omega \frac{\partial C}{\partial q_j} - \left(\frac{\partial K}{\partial q_j} + \frac{\partial K_b}{\partial q_j}\right)\right) c}{d^T \left(2\omega(-M + iG) + iC\right) c}. \tag{5.6}$$

The expressions (4.16) and (4.17) for the unbalance response show that for the determination of its sensitivity, the derivatives of the eigenmodes are required.

Eigenmodes

For the calculation of the derivatives of the eigenmodes there are several options. An overview about different techniques for general complex matrices can be found e.g. in [1] or [43]. One of them is the method by Fox [21], where the derivative is written as a linear combination of all eigenmodes. In this case the task consists in determining the corresponding coefficients. Extensions of this concept are discussed e.g. in [61]. However, this method is very expensive in computational time, if all modes are considered. A more efficient approach was introduced by Nelson [45]. It only needs the knowledge of the eigenvalue whose derivative is calculated. This is the method of our choice. The equation for the derivative of the generalized eigenvalue problem is rewritten as

$$(B - \lambda_i A)\,\frac{\partial \tilde{\phi}_i}{\partial q_j} = \left(\frac{\partial \lambda_i}{\partial q_j} A + \lambda_i \frac{\partial A}{\partial q_j} - \frac{\partial B}{\partial q_j}\right) \tilde{\phi}_i.$$

We use normalization (4.12) where the largest component l of $\tilde{\phi}_i$ has been set to 1,

$$\tilde{\phi}_i^{(l)} = 1.$$

This system is now solved directly. Care must be taken in the solution process because $B - \lambda_i A$ is singular [25]. Nelson's idea is that the l-th column and row can be deleted due to our choice of normalization, resulting in

$$\left(\frac{\partial \tilde{\phi}_i}{\partial q_j}\right)_l = 0.$$

Then the reduced system is solved. The existence of a solution of this system is guaranteed [43]. After that the vectors can be transformed to obtain vectors ϕ_i fulfilling the normalization (4.11) by setting

$$\phi_i = \frac{\tilde{\phi}_i}{(\tilde{\xi}_i A \tilde{\phi}_i)^{1/2}}.$$

The derivative of the eigenvector ϕ_i is then obtained by the chain rule.

In an additional approach the eigenvector derivatives are computed by an iterative procedure. Possible ways to do this are shown in [58].

Unbalance response

To determine the derivative of the unbalance response a we have to know the derivative of each relevant component c_k of the particular solution y of the forced system. It is derived in Section 4.4 as

$$c_k = \sum_{p=1}^{n_f} \sum_{l=1}^{N} \frac{\xi_{\nu_p,l} \phi_{k,l} \hat{f}_{\nu_p}}{i\omega - \lambda_l}.$$

We obtain

$$\begin{aligned} \frac{\partial c_k}{\partial q_j} &= \sum_{p=1}^{n_f} \sum_{l=1}^{N} \frac{\left(\frac{\partial \xi_{\nu_p,l}}{\partial q_j} \phi_{k,l} \hat{f}_{\nu_p} + \xi_{\nu_p,l} \frac{\partial \phi_{k,l}}{\partial q_j} \hat{f}_{\nu_p} + \xi_{\nu_p,l} \phi_{k,l} \frac{\partial \hat{f}_{\nu_p}}{\partial q_j} \right)}{(i\omega - \lambda_l)} + \\ & \sum_{p=1}^{n_f} \sum_{l=1}^{N} \frac{\xi_{\nu_p,l} \phi_{k,l} \hat{f}_{\nu_p} \left(i \frac{\partial \omega}{\partial q_j} - \frac{\partial \lambda_l}{\partial q_j} \right)}{(i\omega - \lambda_l)^2}. \end{aligned}$$

For the absolute value which is needed for the calculation of the unbalance response, we have

$$\begin{aligned} \frac{\partial |c_k|}{\partial q_j} &= \frac{\partial (c_k \cdot \bar{c}_k)^{1/2}}{\partial q_j} = \frac{\frac{\partial c_k}{\partial q_j} \bar{c}_k + c_k \frac{\partial \bar{c}_k}{\partial q_j}}{2 (c_k \cdot \bar{c}_k)^{1/2}} \\ &= \frac{\mathrm{Re} \left(\bar{c}_k \frac{\partial c_k}{\partial q_j} \right)}{|c_k|}. \end{aligned}$$

Having calculated the sensitivities, gradient-based algorithms can be applied to solve the natural frequency and vibration level optimization problems. Before introducing suitable solvers in Chapter 6 the case of multiple eigenvalues has to be discussed which requires an extension of the method.

5.4 Multiple eigenvalues

In points with multiple eigenvalues, attention has to be paid since the eigenvalue function then is no longer differentiable. Only directional derivatives can be calculated in these points. In design optimization problems a coalescence of eigenvalues often happens at the optimized design and in its neighbourhood. Therefore, optimization algorithms reaching the neighbourhood of the optimum have to use the directional derivatives in these points. Then the input of correct sensitivities is guaranteed avoiding a possible source of failure for the algorithm. Research on this topic can be found e.g. in Seyranian et al. [52], where the following method is developed.

The directional derivatives of a multiple eigenvalue with multiplicity s in direction $e \in \mathbb{R}^{n_{dv}}$, $\|e\| = 1$, are obtained as eigenvalues of the $s \times s$-matrix

$$(g_{ij}^T e)_{i,j=1,\ldots,s}.$$

The s^2 vectors $g_{ij} \in \mathbb{C}^{n_{dv}}$ are called the generalized gradients and their entries are given by

$$g_{ij} = \left(\xi_i^T \left(\frac{\partial B}{\partial q_1} - \lambda \frac{\partial A}{\partial q_1} \right) \phi_j, \ldots, \xi_i^T \left(\frac{\partial B}{\partial q_{n_{dv}}} - \lambda \frac{\partial A}{\partial q_{n_{dv}}} \right) \phi_j \right), \quad i,j = 1, \ldots, s$$

and λ is the multiple eigenvalue and ξ and ϕ are the corresponding left and right eigenvectors.

Another possibility was shown by Friswell [22] who works with an extension of Nelson's method.

The situation might occur that during an iterative optimization process modes do not coalesce but simply cross, leading to a multiple eigenvalue only in the crossing point. This is then simply a crossing between two or more differentiable functions (see Figure 5.2). Indeed, in the neighbourhood of an eigenvalue with multiplicity s there are s distinct eigenvalues and there exists a smooth ordering of the directional derivatives of the multiple eigenvalue and the derivatives of the eigenvalues in the neighbourhood (see Haug et al. [28]).

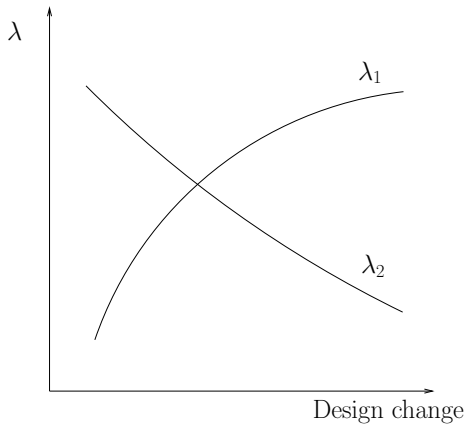

Figure 5.2. Crossing of modes.

Our numerical calculations show that this situation often happens in our applications. We deal with this case by applying a mode tracking procedure which guarantees us to follow the correct mode after the crossing of eigenvalues. This method is described in the next section. Since no coalescence happens the above mentioned directional derivatives are not needed in our calculations, but may become relevant when optimizing other rotating bodies.

5.5 Mode tracking

When optimizing structural dynamic characteristics, specific frequencies and mode shapes must be referenced by a number. In vibration problems, the eigenvalues and eigenvectors are ordered by eigenvalue magnitude. When the design changes in each iteration, frequencies will drift and mode crossings can occur (see Figure 5.3). If the crossings are not tracked, the objective function and constraint functions can be evaluated using modes that are different from those that were intended. Then the design goals can no longer be fulfilled since one might follow a wrong mode (see [13]).

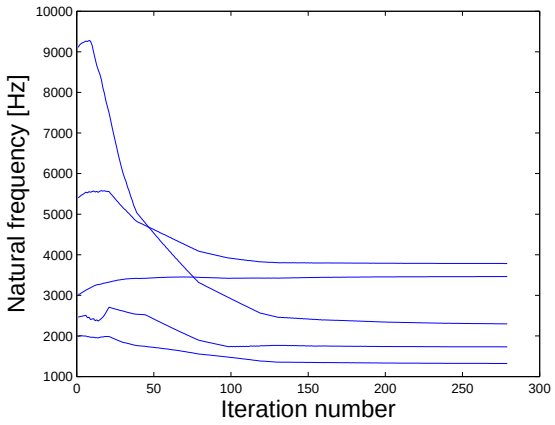

Figure 5.3. Mode crossing in vibration level optimization problem.

To track the modes of our interest we use the following strategy. From the ordered list of eigenvalues we pick the numbers of the frequencies belonging to the modes of interest, i.e. in our case certain rigid or bending modes. The initial shape of these modes is taken as a reference mode shape ϕ_{ref}. After any design change the modal assurance criterion (MAC) value is checked [33]. It is calculated in each iteration step k by

$$MAC(\phi_{\text{ref}}, \phi_j^k) = \frac{|(\phi_{\text{ref}}, \phi_j^{(k)})|^2}{(\phi_{\text{ref}}, \phi_{\text{ref}})(\phi_j^{(k)}, \phi_j^{(k)})}, \quad j = 1, \ldots, N, \tag{5.7}$$

where $(\cdot, \cdot)$ denotes the Euclidean inner product. The MAC value lies between 0 and 1. If two vectors represent the same mode, the value is large. If modes can be distinguished clearly then we expect to have one vector ϕ_j^k for which the value is close to one. However, in order to take into account numerical errors, we take the vector ϕ_j that leads to the largest MAC value, assuming it represents the mode of interest. The new mode number j^* is thus given by

$$j^* = \max_{j=1,\ldots,N} MAC(\phi_{\text{ref}}, \phi_j).$$

The reference vector can now be left as the initial mode shape vector or updated in each iteration. Then in iteration k the mode shape vector of iteration $k-1$ is the reference vector. In our applications we can concentrate on the neighboring modes and do not have to calculate the MAC value for all N eigenvectors.

5.6 Extension to nonlinear bearing model

When applying the optimization method for gyroscopic systems on a model considering nonlinear oil film forces as explained in Section 4.5 certain modifications have to be made. This requires changes in the sensitivity analysis and extensions to include design variables of the bearing configuration.

The diameter of the shaft element, where the bearing is attached to, appears in the expression of the oil film force and hence the derivative with respect to this shaft element has to be modified. Moreover, additional design variables are included in the calculations such as bearing clearance and width. We want to mention how this is included into the optimization program.
The additional damping and stiffness terms due to the nonlinear oil film bearings are expressed by the matrices K_{oil} and C_{oil} in equation (4.23). Therefore the derivatives of these matrices have to be determined in order to include their influence in the calculations. We want to show the proceeding exemplarily for the stiffness coefficient k_{XX}. It is the same for the other stiffness coefficients as well as the damping coefficients.

The formal derivative with respect to a design variable q_j is given by

$$\frac{\partial k_{XX}}{\partial q_j} = \frac{\partial}{\partial q_j}\left(\frac{\partial F_X}{\partial x}\right) = \frac{\partial}{\partial x}\left(\frac{\partial F_X}{\partial q_j}\right).$$

By changing the order of differentiation, the derivatives of the expressions F_X and F_Y with respect to the design variables are evaluated initially. This is possible analytically for the shaft radius and bearing width for which the terms are shown below. For the bearing clearance the derivative is calculated by finite differences. The derivatives of F_X and F_Y are expressed by the derivatives of F_e and F_γ,

$$\frac{\partial F_X}{\partial q_j} = \cos(\gamma)\frac{\partial F_e}{\partial q_j} - \sin(\gamma)\frac{\partial F_\gamma}{\partial q_j}, \quad \frac{\partial F_Y}{\partial q_j} = \cos(\gamma)\frac{\partial F_e}{\partial q_j} + \sin(\gamma)\frac{\partial F_\gamma}{\partial q_j}.$$

For the shaft radius we obtain

$$\frac{\partial F_e}{\partial r} = \frac{\eta\omega b^3}{2c^2}(GA_1 - EA_2), \quad \frac{\partial F_\gamma}{\partial r} = \frac{\eta\omega b^3}{2c^2}(GA_3 - EA_1)$$

and for the bearing width b,

$$\frac{\partial F_e}{\partial b} = \frac{3\eta\omega r b^2}{2c^2}(GA_1 - EA_2), \quad \frac{\partial F_\gamma}{\partial b} = \frac{3\eta\omega r b^2}{2c^2}(GA_3 - EA_1).$$

The subsequent differentiation by the position of the static equilibrium value x is also determined by the method of finite differences as mentioned in Section 4.5.

5.7 Feasibility studies by multiobjective optimization

The successful solution of the optimization problem depends on the existence of a non-empty feasible domain. This is threatened if the target values on the constraints are chosen too restrictive or demanding by the designer. Therefore, in this section we want to present some ideas how to ensure the solvability of the optimization problem. The goal of our approach is not only to find suitable target values, but also to give the engineer some information what could be achieved best and show the trade-off between contradicting targets in the optimization problem. Therefore tools of nonlinear programming capable of handling several conflicting objects are needed. These are called multiobjective or multicriteria optimization techniques and an extensive coverage about them can be found in [42].

Multiobjective optimization problems are solved by scalarization which means converting the problem into a single objective optimization problem. Then standard techniques from nonlinear programming can be used for the solution. Because the different objective functions can be contradictive it is generally not possible to find a solution which would be optimal for the objectives simultaneously. It is the aim to find a solution vector where none of the components can be improved without deteriorating one of the other components. This concept is called Pareto optimality and more theory about that can also be found in [42]. A formal definition is now as follows.

Let $Z \subset \mathbb{R}^n$ be a given compact set of feasible designs. Furthermore, objective functions $f_i : Z \to \mathbb{R}$, $i = 1, \ldots, m$ are given.

Definition 5.1. *A multiobjective optimization problem is defined as*

$$\min_{x \in Z} \{f_1(x), \ldots, f_m(x)\}.$$

Then x^* is called Pareto optimal, if there does not exist $\tilde{x} \in Z$ satisfying $f_i(\tilde{x}) \leq f_i(x^*)$, $i = 1, \ldots, m$ and $f_j(\tilde{x}) < f_j(x^*)$ for some $j \in \{1, \ldots, m\}$. Moreover, x^* is called weakly Pareto optimal, if there does not exist any vector $\tilde{x}$ satisfying m strict inequalities.

Usually, such a problem has infinitely many Pareto optimal solutions and favourable solutions have to be selected out of this set. Therefore, a decision maker is needed to express preference relations between different solutions. This leads to the introduction of aspiration levels that are objective function values which are favourable to the decision maker. A vector consisting of aspiration levels is called a reference point. We want to mention one certain reference point which is the *ideal objective vector*. It is obtained by optimizing each of the objective functions individually subject to constraints.

Definition 5.2. *A vector z^* is called an ideal objective vector, if*

$$z_i^* = \min\{f_i(x) : x \in Z\}, \quad i = 1, \ldots, m.$$

In general, this point is not feasible since the objective functions are contradictive. Nevertheless it can serve as a reference point standing for the ideal case and we use it below.

Let us now present two approaches which we apply to our problem in the following.

- The first one belongs to the so-called no preference methods meaning that the opinions of the decision maker are not taken into consideration. Obviously the solution best satisfying the requirements of the decision maker is not necessarily found with this method. The advantage is that the problem can be solved with a simple nonlinear programming method.

  A standard example for such a method is the **method of the global criterion** in which the distance between some reference point, in our case the ideal objective vector, and the image of the feasible domain is minimized. The optimization problem then is

  $$\min_{x \in Z} \left(\sum_{i=1}^{m} (f_i(x) - z_i^*)^p \right)^{1/p},$$

  where $p \in \mathbb{N}$ and for $p = \infty$

  $$\min_{x \in Z} \max_{i=1,\ldots,m} \{f_i(x) - z_i^*\}.$$

  It can be shown [42] that a solution x^* is Pareto optimal, if $1 \leq p < \infty$ and weak Pareto optimal, if $p = \infty$.

- The second class of methods aims at generating several Pareto optimal solutions and the decision maker selects the one most preferred. It is usually very expensive to calculate the Pareto optimal set or even a part of it. The idea

is to use a weighted sum of the objective functions and this is also called the **weighting method**. The problem is then formulated as

$$\min_{x\in Z} \sum_{i=1}^{m} w_i f_i(x), \quad i = 1, \ldots, m,$$

where $\sum_{i=1}^{m} w_i = 1$. If $w_i > 0$, $i = 1, \ldots, m$, then any solution is Pareto optimal. Of course, only a finite number of parameter settings can be calculated and therefore some information is hidden. But interpolation gives an approximation of the whole Pareto optimal set. A special case is, if only two functions are considered. Then, only one weight parameter appears since $\sum_{i=1}^{2} w_i = 1$ and a sequence of optimization problems varying the weighting parameter can be calculated to yield a trade-off curve between the two functions.

Both methods can also be combined and give the **method of weighted metrics**. The optimization problem is then given by

$$\min_{x\in Z} \left(\sum_{i=1}^{m} w_i (f_i(x) - z_i^*)^p \right)^{1/p}.$$

Application to vibration level optimization problem

As mentioned above it is our aim to obtain reasonable target values for our single objective optimization problem. The model problem (5.2) is given as

$$\begin{aligned} &\min_q f(q) = \text{mass}(q) \\ &\text{subject to} \\ &g_1(q) = -\omega_{\text{m1}}(q) \le g_1^* = -\omega_{\text{m1}}^*, \\ &g_2(q) = a_{\text{m2}}(q) \le g_2^* = a_{\text{m2}}^*, \\ &\underline{q} \le q \le \bar{q}, \end{aligned} \tag{5.8}$$

with two constraint functions g_1 and g_2 and box constraints $\underline{q}$ and $\bar{q}$ for the design variables q. In the vibration level problem the constraint functions are chosen as the critical speed and the unbalance response of certain modes m1 and m2. The task is to find proper target values g_1^* and g_2^*. The idea is to determine the ideal objective vector by taking each constraint function once as objective function of a new optimization problem. The original objective function f is now considered as a constraint and it is demanded that it should not become worse as for the initial design, i.e. for the above case we have $f \le f^* = f(q^0)$. The respective other constraint is neglected. As auxiliary optimization problems we obtain for g_i, $i = 1, 2$,

$$\begin{aligned} &\min_q g_i(q) \\ &\text{subject to} \\ &f(q) \le f^* = f(q^0), \\ &\underline{q} \le q \le \bar{q}. \end{aligned} \tag{5.9}$$

We have $z_i^* = \min_q g_i(q)$, $i = 1, 2$, forming the ideal objective vector. It generally is an infeasible point since no second constraint was included in the optimization problem.

Now the above introduced multicriteria approaches are applied to find Pareto-optimal points in our case.

The method of the global criterion then reads as

$$\begin{aligned} &\min_q \left(\sum_{i=1}^{2}(g_i(q) - z_i^*)^p\right)^{1/p} \\ &\text{subject to} \\ &f(q) \leq f^*, \\ &\underline{q} \leq q \leq \bar{q}. \end{aligned}$$

For our calculation we usually consider $p = 2$. This yields a Pareto optimal solution and the decision maker has to judge whether it is satisfactory.

Using the weighting method and trying different weighting parameters gives the decision maker a bigger choice of Pareto optimal solutions. Here, we are in the favourable case of two parameters. We have

$$\begin{aligned} &\min_q wg_1(q) + (1 - w)g_2(q) \\ &\text{subject to} \\ &f(q) \leq f^*, \\ &\underline{q} \leq q \leq \bar{q}, \end{aligned}$$

where $w \geq 0$. A part of the whole Pareto optimal set can be determined in dependence of the parameter w. Let q_w^* be a solution of the weighting problem. For each parameter w the Pareto optimal points $(g_1(q_w^*), g_2(q_w^*))$ can be drawn in a curve which shows the trade-off (see Figure 5.4).

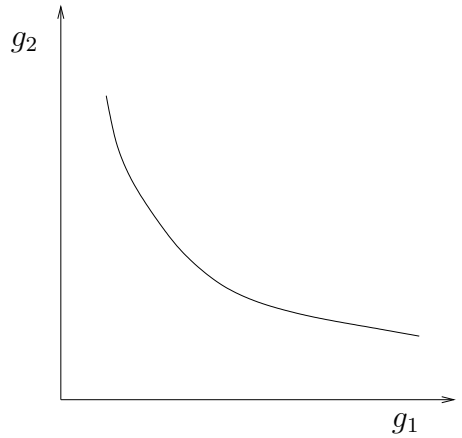

Figure 5.4. Possible curve of Pareto optimal solutions generated with the weighting method.

The decision maker can then set an aspiration level for one constraint and see what can be achieved for the other constraint. Having this knowledge the formulation of an infeasible optimization problem can be avoided.

Remark. In nonlinear programming algorithms based on a sequence of approximating solutions, the Pareto optimal points can in general also be determined only approximately.

Based on these considerations for a numerical determination of target values we can formulate an extended design optimization process. For a given initial design the weighting method performed with different weighting parameters gives the decision maker an overview of possible target values. According to his preferences a suitable combination of values can be chosen such that the actual design optimization problem has a non-empty solution set. However, due to the nonlinearities of the functions, the optimization algorithm does not necessarily reach the point where the constraints with the new target values are active.

Chapter 6

Numerical optimization methods

In this chapter we give an overview about optimization algorithms that are used to solve the optimization problems of interest in this work.

The treated design optimization problems belong to the class of nonlinear constrained programming which are in general given by

$$\begin{aligned} &\min_{x\in\mathbb{R}^n} f_0(x) \\ &\text{subject to} \\ &f_i(x) \geq f_i^*, \quad i = 1,\ldots,m, \\ &\underline{x}_j \leq x_j \leq \bar{x}_j, \quad j = 1,\ldots,n, \end{aligned} \tag{6.1}$$

with a nonlinear differentiable real-valued objective function f_0, nonlinear differentiable real-valued constraint functions f_i and scalar target values f_i^*. As usual in structural optimization problems lower and upper bounds $\underline{x}_j$ and $\bar{x}_j$ on the variables x_j are considered.

The strategy to solve the optimization problem (6.1) is to replace objective and constraint functions by a sequence of approximating functions $\tilde{f}_i,\ i = 0\ldots,m$. The approximating subproblem can be solved directly. In iteration k it is written as

$$\begin{aligned} &\min_{x\in\mathbb{R}^n} \tilde{f}_0^{(k)}(x) \\ &\text{subject to} \\ &\tilde{f}_i^{(k)}(x) \geq f_i^*, \quad i = 1,\ldots,m, \\ &\alpha_j^{(k)} \leq x_j \leq \beta_j^{(k)}, \quad j = 1,\ldots,n. \end{aligned} \tag{6.2}$$

and can be solved by mathematical programming algorithms. It is an important question how the approximations should be chosen. Svanberg [56] considers the class of conservative convex separable approximation methods and we want to follow this approach. The convexity guarantees that dual methods can be used to solve (6.2). *Separability*, meaning that no expressions of mixed variables occur, ensures that the

necessary conditions of optimality do not couple the design variables which reduces the computational effort a lot. Moreover, the approximation scheme is said to be *conservative* if a sequence of steadily improved iterations is generated which provide feasible solutions at any stage of the optimization process [12].

For each subproblem the additional bounds on the design variables x_j have to be tightened since the approximation is assumed to be good only in a small neighborhood of the current iteration point. Therefore, trust region parameters α_j and β_j have to be introduced for each design variable and replace the lower and upper bounds $\underline{x}_j$ and $\bar{x}_j$. The approximating subproblems (6.2) are then solved successively and the algorithm is stopped when the change in design variables becomes sufficiently small.

The whole approach is called sequential convex programming (SCP) and there are many options how to choose the convex approximations. The simplest one is the linearization of objective and constraint functions, called sequential linear programming (SLP), which is described in Section 6.1. An algorithm based on more sophisticated convex approximations is the method of moving asymptotes (MMA) which is explained in more detail in Section 6.2. Modifications of the MMA algorithm were developed that guarantee a convergence towards a KKT point of the discretized problem.

In some cases structural optimization problems can also be treated by semidefinite programming methods (see e.g. [60]). This is possible if the optimization problem can be reformulated as a problem with a linear objective function and constraints that are written as a combination of affine symmetric, positive semidefinite matrices. This works e.g. if a system without gyroscopic effects is optimized subject to constraints on the smallest eigenvalue. The reformulation is in particular attractive if multiple eigenvalues are involved since the algorithms can circumvent differentiability problems [7]. Unfortunately, in our case it is not possible to apply this strategy, because of the nonsymmetric matrices involved and the focus on a certain mode which generally does not belong to the smallest eigenvalue.

6.1 Sequential linear programming

The SLP algorithm is based upon a sequential linearization of the objective function and the constraints. We have for each iteration step k

$$f_i(x) = f_i(x^{(k)}) + \nabla f_i(x^{(k)})(x - x^{(k)})$$

for $i = 0, \ldots, m$. The linearized optimization problem then looks like

$$\begin{aligned}
&\min_x \nabla f_0(x^{(k)})(x - x^{(k)}) \\
&\text{subject to} \\
&\nabla f_i(x^{(k)})^T(x - x^{(k)}) \geq f_i^* - f_i(x^{(k)}), \\
&\alpha_j^{(k)} \leq x - x^{(k)} \leq \beta_j^{(k)}.
\end{aligned}$$

The SLP algorithm is often used in engineering applications and for a wide spectrum of problems acceptable results can be obtained. The big advantage is, that the solution of the subproblems can be realized efficiently by linear programming algorithms like the simplex algorithm or primal-dual interior point methods.

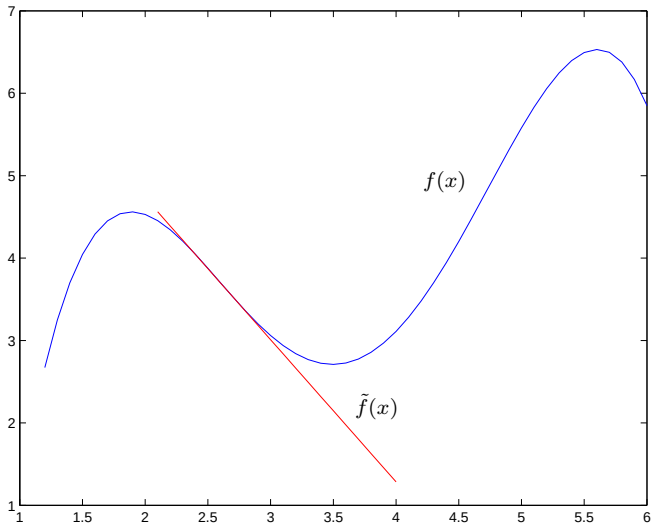

Figure 6.1. SLP approximation $\tilde{f}$ of nonlinear function f.

The success of the algorithm, however, depends strongly on the choice of proper values for the parameters α and β which are usually called *move limits* in this context. Figure 6.1 shows that the approximation is only good in a very small neighbourhood of the current iteration point. Therefore, move limit strategies have to be applied. We used two options.

The first one is based on a large move limit in the beginning allowing big steps to approach quickly the minimum. Then, we successively decrease the move limit to reduce the linearization error, to avoid large oscillations around the optimum and enable a better convergence.

Another possibility is to reduce the design interval when the design variable oscillates and enlarge it when the convergence process is stable (see e.g. Duysinx [12]). After choosing some initial move limit for the first two iterations the update is according

to the following rule.

$$\begin{aligned} \alpha_i^{(k+1)} &= d \cdot \alpha_i^{(k+1)}, \qquad \text{if} \qquad (x_i^{(k+1)} - x_i^{(k)})(x_i^{(k)} - x_i^{(k-1)}) < 0, \\ \alpha_i^{(k+1)} &= u \cdot \alpha_i^{(k+1)}, \qquad \text{if} \qquad (x_i^{(k+1)} - x_i^{(k)})(x_i^{(k)} - x_i^{(k-1)}) \geq 0 \end{aligned}$$

with $0 < d < 1$ and $u > 1$. Again the choice of decrease and increase parameters d and u is decisive. Further strategies can be found in [29].

An extension of the concept of SLP was introduced by Fleury and Braibant [19] with the CONLIN algorithm, which works with a linearization with respect to direct and reciprocal variables. The use of reciprocal variables is motivated by the fact that stresses and displacements are exact linear functions of reciprocal sizing variables in the case of a statically determinate structure and hence this turns out to be the best approach for certain optimal sizing problems (see [18]). However, the drawback of CONLIN is that the curvature of the approximations is fixed which may result in a bad approximation of the original function.

6.2 Method of moving asymptotes

A method which is able to adjust the curvature of the approximation is the method of moving asymptotes (MMA) which was introduced by Svanberg [54]. This method is explained in detail below. It is based on a linearization in terms of the intermediate variables

$$\frac{1}{x_j - l_j} \quad \text{and} \quad \frac{1}{u_j - x_j},$$

dependent on the signs of the derivatives of objective and constraint functions at the current iteration point. The parameters l_j and u_j are called the *moving asymptotes* giving the method its name. They are chosen individually for each design variable x_j and are usually changed in each iteration.

To guarantee that the problem always has feasible solutions the original formulation (6.1) is replaced by the following one where additional variables $y_i, i = 1, \ldots, m$ and z are introduced.

$$\begin{aligned} &\min f_0(x) + a_0 z + \textstyle\sum_{i=1}^{m} (c_i y_i + \frac{1}{2} d_i y_i^2) \\ &\text{subject to} \\ &a_i z + y_i - (f_i(x) - f_i^*) \leq 0, \quad i = 1, \ldots, m, \\ &\underline{x}_j \leq x_j \leq \bar{x}_j, \quad j = 1, \ldots, n, \\ &z \geq 0 \quad \text{and} \quad y_i \geq 0, \quad i = 1, \ldots, m. \end{aligned} \tag{6.3}$$

The parameters a_i, c_i and d_i are given non-negative real numbers and are assumed to satisfy $c_i + d_i > 0$ for each i. Then e.g. setting $z = 0$ and $y_i = \max\{0, f_i(x) - f_i^*\}$ guarantees that the feasible domain is non-empty.

The approximating subproblems are as follows

$$\begin{aligned}
&\min \tilde{f}_0^{(k)}(x) + a_0 z + \textstyle\sum_{i=1}^m (c_i y_i + \frac{1}{2} d_i y_i^2) \\
&\text{subject to} \\
&\tilde{f}_i^{(k)}(x) - a_i z - y_i \geq f_i^*, \quad i = 1, \ldots, m, \\
&\alpha_j^{(k)} \leq x_j \leq \beta_j^{(k)}, \quad j = 1, \ldots, n, \\
&z \geq 0 \quad \text{and} \quad y_i \geq 0, \quad i = 1, \ldots, m.
\end{aligned}$$

The approximating functions are chosen as

$$\tilde{f}_i^{(k)}(x) = \sum_{j=1}^{n} \left(\frac{p_{ij}^{(k)}}{u_j^{(k)} - x_j} + \frac{q_{ij}^{(k)}}{x_j - l_j^{(k)}} \right) + r_i^{(k)}, \quad i = 0, 1, \ldots, m,$$

where

$$p_{ij}^{(k)} = \left(u_j^{(k)} - x_j^{(k)} \right)^2 \max \left\{ 0, \frac{\partial f_i}{\partial x_j}(x^{(k)}) \right\},$$

$$q_{ij}^{(k)} = \left(x_j^{(k)} - l_j^{(k)} \right)^2 \max \left\{ 0, -\frac{\partial f_i}{\partial x_j}(x^{(k)}) \right\},$$

and $r_i^{(k)}$ is a correction term to ensure that the approximating functions $\tilde{f}_i$ equals the original function at the current iteration point, i.e. $\tilde{f}_i(x^{(k)}) = f_i(x^{(k)})$. Either $p_{ij}^{(k)}$ or $q_{ij}^{(k)}$ is equal to zero, so that only one asymptote is active and $\tilde{f}_i$ is a hyperbola (see Figure 6.2). If l_j and u_j become very large the approximating function is almost linear. Indeed, in the limit $l_j^k \to -\infty$ and $u_j^k \to \infty$ the algorithm is identical to the SLP algorithm.

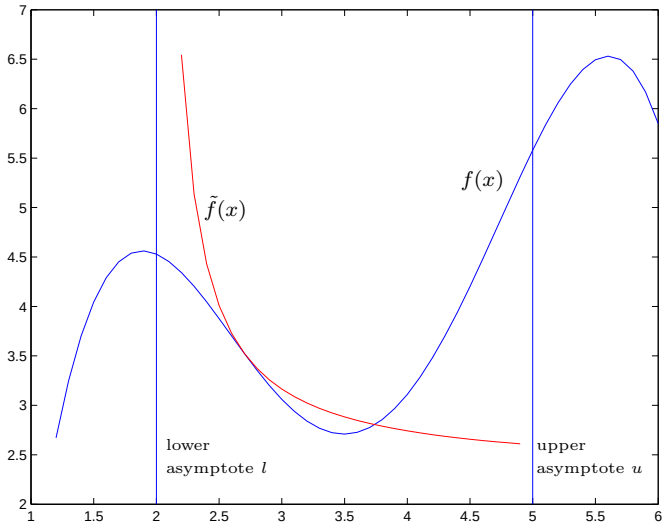

Figure 6.2. MMA approximation $\tilde{f}$ of f.

Moreover, this scheme guarantees that the first derivatives at the current iteration point coincide, i.e.

$$\frac{\partial \tilde{f}_i}{\partial x_j}(x^{(k)}) = \frac{\partial f_i}{\partial x_j}(x^{(k)}).$$

The parameters $\alpha_j^{(k)}$ and $\beta_j^{(k)}$ play the role of move limits and are chosen for example as

$$\alpha_j^{(k)} = \max\{\underline{x}_j, 0.9l_j^{(k)} + 0.1x_j^{(k)}\},$$
$$\beta_j^{(k)} = \min\{\bar{x}_j, 0.9u_j^{(k)} + 0.1x_j^{(k)}\}.$$

For a suitable choice of the vertical asymptotes Svanberg [54] proposed a heuristic strategy based upon the design variable oscillations. For the iterations $k = 1$ and $k = 2$ the following default rules are adopted

$$l_j^{(k)} = x_j^{(k)} - s_0(\bar{x}_j - \underline{x}_j),$$

$$u_j^{(k)} = x_j^{(k)} + s_0(\bar{x}_j - \underline{x}_j)$$

with $s_0 = 0.5$.

For $k > 2$, the update scheme is the following. When the design variables in previous iterations tend in the same direction, i.e.

$$(x_j^{(k-2)} - x_j^{(k-1)})(x_j^{(k-1)} - x_j^{(k)}) \geq 0,$$

the convexity can be reduced not to slow down the convergence rate. Hence the asymptotes can be moved away from the design point

$$l_j^{(k)} = x_j^{(k)} - s_1(x_j^{(k-1)} - l_j^{(k-1)}),$$

$$u_j^{(k)} = x_j^{(k)} + s_1(u_j^{(k-1)} - x_j^{(k-1)})$$

with $s_1 > 1$.

However, when convergence history oscillates , i.e.

$$(x_j^{(k-2)} - x_j^{(k-1)})(x_j^{(k-1)} - x_j^{(k)}) < 0,$$

one wants to make the design space smaller. Then

$$l_j^{(k)} = x_j^{(k)} - s_2(x_j^{(k-1)} - l_j^{(k-1)}),$$

$$u_j^{(k)} = x_j^{(k)} + s_2(u_j^{(k-1)} - x_j^{(k-1)})$$

are chosen with $s_2 < 1$. The numerical studies show that the choice of the parameters s_0, s_1 and s_2 is crucial for the success of the algorithm. More details are mentioned in Chapter 7.

Remark. (i) The MMA algorithm shows good convergence behaviour in many applications. However, it does not guarantee convergence which leads to failure of the method in certain cases.
(ii) If constraint function values strongly differ in magnitude, a normalization might lead to an improvement of the algorithm. The original constraints $f_i(x) \geq f_i^*$ are then replaced by $f_i/f_i^* \geq 1$ for all $i = 1, \ldots, m$.

Since there is no convergence theorem for the original MMA algorithm a method is desired that converges towards a point which fulfills the first order necessary optimality conditions for the optimization problem. These are given by the Karush-Kuhn-Tucker conditions (see e.g. [24]) and make use of the Lagrange function L. For our nonlinear constrained programming problem (6.1) we obtain

Definition 6.1. *The Lagrange function $L : \mathbb{R}^n \times \mathbb{R}^m \to \mathbb{C}$ of the nonlinear constrained optimization problem (6.1) is defined by*

$$L(x, \lambda) = f_0(x) + \sum_{i=1}^{m} \lambda_i (f_i^* - f_i(x)) + \sum_{i=1}^{n} \lambda_{m+i} (\underline{x}_i - x_i) + \sum_{i=1}^{n} \lambda_{m+n+i} (x_i - \bar{x}_i).$$

Definition 6.2. *Let us consider the nonlinear constrained optimization problem (6.1). The conditions*

$$\begin{aligned}
\nabla_x L(x, \lambda) &= 0, \\
f_i^* - f_i(x) &\leq 0 \quad \forall i = 1, \ldots, m, \\
\underline{x}_i - x_i &\leq 0 \quad \forall i = 1, \ldots, n, \\
x_i - \bar{x}_i &\leq 0 \quad \forall i = 1, \ldots, n, \\
\lambda_i &\geq 0 \quad \forall i = 1, \ldots, m + 2n, \\
\lambda_i (f_i^* - f_i(x)) &= 0 \quad \forall i = 1, \ldots, m, \\
\lambda_{m+i} (\underline{x}_i - x_i) &= 0 \quad \forall i = 1, \ldots, n, \\
\lambda_{m+n+i} (x_i - \bar{x}_i) &= 0 \quad \forall i = 1, \ldots, n
\end{aligned}$$

are called Karush-Kuhn-Tucker (or short KKT) conditions. Every point (x^*, λ^*) fulfilling the KKT-conditions is called KKT point of the optimization problem.

We now want to present two extensions of the MMA algorithm that guarantee convergence towards a KKT point. The first one is by Svanberg [56] and works with a modification of the approximating functions. Another possibility is the consideration

of a line search scheme in the original MMA algorithm which was done by Zillober [65, 66].

Globally convergent MMA (GCMMA)

The method proposed by Svanberg uses the following extensions of $p_{ij}^{(k)}$ and $q_{ij}^{(k)}$ to create non monotonous approximations.

$$p_{ij}^{(k)} = (u_j^{(k)} - x_j^{(k)})^2 \left(\max\left\{0, \frac{\partial f_i}{\partial x_j}(x^{(k)})\right\} + \kappa_{ij}^{(k)} \right),$$

$$q_{ij}^{(k)} = (x_j^{(k)} - l_j^{(k)})^2 \left(\max\left\{0, -\frac{\partial f_i}{\partial x_j}(x^{(k)})\right\} + \kappa_{ij}^{(k)} \right),$$

where the additional term $\kappa_{ij}^{(k)} = \frac{\rho_i^{(k)}(u_j^{(k)} - l_j^{(k)})}{2}$.

Both asymptotes l and u are used at the same time to generate the approximating functions. We notice that the tighter the asymptotes are the steeper is the slope of the function (see Figure 6.3).

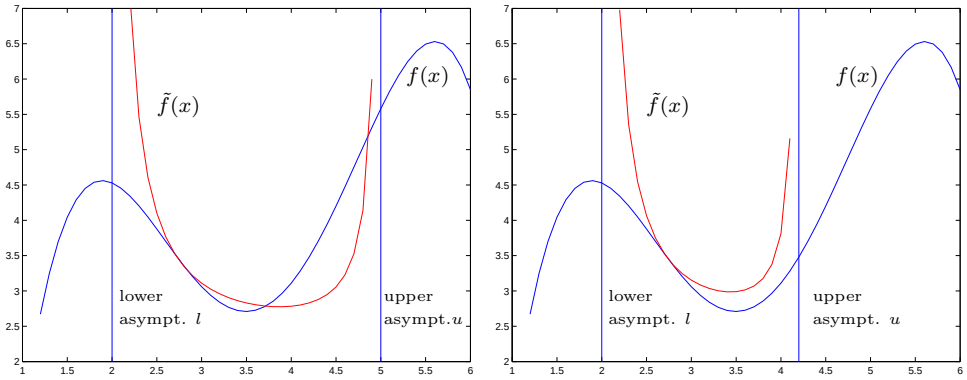

Figure 6.3. GCMMA approximation with different asymptotes.

The additional parameters $\rho_j^{(k)}$ are chosen as follows

$$\rho_j^{(1)} = \varepsilon, \quad \forall j \in \{0, 1, \ldots, m\}, \quad 0 < \varepsilon < 1.$$

The update of the parameters is for $k \geq 2$ done by

$$\rho_j^{(k)} = \begin{cases} 2\rho_j^{(k-1)}, & \text{if} \quad \tilde{f}_j^{(k-1)}(x^{(k)}) < f_j(x^{(k)}), \\ \rho_j^{(k)} = \rho_j^{(k-1)}, & \text{if} \quad \tilde{f}_j^{(k-1)}(x^{(k)}) \geq f_j(x^{(k)}). \end{cases}$$

For the convergence proof it is necessary to update the asymptotes like

$$l_j^{(k)} = x_j^{(k)} - (x_j^{(k-1)} - l_j^{(k-1)}),$$

$$u_j^{(k)} = x_j^{(k)} + (u_j^{(k-1)} - x_j^{(k-1)}),$$

if $\tilde{f}_j^{(k-1)}(x^{(k)}) \geq f_j(x^{(k)})$.

Then it can be shown [56] that the algorithm converges to a KKT-point of problem (6.3). Due to this property the algorithm is often denoted in the literature as globally convergent method of moving asymptotes (GCMMA). However, we want to mention that for any starting point the algorithm converges towards a KKT-point and not necessarily towards a local or even the global optimum.

MMA with line search

Zillober [65, 66] obtains a global convergence of the MMA method by introducing a line search with respect to the augmented Lagrange merit function L_A which is for a fixed parameter r defined by

$$L_A(x,\lambda) = f_0(x) + \sum_{i=1}^{m} \begin{cases} \lambda_i f_i(x) + \frac{r}{2} f_i^2(x), & \text{if } -\frac{\lambda_i}{r} \leq f_i(x), \\ -\frac{\lambda_i^2}{2r}, & \text{otherwise.} \end{cases}$$

To keep the notation simple we just consider it for problem (6.3) without artificial variables. The transformation to the extended case is straightforward. The line search works as follows.

Let $(\tilde{x}, \tilde{\lambda})$ be the solution of the MMA subproblem in iteration k.

1. Let $s^k := \begin{pmatrix} \tilde{x} - x^k \\ \tilde{\lambda} - \lambda^k \end{pmatrix}$, $\delta^k = \|\tilde{x} - x^k\|$, and $\eta^k := \min\limits_{i=1,\ldots,n} \eta_i^k$, where

$$\eta_i^k := \begin{cases} \left(\frac{\partial f}{\partial x_i}(x^k) + \tau_i\right) \frac{2u_i - \tilde{x}_i^k - x_i^k}{(u_i - \tilde{x}_i^k)^2}, & \text{if } \frac{\partial f}{\partial x_i}(x^k) \geq 0, \\ \left(\tau_i - \frac{\partial f}{\partial x_i}(x^k)\right) \frac{-2l_i + \tilde{x}_i^k + x_i^k}{(\tilde{x}_i^k - l_i)^2}, & \text{if } \frac{\partial f}{\partial x_i}(x^k) < 0 \end{cases}$$

   and $\tau_i > 0$.

2. Compute $L_A(x^k, \lambda^k), \nabla L_A(x^k, \lambda^k), \nabla L_A(x^k, \lambda^k)^T s^k$.

The next step guarantees that the descent direction is sufficiently good. This is done by an adaptation of the parameter r of the augmented Lagrangian function, which is not changing the descent direction s^k itself, but instead the merit function for which the decrease is desired.

3. If $\nabla L_A(x^k, \lambda^k)^T s^k > -\eta^k (\delta^k)^2/2$ update penalty parameter r, $r^{new} = 10r$, and goto 2, otherwise let $\sigma = 1$.

4. Compute $f_0(x^k + \sigma(\tilde{x} - x^k))$ and $f_i(x^k + \sigma(\tilde{x} - x^k))$ for $i = 1, \ldots, m$ and $L_A((x^k, \lambda^k) + \sigma s^k)$.

Now an appropriate steplength has to be found. An Armijo condition is used for this.

5. If $L_A(x^k, \lambda^k) - L_A((x^k, \lambda^k) + \sigma s^k) < -c\sigma \nabla L_A(x^k, \lambda^k)^T s^k$, let $\sigma = \sigma \cdot \psi$ (where $0 < \psi, c < 1$) and goto step 4; otherwise let $\sigma^k = \sigma$.

6. Let $\begin{pmatrix} x^{k+1} \\ \lambda^{k+1} \end{pmatrix} := \begin{pmatrix} x^k \\ \lambda^k \end{pmatrix} + \sigma^k s^k$. Set $k := k + 1$ and solve the next MMA subproblem.

This procedure is repeated until a given termination criterion such as a sufficient small difference between two consecutive designs is fulfilled.

Zillober shows that under certain assumptions the penalty parameters r_j are bounded and that the sequence of iteration points x_j obtained by the SCP algorithm has an accumulation point and each accumulation point is a KKT point [66]. One of the assumptions says that in the neighbourhood of stationary points the multipliers have to decrease with at least the same order as the primal variables. If this assumption is not fulfilled a weaker convergence result can be proven which says that the iteration sequence has an accumulation point and at least one of the accumulation points is stationary.

All algorithms shown so far only used first derivatives. The drawback of these first order approximations is that once they have reached the neighbourhood of the optimum the convergence towards the optimum is very slow. To speed up the convergence process better approximations are needed which are based on curvature information. The inclusion of second order information into the approximation scheme can improve the quality of the approximation and leads to faster convergence rates. Svanberg extended his MMA approach by the consideration of non-mixed second-order derivatives [55]. However, it is generally very expensive to calculate the second derivatives and therefore this approach is often rejected. A possible remedy is shown in [9] where information from previous iterations is used to approximate the second derivative of the current iteration point.

Chapter 7

Computational results

This chapter presents the results of the calculations for the natural frequency optimization problem (5.1) and the vibration level optimization problem (5.2). As an example, the turbocharger in the engine of a passenger car as introduced in Chapter 1 is studied. At first, the configurations of two different finite element models are described which serve as initial design for the optimization process. Then results for the natural frequency optimization problem are presented in Section 7.2. The central optimization problem with vibration level constraints is treated in Section 7.3. In the latter case, additional calculations were performed for an extended set of design variables, including also variables for the bearing configuration. As support linear spring and damper support as well as nonlinear fluid-film bearings were considered. Numerical results are presented for all cases. Section 7.4 deals with the important question when feasible solution exists. Since the target values in the optimization problem are often set heuristically, it is not guaranteed that feasible solutions exist for our optimization problem. Therefore, it is our aim to determine target values for which it can be assured that the solution set of the optimization problem is nonempty. This is done by using the multicriteria optimization approaches which were explained in Chapter 5.

7.1 Description of rotor models

The two rotor models presented in this section are models representing current prototypes of turbochargers of TCRDL. They are taken as initial design for the optimization process. Later, when evaluating the numerical results, the optimized designs are compared with the initial ones. The complete specification of the shaft is given in Appendix C.

Model 1

Model 1 consists of 13 beam elements and two rigid disks which are attached at nodes 3 and 12. There exists spring support at nodes 7 and 9 and unbalance forces are assumed to act at nodes 2, 4, 11 and 13. The complete model is shown in Figure 7.1. The unbalance forces are indicated by arrows. Later this model is also studied with four times the number of beam elements to observe the behaviour for a finer discretization.

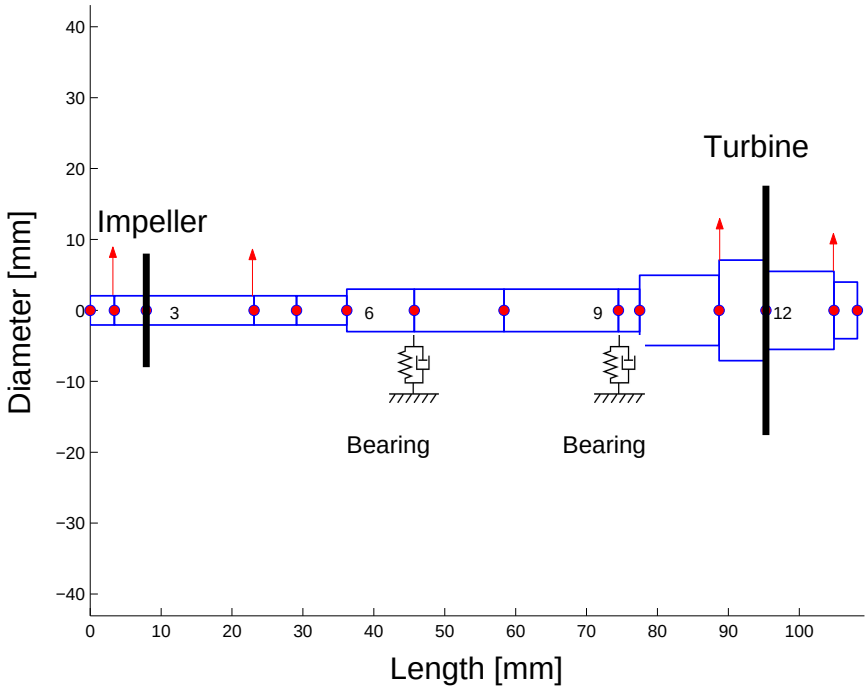

Figure 7.1. Initial design of model 1 with shaft, impeller, turbine, bearings and unbalance forces (red arrows).

For the formulation of the design optimization problem the choice of design variables is crucial. In our case the diameters d_i of the beam elements and the mass m_{τ_i} and moments of inertia $I_{d_{\tau_i}}, I_{p_{\tau_i}}$ of the rigid disks τ_i, $(i = 1, 2)$, representing impeller and turbine, are selected. The optimized values for mass and moments of inertia of the rigid disk are in a subsequent step transformed into a corresponding blade geometry by the engineer. The design variable vector q is written as

$$q = (d_1, \ldots, d_{n-1}, m_{\tau_1}, m_{\tau_2}, I_{d_{\tau_1}}, I_{d_{\tau_2}}, I_{p_{\tau_1}}, I_{p_{\tau_2}}).$$

The lower and upper bounds on the diameter of the beam elements are given by $\underline{q} = 0.003$ m and $\bar{q} = 0.05$ m except in the vicinity of the bearings where we have $\underline{q} = 0.004$ m and $\bar{q} = 0.008$ m due to limitations of the casing size. These bounds

are set to avoid critical stress and guarantee stability for the optimized design. For the other design variables we have $\underline{q} = \underline{\beta} \cdot q^{(0)}$ and $\bar{q} = \bar{\beta} \cdot q^{(0)}$, where $\underline{\beta} = 0.9$ and $\bar{\beta} = 1.1$ and $q^{(0)}$ contains the values for the initial design.

Model 2

To be able to take care of different material used in the manufacturing of the rotor, modifications of the model were made that allow an inner and an outer shaft part of certain beam elements. In our element matrices (see Appendix B) we have to modify the expressions for μ, I_p and EI_a. The mass per unit length $\mu = r^2\pi\rho$ becomes

$$\mu = \pi(r_i^2\rho_i + (r_o^2 - r_i^2)\rho_o),$$

where r_i and ρ_i are radius and density of the inner shaft part and r_o and ρ_o the corresponding values of the outer shaft. Analogously, we can transform the expression for the polar moment of inertia

$$I_p = \frac{\pi}{2}(r_i^4\rho_i + (r_o^4 - r_i^4)\rho_o)$$

and for the bending rigidity we have

$$EI_a = \frac{\pi}{4}(r_i^4 E_i + (r_o^4 - r_i^4)E_o),$$

where E_i and E_o are the values of Young's modulus for inner and outer shaft part.

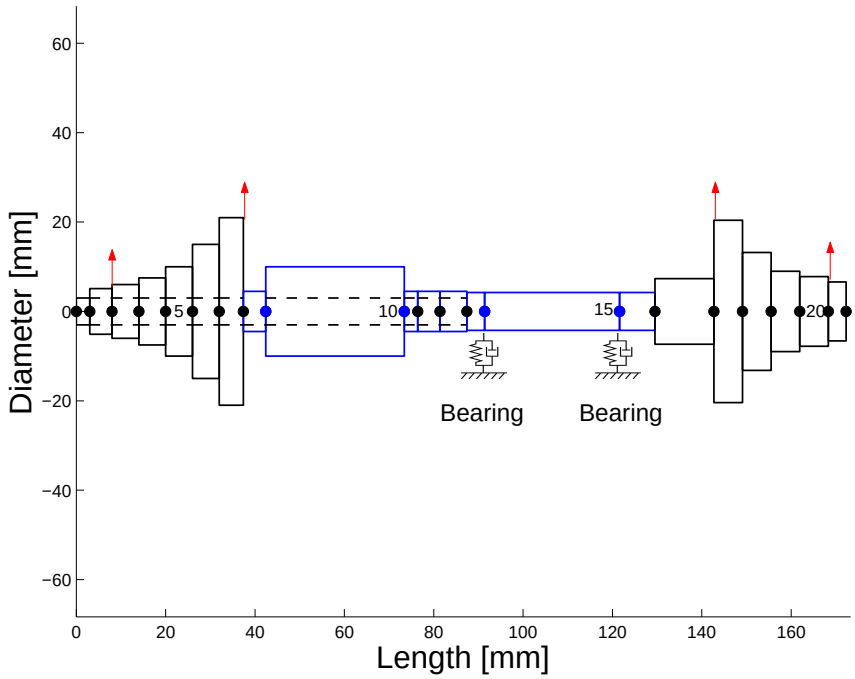

Figure 7.2. Initial design of model 2 with shaft, bearings and unbalance forces (red arrows). Blue shaft elements indicate design variables.

These modifications are realized in model 2 (see Figure 7.2) which consists of 21 beam elements. No rigid disks are used here but instead turbine and impeller are modeled by a larger diameter of the beam elements. In this model only the diameters d_i (of the outer shaft) of some beam elements are selected as design variables. Those elements are indicated in blue color in the figure. Moreover, the lengths l_i of certain elements are chosen as variables. The nodes of these two elements are drawn in blue. The design variable vector q in our concrete case is given by

$$q = (d_8, d_9, d_{10}, d_{11}, d_{12}, d_{13}, d_{14}, d_{15}, l_9, l_{14}).$$

We refer again to Appendix C for the complete specification of the shaft.

Remark. The approach presented in Chapters 1-6 holds for a general class of rotating bodies. The physical model which is used captures effects common to all such bodies. For certain applications, like the turbocharger as considered example, additional effects such as aerodynamic effects, might play a role. However, in our research we want to focus on the validity of the optimization approach for the general class of rotors and neglect the additional effects.

7.2 Natural frequency optimization problem

We start with some calculations which were done for model 1. If the support is not mentioned explicitly, linear spring and damper support is assumed. It is the aim to minimize the mass while raising the natural frequencies of the first and second bending mode (denoted with subscript bm1 and bm2) by 10%. The formulation of this natural frequency optimization problem is then

$$\begin{aligned}
&\min_q \operatorname{mass}(q)\\
&\text{subject to}\\
&\lambda_{\mathrm{bm1}}(q) \geq \alpha_{\mathrm{bm1}} \cdot \lambda^{(0)}_{\mathrm{bm1}},\\
&\lambda_{\mathrm{bm2}}(q) \geq \alpha_{\mathrm{bm2}} \cdot \lambda^{(0)}_{\mathrm{bm2}},\\
&\underline{q}_i \leq q_i \leq \bar{q}_i, \quad i = 1, \ldots, n_{dv},
\end{aligned}$$

where we set $\alpha_{\mathrm{bm1}} = \alpha_{\mathrm{bm2}} = 1.1$ and $\lambda^{(0)}_{\mathrm{bm1}}$ and $\lambda^{(0)}_{\mathrm{bm2}}$ are the values for the initial design.

The mass of the initial model is 0.0929 kg and in the static case of 0 Hz we obtain as frequency for the initial design

$$\lambda^{(0)}_{\mathrm{bm1}} = 1636\,\mathrm{Hz} \quad \text{and} \quad \lambda^{(0)}_{\mathrm{bm2}} = 2635\,\mathrm{Hz}$$

and the assignment is determined by drawing the modes. In Figure 7.3 it can be seen that below the bending modes there are two other natural frequencies. These lower

frequencies belong to rigid modes. Due to the gyroscopic terms the natural frequencies depend on the rotational speed and this behaviour can be seen in the figure. For every mode the frequency splits into two parts which are, respectively, above and below their associated zero-running-speed natural frequency. The increasing one represents the forward whirling direction of the mode. It is subject to unstable whirling motion. and therefore the frequency which we study. The decreasing one is the backward whirling direction which we neglect, since no excitation occurs (see e.g [11]).

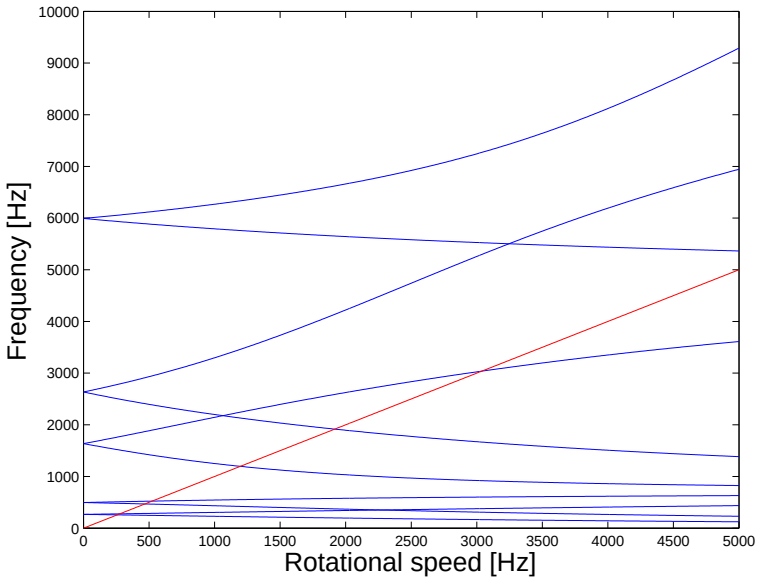

Figure 7.3. Natural frequencies of first ten modes for initial design in dependence of rotational speed and bisecting line (red).

Moreover, we added the bisecting line which represents the resonance case. The intersection of this line with the frequencies of the modes gives us the critical speeds of the different modes which is of major interest for us. Figure 7.3 serves as a good illustration for the frequency and critical speed pattern. In numerical calculations the critical speeds are of course determined analytically by the method introduced in Section 4.4.

Calculations were done for a rotational speed $\omega = 1000$ Hz and model 1 with 13 and 52 beam elements, respectively. The latter model is a refinement of the former one to obtain a smoother design and every beam element is divided into four equal parts. Initial and target frequencies for the two cases are obviously equal and are as follows.

For the initial design we have

$$\lambda_{\mathrm{bm1}}^{(0)} = 2145\,\mathrm{Hz} \quad \text{and} \quad \lambda_{\mathrm{bm2}}^{(0)} = 3297\,\mathrm{Hz},$$

which gives the target frequencies

$$\lambda^*_{\mathrm{bm1}} = 1.1 \cdot \lambda^{(0)}_{\mathrm{bm1}} = 2359\,\mathrm{Hz} \quad \text{and} \quad \lambda^*_{\mathrm{bm2}} = 1.1 \cdot \lambda^{(0)}_{\mathrm{bm2}} = 3626\,\mathrm{Hz}.$$

Model 1 with 13 beam elements

The numerical results show that we obtain the same optimized structure for SLP and MMA. In Figure 7.4 the initial and the optimized model are drawn in one picture to make the difference clear between both designs. The initial model is indicated by the dashed black line and the optimized model is drawn in blue. Design variables, where the lower bound constraint is active, are drawn in red.

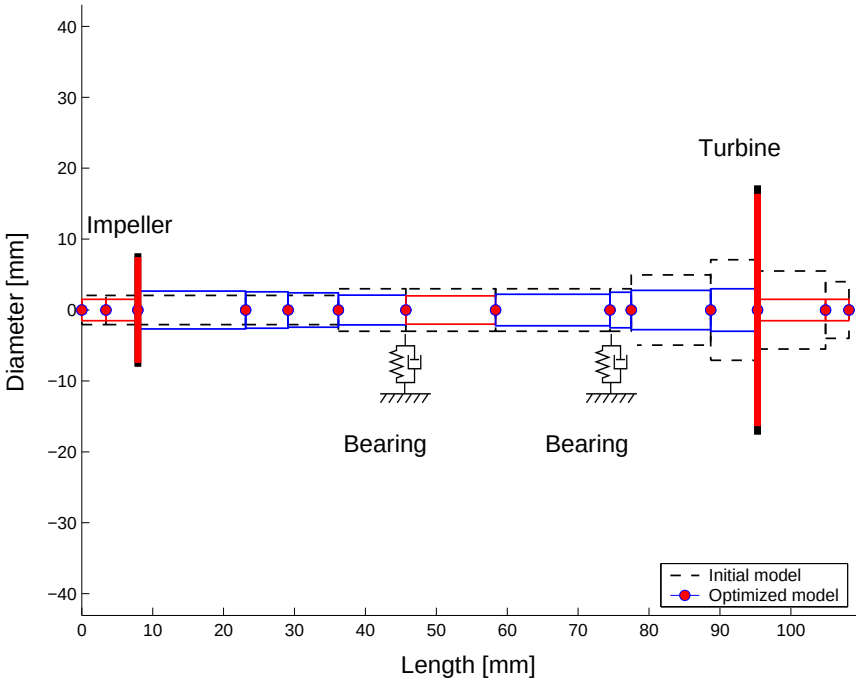

Figure 7.4. Initial and optimized structure of model 1 with 13 beam elements for natural frequency optimization problem and $\omega = 1000$ Hz.

We notice that the rotor becomes thin at the end parts and in the center part. The diameters of the beam elements at the end even attain the lowest possible value. The same holds for the mass of the rigid disks leading to a large contribution for the reduction of the total mass. The mass of the optimized design is 0.0651 kg, which is 70.1% of the initial mass. This reduction of weight leads to a better response and higher efficiency of the rotor. Figure 7.5 shows the iteration history of the objective function for the SLP and the MMA algorithm.

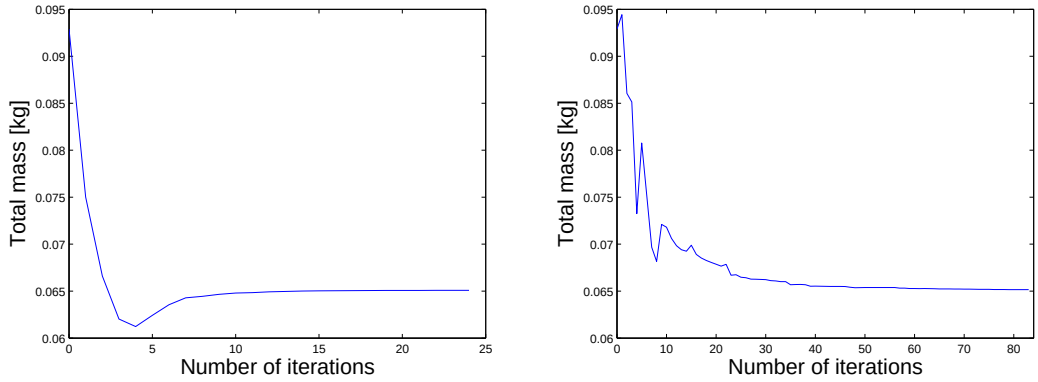

Figure 7.5. History of objective function for SLP (left) and MMA (right) algorithm for natural frequency optimization problem and model 1 with 13 beam elements.

Typical features of the algorithms can be observed. Using a proper choice of move limits the SLP algorithm quickly reaches a design satisfying the termination criterion. However, the algorithm tends to stay in the infeasible design space due to the linearization error which becomes obvious at the iteration history of the constraint on the second bending mode (see Figure 7.7).
The MMA algorithm immediately produces designs belonging to the feasible domain. After few iterations the designs are in the neighbourhood of an optimum but some more iterations are needed until the termination criterion is fulfilled. The big difference to SLP is that after a small number of iterations each design during the iteration process is feasible (see Figure 7.6 and 7.7) and hence the algorithm can be terminated earlier while satisfying all constraints.

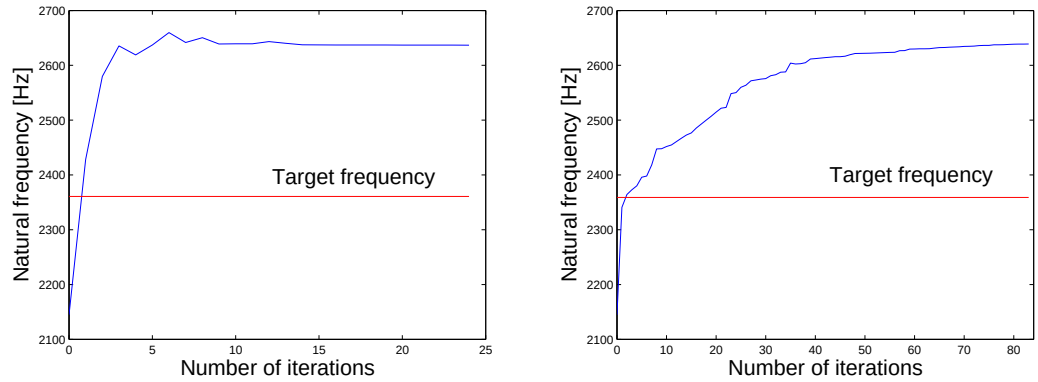

Figure 7.6. History of constraint function for natural frequency of first bending mode for SLP (left) and MMA (right) algorithm and target frequency (red) as lower bound.

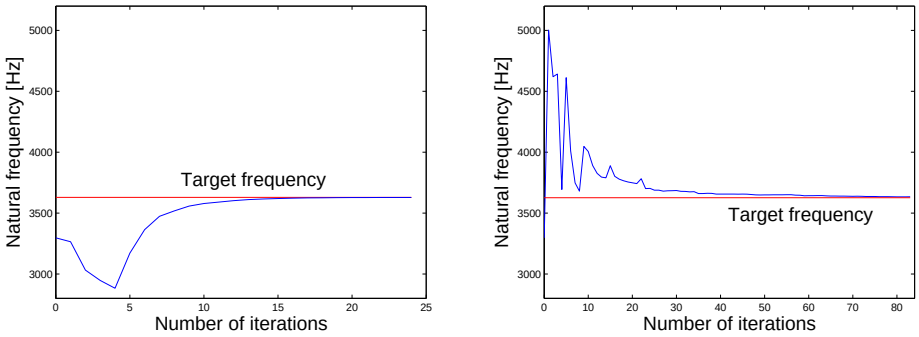

Figure 7.7. History of constraint function for natural frequency of second bending mode for SLP (left) and MMA (right) algorithm and target frequency (red).

The numerical calculations show that for the convergence of the algorithm a proper choice of the parameters is essential. The increase and decrease parameters given by the move limit strategies explained in Chapter 6 have to be chosen to be quite tight to avoid convergence to a bad point and oscillations in the convergence process.

Model 1 with 52 beam elements

Calculations for a refined model with four times the number of beam elements were performed to consider more degrees of freedom. The calculation time then, of course, rises. The shape of the rotor does not change significantly. As expected the design is smoother than previously and greater jumps in diameter only occur at the position of impeller and turbine. The initial and optimized design is shown in Figure 7.8.

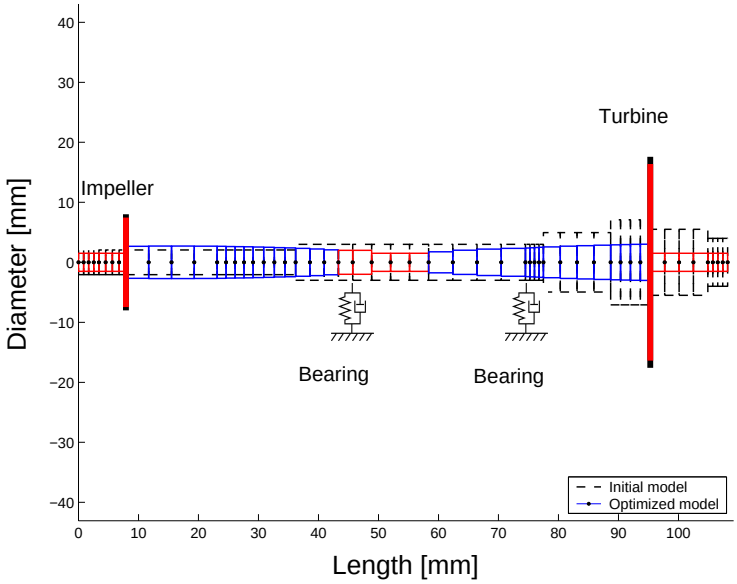

Figure 7.8. Initial and optimized structure of model 1 for natural frequency optimization problem for $\omega = 1000$ Hz and 52 beam elements.

Due to the finer model the flexibility is increased and the mass is further reduced. It is now 0.0646 kg compared with 0.0651 kg in the model with 13 beam elements, which is 69.5% of the mass of the initial design.

7.3 Vibration level optimization problem

We now turn to our central optimization problem, i.e. the minimization of the mass of the rotor subject to constraints on the vibration level. In general it is our aim to increase a certain critical speed by 10% and to decrease the unbalance response of a certain mode by 20%. These percentage values are set according to experience and desire of the engineer. In order to solve the optimization problem, the critical speeds lying in the frequency range of interest, have to be determined at first. Then the unbalance response which is the main target of our studies is calculated.

The first step is to look at the initial design to figure out the modes of interest. To get an impression which modes lead to problems the unbalance responses are calculated in a rotational speed range from 0 to 5000 Hz. This gives an overview about the vibration levels in the relevant operating speed range. Modes with extremely high amplitude are then selected to be targets of our optimization process and their amplitudes need to be reduced.

I) Results for model 1 with spring support

For model 1 the Euclidean norm of the displacement vector $\tilde{y}$ is taken as measure for the unbalance response (see equation (4.17)).

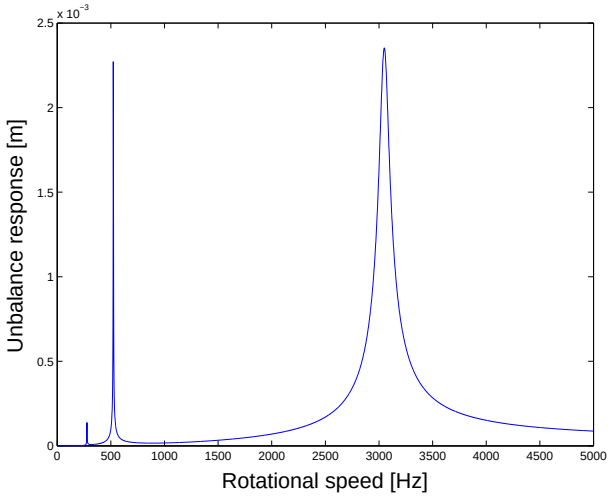

Figure 7.9. Vibration level for initial design of model 1.
Large unbalance response for conical mode (left) and first bending mode (right).

We can see that for two modes the unbalance responses in the resonance case are extremely high. These are therefore the modes we should take care of and include in our optimization problem. Mode shapes can be drawn since the eigenmode vector contains information about the lateral displacements at each node. Drawing the mode shapes shows that the two critical modes are the second rigid mode, which is a conical mode, and the first bending mode. The critical speeds are determined analytically by the method described in Section 4.4 and the exact unbalance response for each critical speed is calculated by equation (4.17).

The values of the critical speeds of rigid and bending modes and the amplitudes for the initial design are

$$\omega_{\mathrm{rm}} = 523\,\mathrm{Hz}, \quad \omega_{\mathrm{bm}} = 3049\,\mathrm{Hz},$$
$$a_{\mathrm{rm}} = 0.00239\,\mathrm{m}, \quad a_{\mathrm{bm}} = 0.00235\,\mathrm{m}.$$

We study the following vibration level optimization problem and demand a decrease of the unbalance response of the initial design by 20%,

$$\begin{aligned} &\min_q \mathrm{mass}(q) \\ &\text{subject to} \\ &\omega_{\mathrm{bm1}}(q) \geq \omega^*_{\mathrm{bm1}} = 1.1 \cdot \omega^{(0)}_{\mathrm{bm1}}, \\ &\omega_{\mathrm{rm}}(q) \geq \omega^*_{\mathrm{rm}} = 1.05 \cdot \omega^{(0)}_{\mathrm{rm}}, \\ &a_{\mathrm{bm1}}(q) \leq a^*_{\mathrm{bm1}} = 0.8 \cdot a^{(0)}_{\mathrm{bm1}}, \\ &a_{\mathrm{rm}}(q) \leq a^*_{\mathrm{rm}} = 0.8 \cdot a^{(0)}_{\mathrm{rm}}, \\ &\underline{q}_i \leq q_i \leq \bar{q}_i, \quad i = 1, \ldots, n_{dv}, \end{aligned} \tag{7.1}$$

where $\omega^{(0)}_{\mathrm{bm1}}, \omega^{(0)}_{\mathrm{rm}}, a^{(0)}_{\mathrm{bm1}}$ and $a^{(0)}_{\mathrm{rm}}$ are critical speeds and unbalance responses for the initial design. The increase of the critical speed of the rigid mode is of minor importance. Therefore we choose a factor of only 1.05. This results in the target values

$$\omega^*_{\mathrm{rm}} = 549\,\mathrm{Hz}, \quad \omega^*_{\mathrm{bm}} = 3354\,\mathrm{Hz}, \quad a^*_{\mathrm{bm}} = 0.00188\,\mathrm{m}, \quad a^*_{\mathrm{rm}} = 0.00191\,\mathrm{m}.$$

The mass of the initial model is 0.0929 kg.

As derived in Section 5.3, the expression for one component of the unbalance response vector is given by

$$c_k = \sum_{j=1}^{n_f} \sum_{l=1}^{N} \frac{\xi_{\nu_j,l} \phi_{k,l} \hat{f}_{\nu_j}}{i\omega - \lambda_l}, \tag{7.2}$$

where ν_j are the indices of the nonzero components of $\tilde{f}$ and ξ and ϕ are left and right eigenmodes. In this term the sum over all modes is considered. This increases computational time for the sensitivities a lot. Therefore we want to study whether

the number of considered modes could be reduced. Indeed, it shows that in the eigenvalue analysis for the critical speed of the specific mode, the natural frequency of this mode is close to its critical speed, thus contributing to a dominating part to the unbalance response expression (7.2). This behaviour was examined numerically and can be seen in the Figures 7.10 and 7.11.

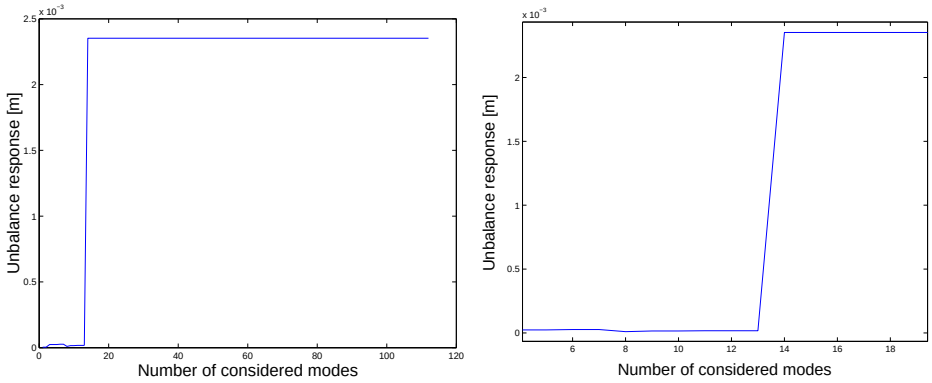

Figure 7.10. Dependence of unbalance response of bending mode on number of considered modes and close-up of left figure.

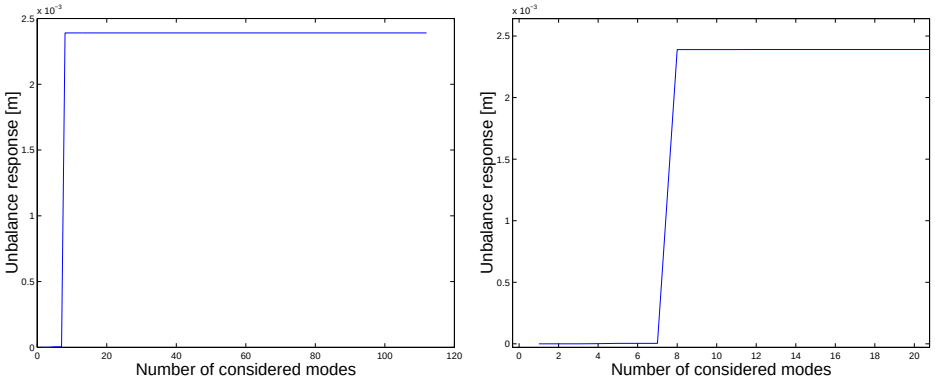

Figure 7.11. Dependence of unbalance response of rigid mode on number of considered modes and close-up of left figure.

We see that the decisive mode numbers for the second rigid mode and the first bending mode are $l^* = 8$ and $l^* = 14$, respectively. Considering only one of these modes for the calculations of the derivatives is sufficient and formula (7.2) becomes

$$\hat{c}_k = \sum_{j=1}^{n_f} \frac{\xi_{\nu_j,l^*}\phi_{k,l^*}\hat{f}_{\nu_j}}{i\omega - \lambda_{l^*}}.$$

This speeds up calculations a lot. In both cases the approximation error compared with the full set of modes is less than 0.0001%, i.e.

$$\frac{|\hat{a} - a|}{a} < 10^{-4}.$$

The numerical calculations then yield for problem (7.1) the optimized structure which is shown in Figure 7.12.

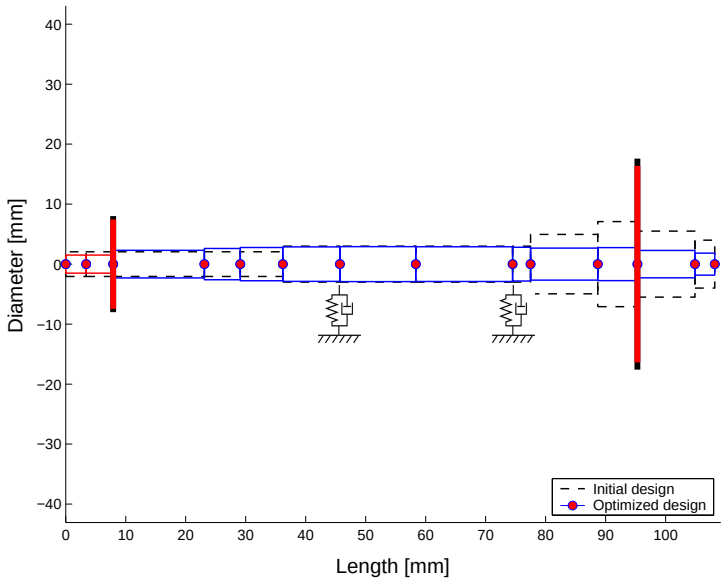

Figure 7.12. Initial and optimized design for vibration level optimization problem for model 1.

The optimized rotor in this case is slightly thicker than in the case of the natural frequency problem. Only the design variables of the diameters at the left end and the mass of the rigid disk hit the lower bound constraint. The values for the optimized design are

$$\omega_{\mathrm{bm}} = 3354\,\mathrm{Hz}, \quad \omega_{\mathrm{rm}} = 603\,\mathrm{Hz}, \quad a_{\mathrm{bm}} = 0.00181\,\mathrm{m}, \quad a_{\mathrm{rm}} = 0.00191\,\mathrm{m}$$

with the mass being 0.06898 kg. This corresponds to 74.3% of the initial mass. We recognize that the constraints on the critical speed of the bending mode as well as on the vibration level of the rigid mode are active. Figure 7.13 shows that the desired increase in critical speed and decrease in vibration level can be achieved. Hence the rigid and conical modes of the optimized rotor have smaller amplitudes (see small figures in Figure 7.13) which leads to less noise and increased reliability.

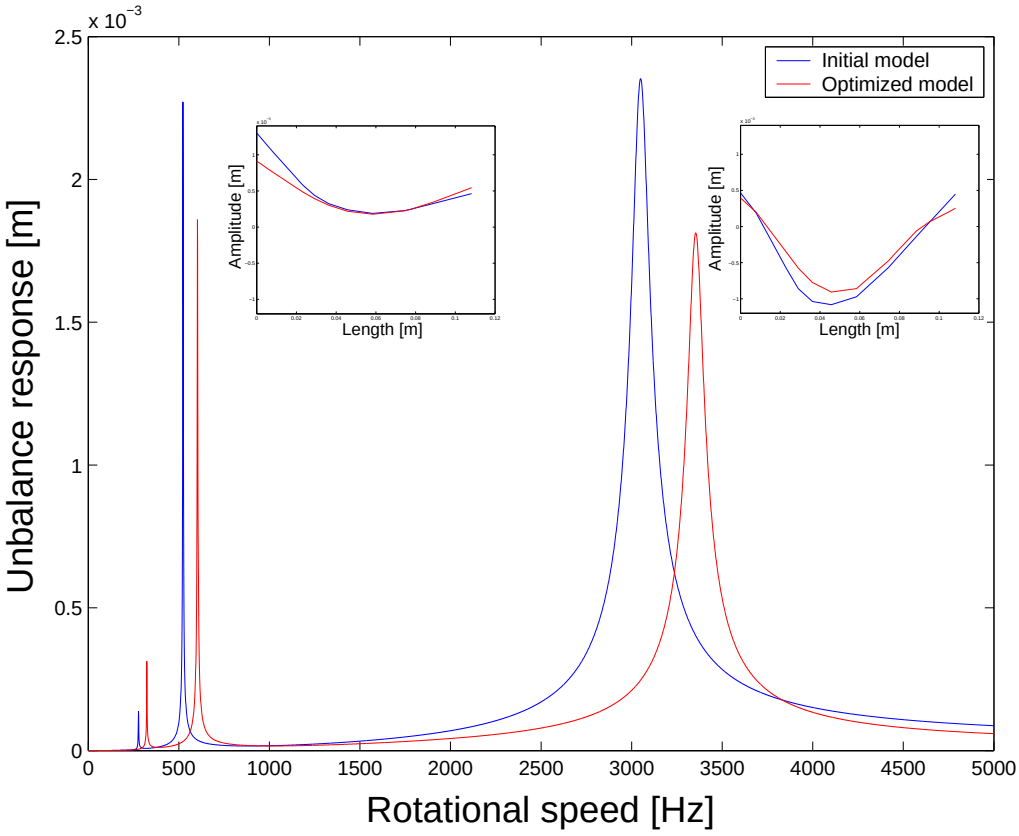

Figure 7.13. Vibration level of initial and optimized design for model 1. Initial and optimized mode shapes of conical mode (left) and bending mode (right) can be seen in the small figures.

The SLP and MMA algorithms show qualitatively the same behaviour as for the natural frequency optimization problem.

Additional design variables for model 1

Bearings have a great influence on the behaviour of the turbocharger. Hence we expect changes to the previous optimization process if we consider bearing coefficients as design variables. This is in the first step done by keeping the linear spring and damper assumption but taking the previously constant damping and stiffness coefficients c_{b_i} and k_{b_i} as design variables. The change of values of the bearing coefficients in the optimization process is then transformed into a different bearing configuration. The extended design variable vector is given by

$$\tilde{q} = (d_1, \ldots, d_{n-1}, m_{\tau_1}, m_{\tau_2}, I_{d_{\tau_1}}, I_{d_{\tau_2}}, I_{p_{\tau_1}}, I_{p_{\tau_2}}, c_{b_1}, c_{b_2}, k_{b_1}, k_{b_2}).$$

Each matrix in the equation of motion is depending on certain design variables, i.e. we have

$$M(\tilde{q})\ddot{x} + (\omega G(\tilde{q}) + C(\tilde{q}))\dot{x} + (K(\tilde{q}) + K_b(\tilde{q}))x = fe^{i\omega t}.$$

Numerical calculations indeed show that we obtain a significant reduction of the vibration level if we additionally consider damping and stiffness coefficients as design variables. The SLP, MMA and GCMMA algorithms are applied to this problem. It shows that the calculations are highly dependent on the choice of parameters. Even small changes in the move limit strategy or choice of asymptotes, respectively, lead to different results of the optimization problem.

Figure 7.14 shows the optimized structure for the choice of parameters, which led to the smallest mass.

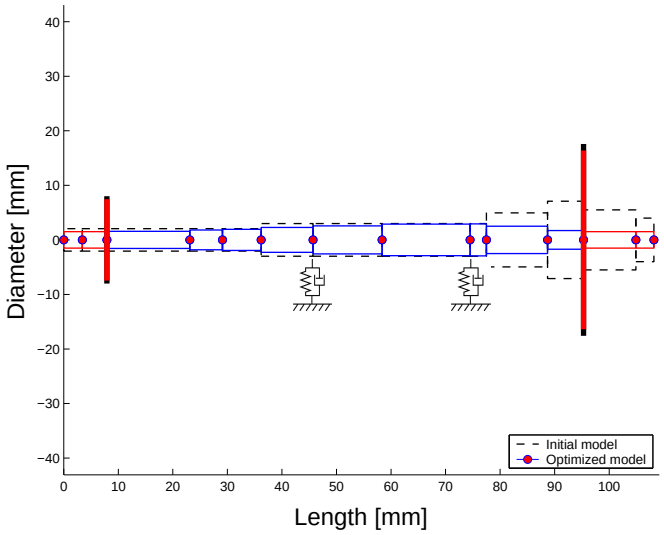

Figure 7.14. Initial and optimized design for vibration level optimization problem under consideration of additional design variables representing bearing parameters for model 1.

The values for the optimized design of the three algorithms are given in Table 7.1.

	SLP	MMA	GCMMA	Target values
Mass [kg]	0.06409	0.06512	0.06438	
ω_{rm} [Hz]	549	593	556	549
ω_{bm} [Hz]	3354	3400	3400	3354
a_{rm} [m]	0.0019	0.0018	0.0018	0.0019
a_{bm} [m]	$5.25 \cdot 10^{-4}$	$4.66 \cdot 10^{-4}$	$4.52 \cdot 10^{-4}$	0.0019

Table 7.1. Values for optimized designs for vibration level optimization problem for model 1 for SLP, MMA and GCMMA algorithm.

We observe that the introduction of the additional design variables makes a further reduction of mass possible which is now 0.064 kg being only 68.8% of the initial mass. The three algorithms reach slightly different local optimums. This can be explained by the high nonlinearity of the constraint functions. The GCMMA algorithm guarantees that we indeed obtain a KKT point.

The most remarkable observation is that the amplitude of the second bending mode is further decreased to a large extent. The unbalance response of the first bending mode is now only 23.8% of the unbalance response of the initial design. This is possible without changing the constraint explicitly. The behaviour can be explained by an increased damping coefficient after the design optimization process. The new unbalance response behaviour can be seen in Figure 7.15.

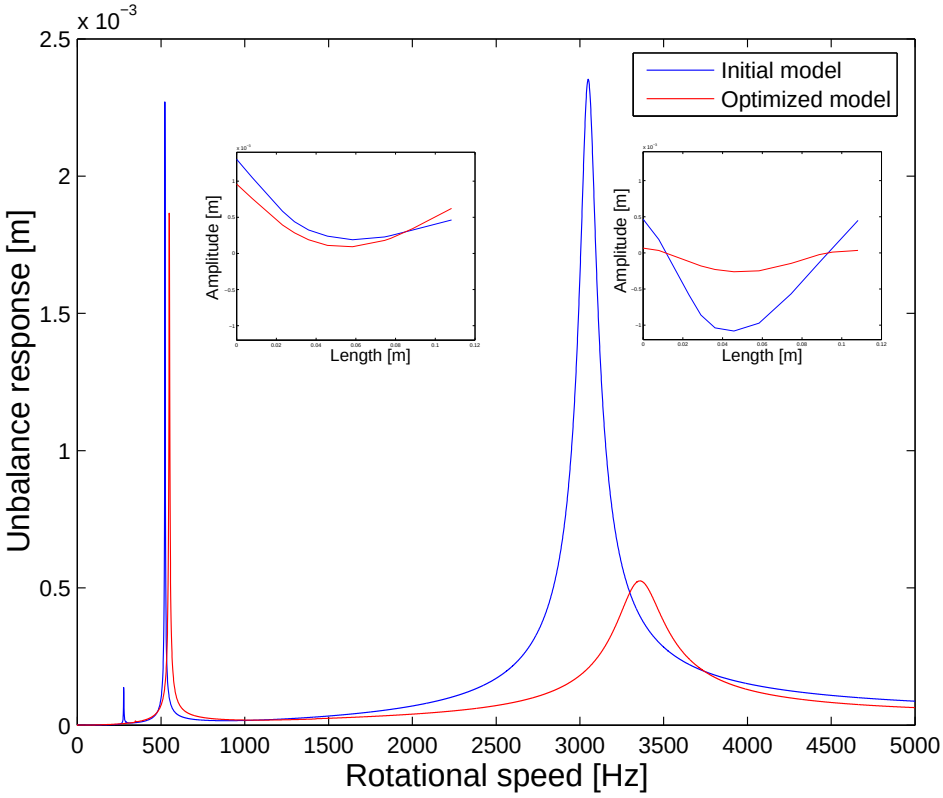

Figure 7.15. Vibration level of initial and optimized design for vibration level problem for model 1 under consideration of additional design variables representing bearing parameters. Initial and optimized mode shapes of conical mode (left) and first bending mode (right) can be seen in the small figures.

The iteration history of the three algorithms (see Figure 7.16) show again their typical behaviour. The SLP algorithm reaches temporarily a smaller mass, but this is at the expense of a violation of the constraints. Compared to the previous example of the natural frequency optimization problem (see Figure 7.5), MMA reaches faster the neighbourhood of the optimum and needs slightly fewer iterations until termination. The GCMMA algorithm shows a monotone decrease and is a little bit slower than MMA.

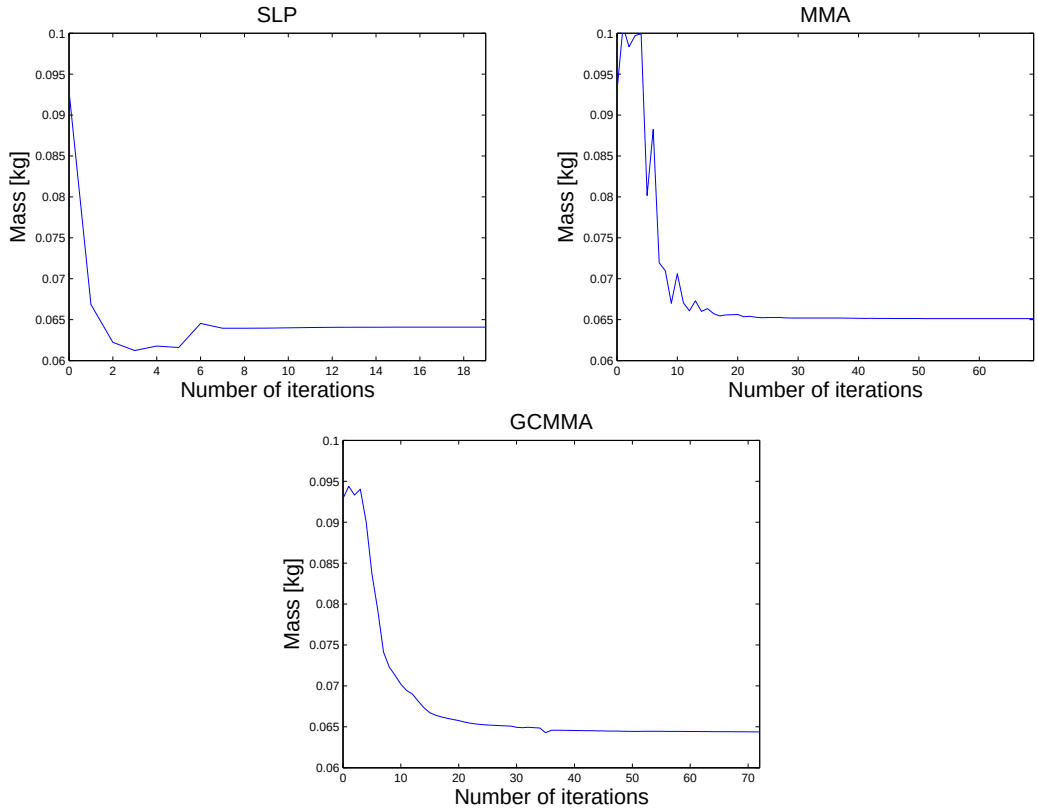

Figure 7.16. History of objective function for SLP (upper left), MMA (upper right) and GCMMA (bottom) algorithm for vibration level problem with extended design variable vector.

Remark. The given optimization problem with constraints on the vibration level can be solved successfully fulfilling all constraints and leading to a substantial reduction of mass of the rotor. The used optimization algorithms tend to reach quickly the neighbourhood of a local optimum, though it may take a while until they terminate depending on the termination criterion. MMA generates usually feasible designs, whereas SLP happens to iterate also in the infeasible design space. By considering additional design variables like bearing parameters better results, i.e. a lighter structure and reduced amplitudes, can be obtained.

II) Results for model 2 with spring support

The solution of a vibration level optimization problem is now performed for **model 2** in the same way as above.

The initial mass of the turbocharger is 0.28934 kg. To determine the modes that cause problems the unbalance response on the whole rotational speed range is calculated and is drawn in Figure 7.17.

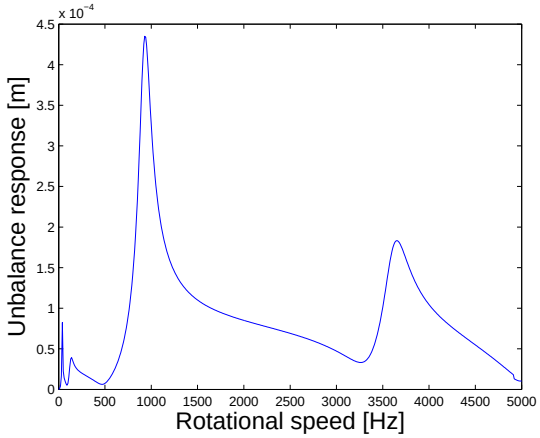

Figure 7.17. Vibration level of initial design for model 2.

It can be seen that the largest amplitude occurs at $\omega_1 = 924$ Hz and $\omega_2 = 3608$ Hz. Drawing the modes shows that these are the first and second bending mode.

In this model the unbalance response is measured by the displacement at node 1 and for the amplitude belonging to the first bending mode we obtain a value of

$$a(\omega_{\mathrm{bm1}}(q)) = 4.311 \cdot 10^{-4}\,\mathrm{m}.$$

The target of the optimization is to reduce the large amplitude of the first bending mode. Moreover, the critical speed of the second bending mode should be shifted to a higher frequency so that it is not reached under operating conditions. The desired target values [30] are then

$$\omega^*_{\mathrm{bm2}} = 3900\,\mathrm{Hz}, \quad a^*_{\mathrm{bm1}} = 3.8 \cdot 10^{-4}\,\mathrm{m}.$$

Thus, the optimization problem we solve is given by

$$\begin{aligned} &\min_q \mathrm{mass}(q) \\ &\text{subject to} \\ &\omega_{\mathrm{bm2}}(q) \geq 3900\,\mathrm{Hz}, \\ &a(\omega_{\mathrm{bm1}}(q)) \leq 0.38\,\mathrm{mm}, \\ &\underline{q}_i \leq q_i \leq \bar{q}_i, \quad i = 1, \ldots, n_{dv}. \end{aligned} \tag{7.3}$$

Again we speed up the calculations by simplifying the unbalance response expression. The mode we have to consider is in this case mode number 12.

The optimized structure obtained by SLP, MMA and GCMMA is shown in Figure 7.18.

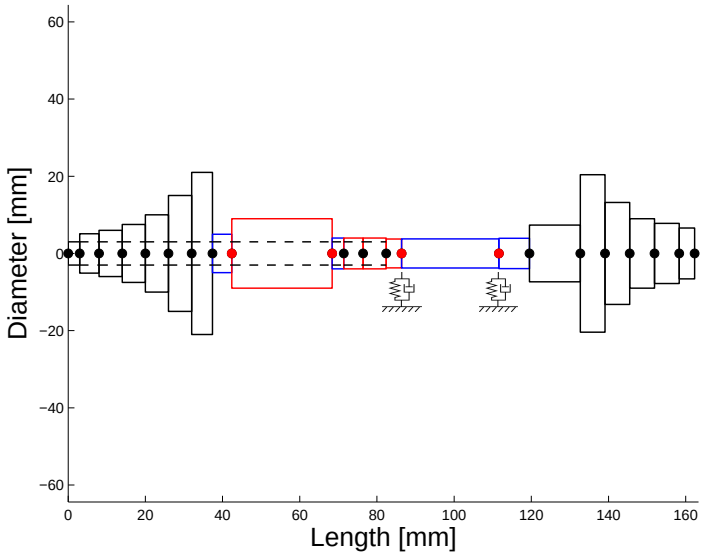

Figure 7.18. Optimized design for vibration level optimization problem for model 2.

Again the design variables that are active at the lower bound are drawn in red. These are the diameters of beam elements 9, 11, 12 and 13 as well as both length design variables. The mass of the optimized structure is 0.2585 kg, which is 89.4% of the initial mass. All values for this case are summarized in Table 7.2.

	SLP	MMA	GCMMA	Target values
Mass [kg]	0.25854	0.25858	0.25852	
ω_{bm2} [Hz]	3900	3902	3900	3900
a_{bm1} [m]	$3.34 \cdot 10^{-4}$	$3.33 \cdot 10^{-4}$	$3.26 \cdot 10^{-4}$	$3.8 \cdot 10^{-4}$

Table 7.2. Values for optimized design for vibration level optimization problem for model 2.

The differences in the results for the three algorithms are smaller than in the case of model 1 (compare Table 7.1). The critical speed constraint is almost hit exactly by all algorithms. An interesting observation is that the important unbalance response value a not only fulfills the constraint but can even be decreased below the target value. The optimized values is about 77 % of the initial value. The complete

vibration level behaviour is shown in Figure 7.19. We notice that even the second large amplitude, in our case the second bending mode with the initial critical speed $\omega_2 = 3608$ Hz, is significantly smaller for the optimized design. This happens without being explicitly targeted in the optimization problem.

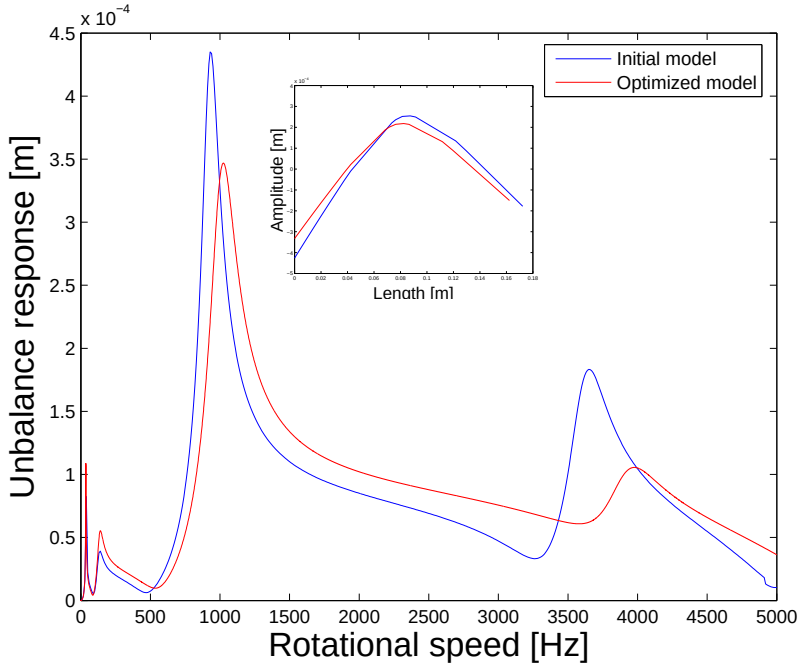

Figure 7.19. Vibration level for initial and optimized design for vibration level problem for model 2. Initial and optimized mode shape of the first bending mode in the small figure.

Again, we want to have a look at the iteration history of the objective functions of the three algorithms (see Figure 7.20). The fast convergence to the optimum can be seen in all cases. For MMA we have no longer any oscillations at the beginning and instead as in the case of GCMMA a monotone decrease to the optimum. In the SLP algorithm the minimum is still approached from the infeasible design space. SLP and MMA both need only around 20 iterations until termination, whereas GCMMA needs some more iterations. An interesting alternative to the SLP, MMA and GCMMA algorithms is the MMA with line search, also introduced in Chapter 6. It shows a nice monotone decrease towards a point, which is guaranteed to be a KKT-point.

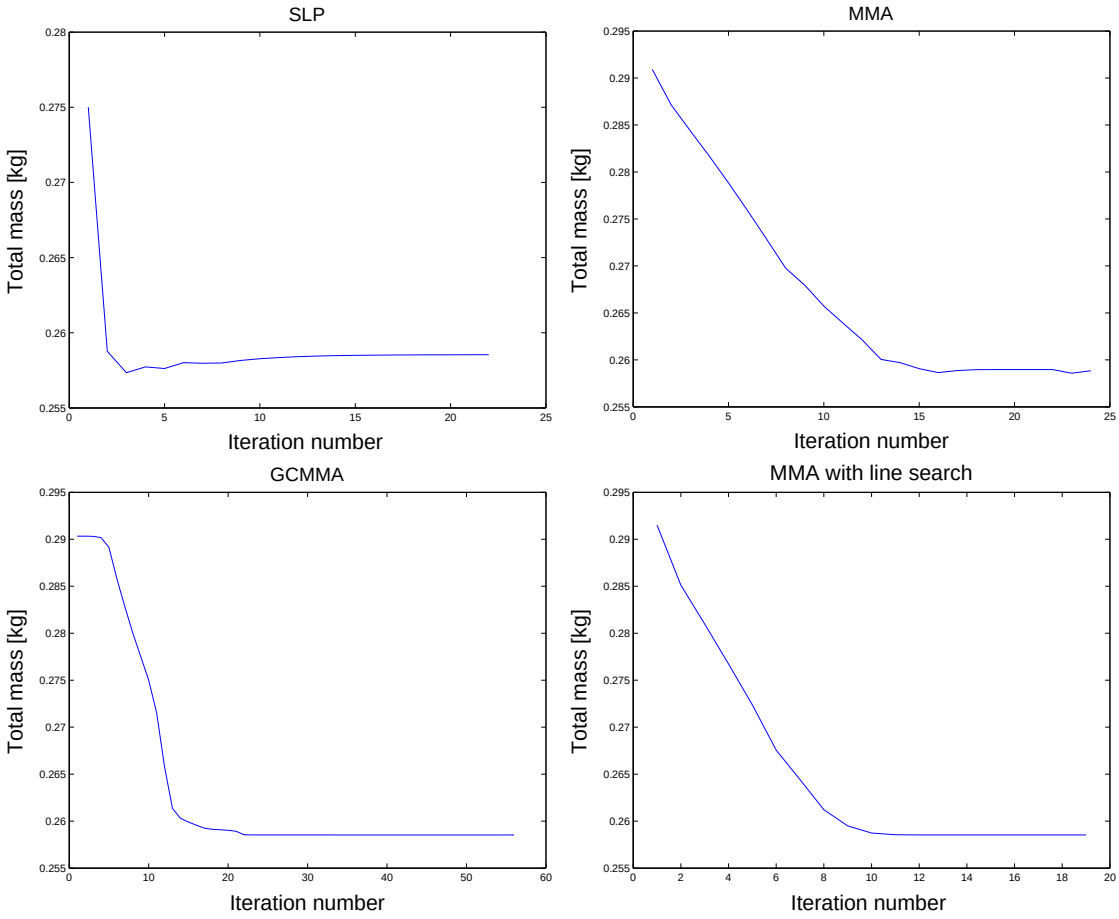

Figure 7.20. History of objective function for SLP (upper left), MMA (upper right), GCMMA (bottom left) and MMA with line search (bottom right) algorithm for vibration level problem for model 2.

Additional design variables for model 2

Calculations for model 2 were also done for the case capturing additional design variables. Again, a further decrease in the vibration level can be observed, which occurs without tightening the constraint. The new value of the unbalance response for the amplitude of the first bending mode is

$$a = 2.58 \cdot 10^{-4}\,\mathrm{m},$$

which is only 60% of the initial value.

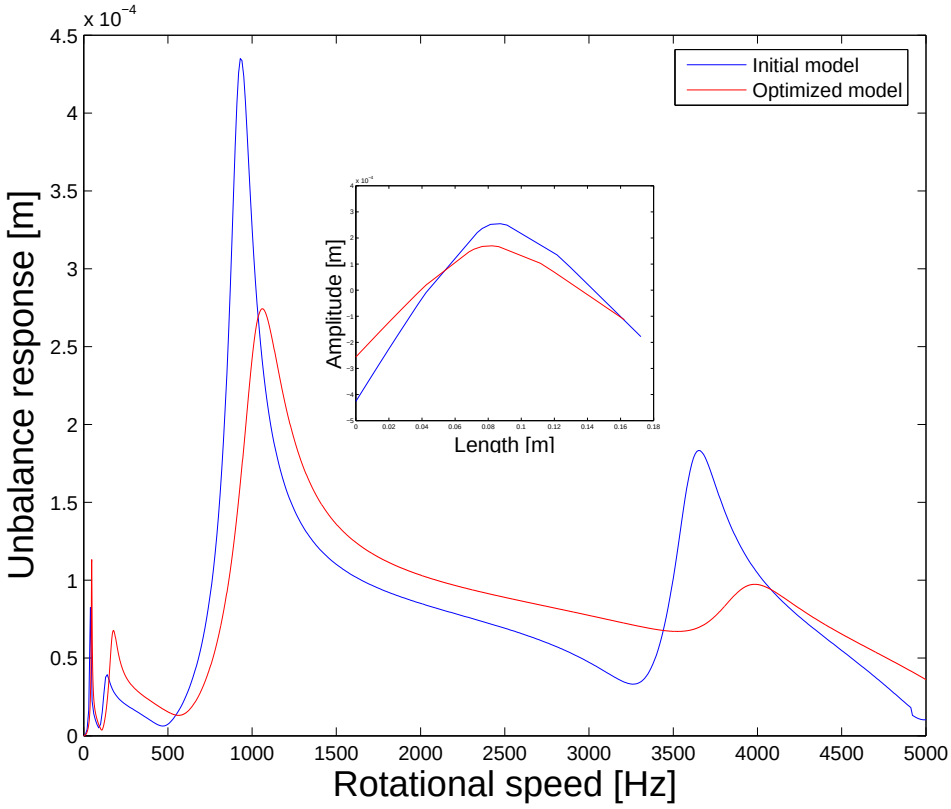

Figure 7.21. Vibration level for initial and optimized design for vibration level problem for model 2 in the case of an extended design variable vector including bearing coefficients. Initial and optimized mode shape of the first bending mode in the small figure.

We observe that also in the case of model 2 the given optimization problem can be solved successfully while satisfying all constraints. All considered algorithms showed fine convergence behaviour. Additional design variables representing bearing coefficients led to a further improvement of the results.

III) Results for models including nonlinear oil film forces

Model 1

We now want to give results for the vibration level optimization problem for our models including nonlinear bearing forces. The sensitivity analysis of the optimization algorithms has to respect the nonlinear terms as explained in Section 5.6.

Before solving the vibration level optimization problem we have to look again at the vibration behaviour of the initial models. We observe, that the oil film forces

significantly change the behaviour of the shaft. Figure 7.22 shows the vibration behaviour of this new case for model 1.

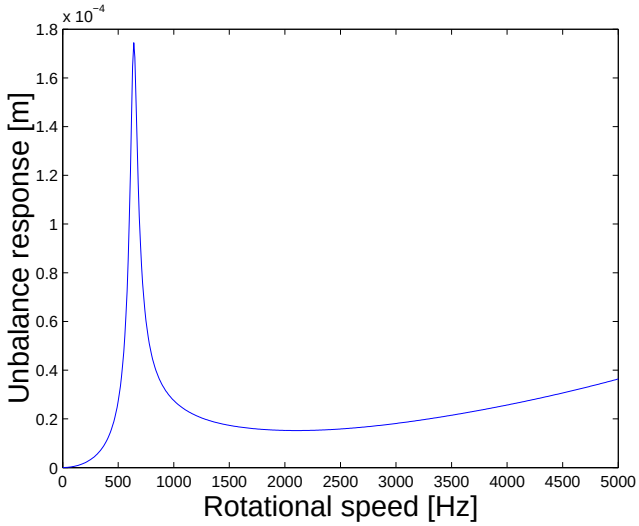

Figure 7.22. Vibration level of initial design of model 1 with nonlinear oil film bearings.

The critical mode is a conical mode which now has a critical speed of $\omega_{\mathrm{rm}} = 639$ Hz. Over the range we plotted and which includes the operational speed range the amplitude of this mode is by far the largest one and thus target of our optimization program. The initial value for the unbalance response is $a_{\mathrm{rm}} = 1.39 \cdot 10^{-4}$ m.

We now solve the following optimization problem for the oil film model. As for the other models, we consider an increase of the critical speed by 10% and a decrease of the unbalance response by 20%. Here, the constraints are set for the same mode.

$$\begin{aligned} &\min_q \mathrm{mass}(q) \\ &\text{subject to} \\ &\omega_{\mathrm{rm}}(q) \geq \omega^*_{\mathrm{rm}} = 1.1 \cdot \omega^{(0)}_{\mathrm{rm}}, \\ &a(\omega_{\mathrm{rm}}(q)) \leq a^*_{\mathrm{rm}} = 0.8 \cdot a^{(0)}_{\mathrm{rm}}, \\ &\underline{q}_i \leq q_i \leq \bar{q}_i, \quad i = 1, \ldots, n_{dv}. \end{aligned} \tag{7.4}$$

We obtain the optimized structure as shown in Figure 7.23.

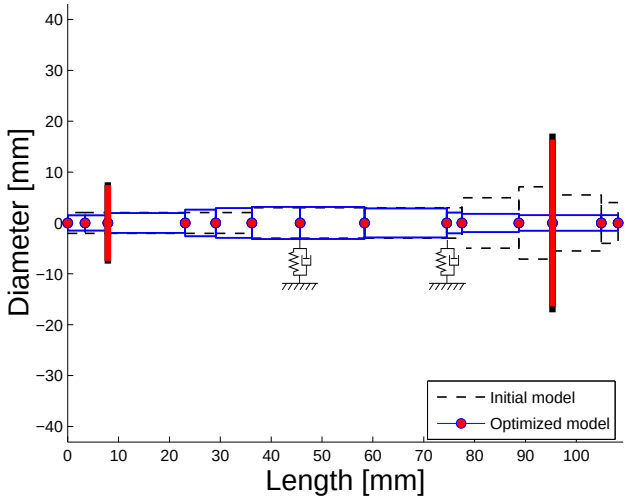

Figure 7.23. Initial and optimized model for vibration level optimization problem for model 1 with nonlinear oil film bearings.

In this case only the design variable of the mass of the rigid disk is active, but no diameter constraint. Nevertheless, the rotor becomes thinner at the left and right end and remains thicker in the centre part. The mass of the optimized model is 0.06635 kg. The critical speed and vibration level constraints can be fulfilled as shown in Figure 7.24.

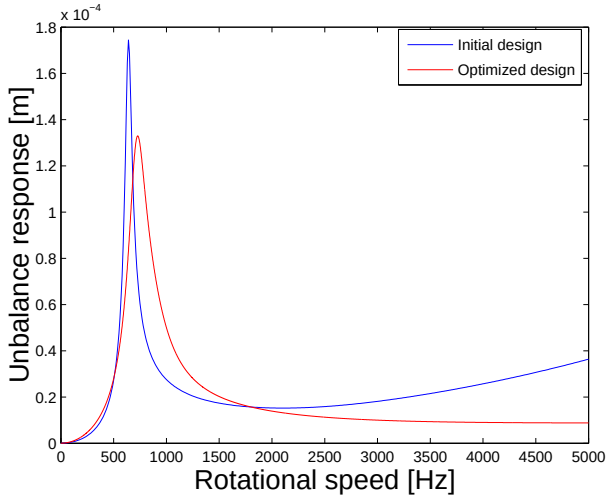

Figure 7.24. Vibration level of initial and optimized design for vibration level problem for model 1 with nonlinear oil film bearings.

We observe, that not only the unbalance response of our target mode is reduced, but also a further increase for higher rotational speeds is avoided. Over the considered

speed range there is a monotone decrease of the unbalance response after passing the peak for the conical mode.

Model 2

The critical modes in this case are a conical and a second bending mode. Our optimization program focuses on reducing the amplitude of the bending mode which is the larger one. The optimization problem is formulated as follows, where explicit target values ω^*_{bm} and a^*_{bm} are set.

$$\begin{aligned} &\min_q \text{mass}(q) \\ &\text{subject to} \\ &\omega_{\text{bm}}(q) \geq \omega^*_{\text{bm}} = 3000\,\text{Hz}, \\ &a(\omega_{\text{bm}}(q)) \leq a^*_{\text{bm}} = 2.0 \cdot 10^{-4}\,\text{m}, \\ &\underline{q}_i \leq q_i \leq \bar{q}_i, \quad i = 1, \ldots, n_{dv}. \end{aligned} \tag{7.5}$$

Numerical calculations show that the MMA algorithm produces a feasible optimized design for this case. The SLP algorithm converges even for various choice of parameters to an infeasible design, violating the unbalance response constraint. Using a small move limit throughout the whole optimization process might be a remedy. However, this would lead to a significant increase in computational time and is therefore declined. The MMA algorithm, however, yields an optimized structure fulfilling all constraints (see Figure 7.25). The constraint on the unbalance response is here active.

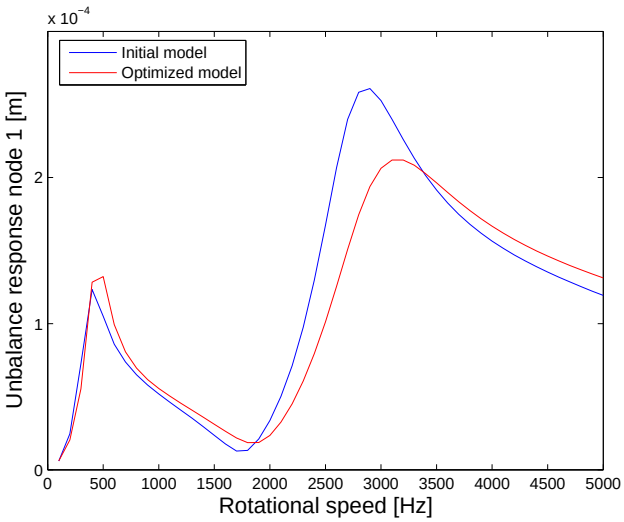

Figure 7.25. Vibration level for initial and optimized design for vibration level problem for model 2 with nonlinear oil film forces.

It shows that the suggested optimization approach works well for a model including nonlinear oil film forces. For model 1 and 2 the given targets could be fulfilled.

7.4 Numerical determination of target values

In Section 5.7 some ideas are presented that aim at a numerical determination of suitable target values based on multiobjective approaches. In this section numerical results for the corresponding optimization problems are shown.

The approach is done here for our model vibration level optimization problem as mentioned in Section 5.7. Firstly, we want to determine the ideal objective vector. The optimization problems (5.9), where the original constraint and objective functions are interchanged are written as

$$\begin{aligned} &\min_q J_1(q) = -\omega_{\mathrm{rm}}(q) \\ &\text{subject to} \\ &\mathrm{mass}(q) \le m^{(0)}, \\ &\underline{q}_i \le q_i \le \bar{q}_i, \quad i = 1, \ldots, n_{dv}, \end{aligned} \tag{7.6}$$

and

$$\begin{aligned} &\min_q J_2(q) = a_{\mathrm{rm}}(q) \\ &\text{subject to} \\ &\mathrm{mass}(q) \le m^{(0)}, \\ &\underline{q}_i \le q_i \le \bar{q}_i, \quad i = 1, \ldots, n_{dv}, \end{aligned} \tag{7.7}$$

where $m^{(0)}$ is the mass of the intial design.
The ideal objective vector is then given by

$$(z_1^*, z_2^*) = (-\min_q J_1, \min_q J_2).$$

Remark. For the optimization problems (7.6) and (7.7) the initial design is feasible in contrast to the previous design optimization problems.

Model 1 with nonlinear oil film forces

At first, we take model 1 including nonlinear oil film forces and determine the ideal objective vector by solving (7.6) and (7.7). Applying the MMA algorithm we obtain for (7.6)

$$\omega_{\mathrm{rm}} = 1227\,\mathrm{Hz}, \quad a_{\mathrm{rm}} = 1.211 \cdot 10^{-4}\,\mathrm{m}, \quad \mathrm{mass} = 0.0852\,\mathrm{kg}$$

and for (7.7) we have

$$\omega_{\mathrm{rm}} = 450\,\mathrm{Hz}, \quad a_{\mathrm{rm}} = 1.97 \cdot 10^{-5}\mathrm{m}, \quad \mathrm{mass} = 0.0929\,\mathrm{kg}.$$

Our ideal objective vector is thus $(z_1^*, z_2^*) = (1227\,\text{Hz}, 1.97 \cdot 10^{-5}\,\text{m})$.
Not surprisingly, we recognize that we can achieve much more if we focus on each value separately. But we have to pay for this by an unfavourable value of the other constraint. Indeed the minimization of unbalance response in optimization problem (7.7) yields a large reduction. But on the other hand, the critical speed also decreases which is against our desire.

As introduced in Section 5.7 the method of the global criterion can be used to combine both functions in one objective function. Its solution yields a Pareto optimal point for the multicriteria optimization problem. Before applying the SLP or MMA algorithm, the objective functions are scalarized to avoid an undesired weighting in the numerical calculations. As scalarizing factor the values in the ideal objective vector are used and we set $\tilde{J}_1 = J_1/z_1^*$ and $\tilde{J}_2 = J_2/z_2^*$.

The optimization problem for the method of the global criterion is now written as

$$\begin{aligned} &\min_q \left(\tilde{J}_1(q) - 1\right)^2 + \left(\tilde{J}_2(q) - 1\right)^2 \\ &\text{subject to} \\ &\text{mass}(q) \le m^{(0)} \\ &\underline{q}_i \le q_i \le \bar{q}_i, \quad i = 1, \ldots, n_{dv}. \end{aligned} \tag{7.8}$$

The numerical calculations give the values

$$\omega_{\text{bm2}} = 795\,\text{Hz}, \quad a_{\text{bm1}} = 2.87 \cdot 10^{-5}\text{m}, \quad m = 0.0929\,\text{kg}.$$

and the obtained result is very convincing since the vibration level is reduced significantly as can be seen in Figure 7.26.

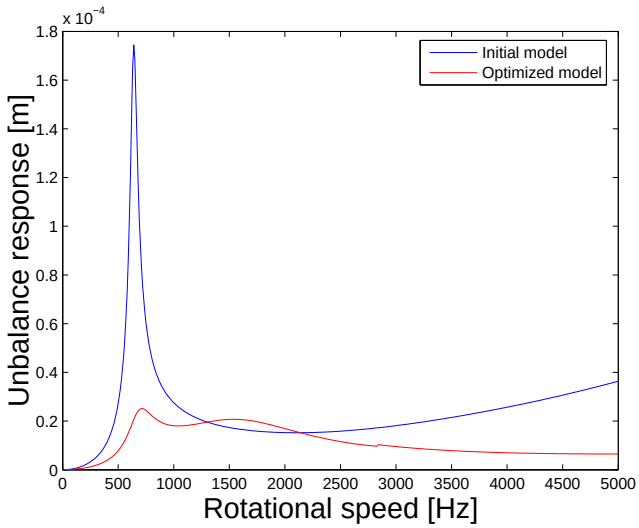

Figure 7.26. Vibration level for initial and optimized design of method of the global criterion for model 1 with nonlinear oil film forces.

Of course, we are interested in as many Pareto optimal points as possible. This can either be achieved by varying the reference vector in the method of the global criterion or by considering the weighting method introduced in Section 5.7. The latter approach is followed here and the optimization problem reads as

$$\begin{aligned} &\min_q w\tilde{J}_1(q) + (1-w)\tilde{J}_2(q) \\ &\text{subject to} \\ &\text{mass}(q) \leq m^{(0)}, \\ &\underline{q}_i \leq q_i \leq \bar{q}_i, \quad i = 1, \ldots, n_{dv}. \end{aligned} \tag{7.9}$$

Now different weighting parameters can be tried. In our case 26 different parameters from 0 to 1 were used yielding combinations of critical speed and unbalance response. Interpolation of these points gives the trade-off-curve which is shown in Figure 7.27.

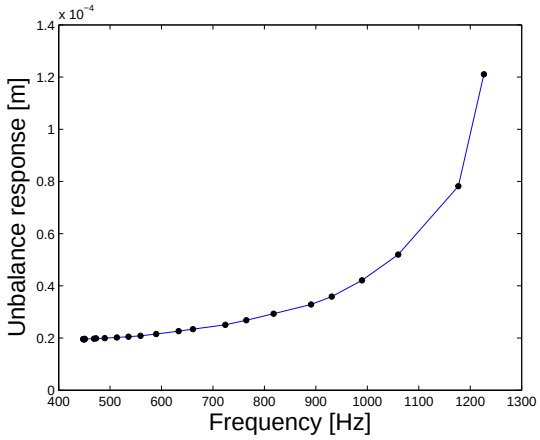

Figure 7.27. Pareto optimal combinations of critical speed and unbalance response for model 1 with nonlinear oil film forces.

The decision maker can now choose a suitable combination that fits best to his preferences and take this combination as target values. Another possibility is to select the constraint which is more important, fix the desired target value and look what can be achieved for the other constraint. Of course, this concept can not completely prevent that the algorithm gets stuck in a local minimum though it is known that a feasible solution exists. Usually, the behaviour of the algorithm depends a lot on the starting point (i.e. the initial design) and a proper choice of parameters for the algorithms. Therefore, the introduced concept should be regarded more as a guideline which indicates obvious unreachable aspiration levels.

The same approach shown for model 1 is also applied to model 2 with and without oil film forces. The corresponding results are summarized briefly now. The model without oil film forces is studied first.

Model 2 without oil film forces

The ideal objective vector is in this case given by

$$z_1^* = 4487\,\text{Hz}, \quad \text{and} \quad z_2^* = 1.978 \cdot 10^{-4}\,\text{m}.$$

Figure 7.28 shows the vibration level for the optimized design obtained by the method of the global criterion for this case. The behaviour is very similar to the result using additional design variables (see Figure 7.21). Compared with the case of model 1 with oil film forces (see Figure 7.26), only a smaller decrease of unbalance response is achieved.

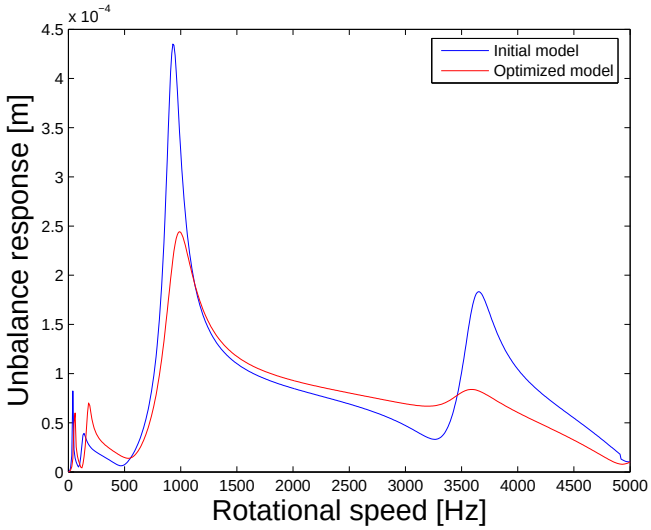

Figure 7.28 Vibration level for initial and optimized design of method of the global criterion for model 2 without oil film forces.

Model 2 with nonlinear oil film forces

Finally, the multiobjective approach which was described for model 1 with nonlinear oil film forces is applied to model 2 with nonlinear oil film forces. Solving (7.6) and (7.7) the ideal objective vector is

$$z_1^* = 3407\,\text{Hz}, \quad z_2^* = 1.956 \cdot 10^{-4}\,\text{m}.$$

The application of the method of the global criterion yields a result for the vibration level behaviour (see Figure 7.29) which is similar to the result of optimization problem (7.5) which is shown in Figure 7.25.

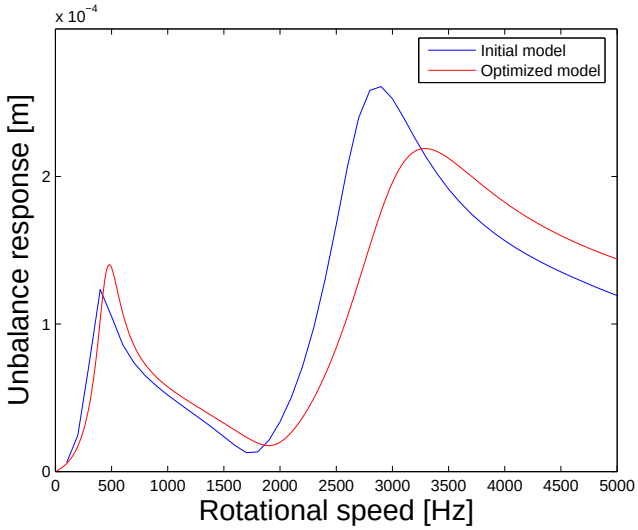

Figure 7.29. Vibration level for initial and optimized design of method of the global criterion for model 2 with nonlinear oil film forces.

The calculations for a trade-off curve of combinations of critical speed and unbalance response with 51 different parameters from 0 to 1 show an interesting behaviour (see Figure 7.30). A coalescence of Pareto optimal points occurs around the values (2503 Hz, $1.956{\cdot}10^{-4}$ m) and (3185 Hz, $1.962{\cdot}10^{-4}$ m). The first point is reached for weighting factors $w = 0$ to $w = 0.4$ and the second point for $w = 0.6$ to $w = 0.9$, i.e. for most of the weighting factors the optimization algorithm converges to one of the two points.

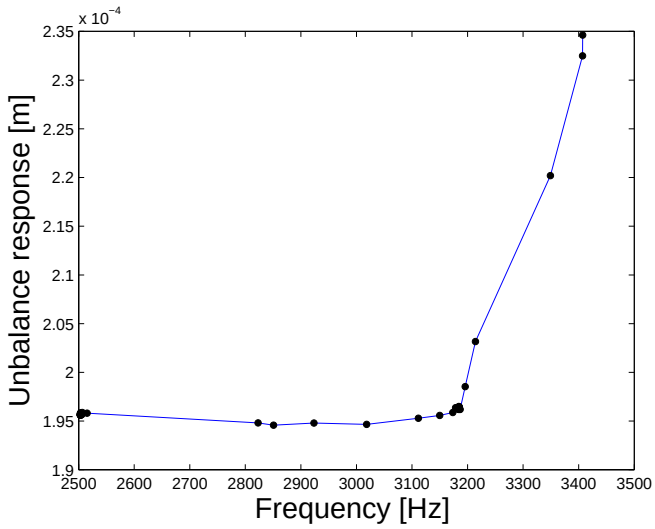

Figure 7.30. Pareto optimal combinations of critical speed and unbalance response for model 2 with nonlinear oil film forces.

We notice that the reduction of the unbalance response is dominant. Indeed, the critical speed can be increased up to almost 3200 Hz without increase in unbalance response. However, if the decision maker is interested in a higher critical speed, this has to be paid for by a quick increase in unbalance response. Therefore this point, where the kink occurs, seems to present a desirable combination of target values.

Remark. A consideration of the clearance as additional design variable showed that a further decrease of the vibration level of the second bending mode is possible. However, this is at the expense of the increase of its critical speed.

The calculations performed for the multiobjective optimization problem yield various Pareto optimal points which may represent favourable designs. But it has to be mentioned that these points are determined under the assumption that the mass is not higher than that for the initial design. Usually, this constraint is active for the optimized design of the multiobjective optimization problem. On the other hand, this implies that a solution of the vibration level optimization problem with new strict target values for the critical speed and unbalance response constraints need not be feasible. The reason is that in the original optimization problem the minimization of the mass is the major goal. Therefore, the reduction of mass might lead to a violation of the tight constraints.

Chapter 8

Conclusion

In the preceding work we have developed a comprehensive design optimization approach for a general class of rotating bodies focusing on the reduction of mass and unbalance response as well as the shift of critical speeds. We have formulated a suitable design optimization problem which meets these targets. For rotating bodies effects of rotary inertia and gyroscopic moments are very important. Considering these effects changes the theoretical and numerical analysis of the problem compared to existing approaches for the non-rotating case. In this regard, the presented research extends results found in the literature. Our results include statements about the existence and description of solutions of the considered design optimization problems as well as their numerical solution based on a suitable finite element discretization. The optimization goals are best treated by a design optimization problem where the mass function is the objective function which is to be minimized. Natural frequencies or critical speed and unbalance response are considered as constraints which are increased and decreased above and below certain target values, respectively.

One central result of the thesis is the proof of the existence and the description of solutions for this design optimization problem for a continuous rotor with simple support boundary conditions. Hence the formulation of the optimization problem makes sense and a solution can be determined. It is obtained numerically by using a suitable finite element discretization of the infinite dimensional original problem. We have shown the convergence of the optimal solutions of the discretized problem towards those of the continuous problem by using the convergence of the corresponding eigenvalues and eigenvectors. Thus, by choosing a sufficient fine discretization scheme, results in good approximation of the solution of the continuous problem can be obtained.

For the numerical solution of the problem the finite element discretization has been realized by the approximation with piecewise cubic polynomials. This results in the

algebraic fomulation of the equation of motion and the generalized discretized eigenvalue problem has been obtained. As algorithms to solve the design optimization problem sequential linear programming (SLP) and the method of moving asymptotes (MMA) were chosen and their performance was compared. Whereas SLP iterations were sometimes in the infeasible design space, MMA generated usually feasible designs throughout the optimization process and is therefore preferred. Modifications of the MMA algorithm like GCMMA and MMA with line search guarantee convergence towards a Karush-Kuhn-Tucker point of the discretized problem. However, these algorithms generally need longer until they converge. Since the results often do not differ much from SLP or MMA results, the former algorithms are chosen due to their faster termination. Mode crossing took place in the design optimization process but was successfully dealt with by a mode tracking procedure. No coalescence of eigenvalues occurred in our application such that a consideration of strategies taking care of points of nondifferentiability of the eigenvalue function was not necessary.

The numerical results for the turbocharger application show that a substantial reduction of mass and unbalance response for the considered design optimization problems is achieved. Moreover, certain critical speeds can be shifted out of the operating speed range of the rotor. Hence they are no longer excited. The presented results lead to the desired reduction of noise and less fatigue of material of the rotor. The consideration of parameters of the bearing geometry yields a further improvement. In addition to that, calculations for a model including nonlinear bearing forces have shown that the developed optimization method gives good results. The application of multiobjective optimization methods ensures feasible solutions by determining suitable target values for the respective constraint functions. Several Pareto optimal combinations of target values were computed from which the preferred one can be chosen.

The presented approach shows good results for the design optimization problems for two different models of the turbocharger with different support conditions. All considered problems could be solved by the presented algorithms. However, due to the strong nonlinearity of the critical speed and the unbalance response functions the result of the optimization algorithms depends on move limit parameters of the algorithms. In most cases only minor differences appeared.

The research presented in this thesis can be extended in various directions. An extension of the theoretical work is possible by proving the existence theorems for models with linear spring and damper support. Then discrete forces at the position of the support have to be taken into account. For rotating bodies supported by fluid film bearings a modified calculation of the oilfilm forces capturing further effects can be considered. An appropriate model is currently developed in collaboration with TCRDL [51] and can be included in our method after completion. This requires

the modification of the sensitivity analysis and enables the consideration of further design variables of the bearing configuration.

For the design optimization of other examples of rotating bodies, multiple eigenvalues might be a bigger problem than for the shown example of the turbocharger. A coalescence of eigenvalues might occur around the optimum and not only a mode crossing as in our case. A remedy is the inclusion of directional derivatives at these points into the method. Another possibility is to switch to solvers of nonsmooth optimization for such critical points.

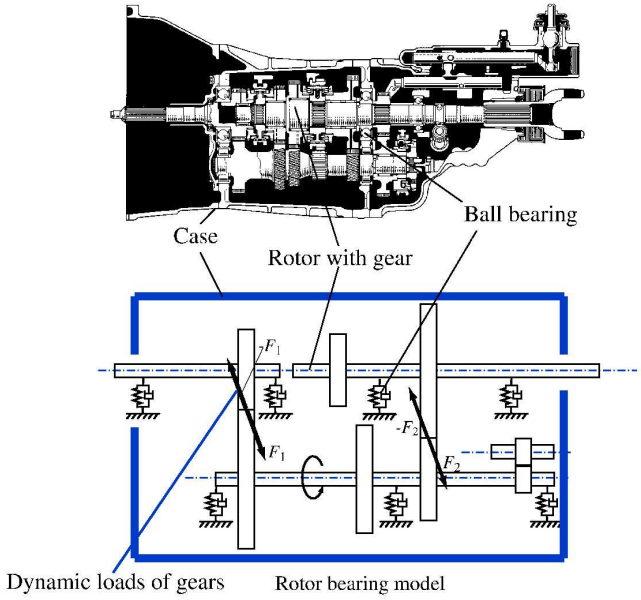

Figure 8.1. Gear-train system (Figure by TCRDL).

The presented method is already used at TCRDL for the design optimization of turbochargers. TCRDL plans to apply the method to other rotating bodies such as a gear-train system in a passenger car (see Figure 8.1) in the future. This object can also be described by the introduced physical model and the optimization approach can be applied.

Appendix A

Basic tools from functional analysis

This appendix collects some results from functional analysis which are needed to prove the theorems of the existence of solutions for the natural frequency and vibration level optimization problem. The following theorems are summarized from [2], [62] and [64].

In infinite dimensional spaces the eigenvalue theory for matrices in finite dimensional spaces no longer holds. A more general concept has to be introduced.

Definition A.1. *Let $T \in L(X)$.*

(a) The resolvent set of T is

$$\rho(T) = \{\lambda \in \mathbb{K} : (\lambda - T)^{-1} \in L(X)\}.$$

(b) The mapping

$$R : \rho(T) \to L(X), \quad R_\lambda(T) := (\lambda - T)^{-1}$$

is called the resolvent of T.

(c) The spectrum of T is given by

$$\sigma(T) = \mathbb{K} \setminus \rho(T).$$

The elements of $\sigma(T)$ are called eigenvalues, an $x \neq 0$ with $Tx = \lambda x$ is called eigenvector (or eigenfunction if X is a function space).

If $K = \mathbb{C}$, then $\sigma(T) \neq \emptyset$.

The class of compact operators denoted by $K(X)$ is of special importance for our analysis. The spectrum of these operators can be described by the following theorem.

Theorem A.1 (Riesz-Schauder). *Let $T \in K(X)$. The spectrum $\sigma(T)$ is an at most countable set with no accumulation point different from zero. Each nonzero $\lambda \in \sigma(T)$ is an eigenvalue of T with finite multiplicity and $\bar{\lambda}$ is an eigenvalue of T^* with the same multiplicity.*

The theorem says that the spectrum consists of a sequence of eigenvalues λ tending to zero.

To show the existence of solutions of linear partial differential equations of elliptic type, the theorem of Lax-Milgram is a useful tool.

Theorem A.2 (Lax-Milgram). *Let X be a Hilbert space and $a : X \times X \to \mathbb{K}$ a sesquilinear form which satisfies for any $x, y \in X$ the conditions*

(i) $|a(x,y)| \leq C_0 \|x\|_X \|y\|_X$ *(Continuity),*

(ii) $\mathrm{Re}(a(x,x)) \geq c_o \|x\|_X^2$ *(Coercivity),*

where $0 < c_0 \leq C_0 < \infty$. Then there exists a uniquely determined bounded linear operator A with a bounded linear inverse A^{-1} such that

$$a(y,x) = (y, Ax)_X \quad \text{for all} \quad x, y \in X$$

and

$$\|A\| \leq C_0 \quad \text{and} \quad \|A^{-1}\| \leq \frac{1}{c_0}.$$

To verify the conditions of the Lax-Milgram theorem, the Poincaré inequality as well as a generalized form of it might be helpful.

Theorem A.3 (Poincaré inequality). *Let $\Omega \subset \mathbb{R}^n$ be a bounded open set. Then there exists a constant C_0 (depending on Ω) such that*

$$\int_\Omega |u|^2 \leq C_0 \int_\Omega |\nabla u|^2 \quad \text{for all } u \in H_0^1(\Omega).$$

Theorem A.4 (Generalized Poincaré inequality). *Let Ω be a bounded, open, connected set with Lipschitz-boundary $\partial\Omega$. Moreover, let $S \subset H^1(\Omega)$ be nonempty, convex and closed. Then the following two statements are equivalent.*

(1) There exists a $u_0 \in S$ and a constant $C_0 < \infty$, such that for all $\xi \in \mathbb{R}^m$

$$u_0 + \xi \in S \Rightarrow |\xi| \leq C_0$$

(2) There exists a constant $C < \infty$ such that

$$\|u\|_{L^p(\Omega)} \leq C(\|\nabla u\|_{L^p(\Omega)} + 1) \quad \text{for all } u \in S$$

If S is a cone with apex 0, i.e.

$$u \in S, \alpha \geq 0 \Rightarrow \alpha u \in S,$$

then inequality (2) can be replaced by

$$\|u\|_{L^p(\Omega)} \leq C\|\nabla u\|_{L^p(\Omega)} \quad \textit{for all } u \in S.$$

Appendix B

Structural matrices of FE model

In this appendix the formulation of the mass, gyroscopic and stiffness matrices for one beam element with uniform cross-section and material properties is given.

The algebraic formulation of the strucutral matrices is derived in Section 4.3. With the choice of the Hermite polynomials as basis functions the matrices for the numerical applications can be formulated. They are as follows.

The mass matrix for one beam element given by (4.3) is split into a part for translational motion M_{kt} and one for rotational motion M_{kr}. For the symmetric M_{kt} we obtain

$$M_{kt} = \frac{r^2\pi\rho l}{420}\begin{pmatrix} 156 & & & & & & & \\ 0 & 156 & & & & Sym. & & \\ 0 & -22l & 4l^2 & & & & & \\ 22l & 0 & 0 & 4l^2 & & & & \\ 54 & 0 & 0 & 13l & 156 & & & \\ 0 & 54 & -13l & 0 & 0 & 156 & & \\ 0 & 13l & -3l^2 & 0 & 0 & 22l & 4l^2 & \\ -13l & 0 & 0 & -3l^2 & -22l & 0 & 0 & 4l^2 \end{pmatrix},$$

where r is the radius and l the length of the beam element and ρ the density of the shaft material. The symmetric mass matrix for one beam element for rotational motion M_{kr} is given by

$$M_{kr} = \frac{r^2\pi\rho r^2}{120l}\begin{pmatrix} 36 & & & & & & & \\ 0 & 36 & & & & Sym. & & \\ 0 & -3l & 4l^2 & & & & & \\ 3l & 0 & 0 & 4l^2 & & & & \\ -36 & 0 & 0 & -3l & 36 & & & \\ 0 & -36 & 3l & 0 & 0 & 36 & & \\ 0 & -3l & -l^2 & 0 & 0 & 3l & 4l^2 & \\ 3l & 0 & 0 & -l^2 & -3l & 0 & 0 & 4l^2 \end{pmatrix}.$$

The symmetric stiffness matrix for one beam element K_k as derived in (4.4) is given by

$$K_k = \frac{EI_a}{l^3} \begin{pmatrix} 12 & & & & & & & \\ 0 & 12 & & & & Sym. & & \\ 0 & -6l & 4l^2 & & & & & \\ 6l & 0 & 0 & 4l^2 & & & & \\ -12 & 0 & 0 & -6l & 12 & & & \\ 0 & -12 & 6l & 0 & 0 & 12 & & \\ 0 & -6l & 2l^2 & 0 & 0 & 6l & 4l^2 & \\ 6l & 0 & 0 & 2l^2 & -6l & 0 & 0 & 4l^2 \end{pmatrix},$$

where EI_a is the bending rigidity of the beam element.

The skew-symmetric gyroscopic matrix for one beam element G_k which is given by (4.5) reads here as

$$G_k = \frac{I_p}{30l} \begin{pmatrix} 0 & & & & & & & \\ -36 & 0 & & & Skew-sym. & & & \\ 3l & 0 & 0 & & & & & \\ 0 & 3l & -4l^2 & 0 & & & & \\ 0 & -36 & 3l & 0 & 0 & & & \\ 36 & 0 & 0 & 3l & -36 & 0 & & \\ 3l & 0 & 0 & -l^2 & -3l & 0 & 0 & \\ 0 & 3l & l^2 & 0 & 0 & -3l & -4l^2 & 0 \end{pmatrix},$$

where I_p is the polar moment of inertia of the beam element.

Derivatives of the matrices with respect to the radius r and length l can be determined straightforwardly.

Appendix C

Specification of turbocharger models

In this appendix we give the concrete specification of shaft, rigid disks, bearing support and unbalance forces for the two turbocharger models which we consider in our numerical calculations.

The specification for model 1 (see Figure 7.1) is given as follows.

The shaft specification is given by

Element number	Length [mm]	Diameter [mm]	Density [kg/m^3]	Young's modulus [N/m^2]
1	3.4	4.1	7800	$2.10 \cdot 10^{11}$
2	4.5	4.1	7800	$2.10 \cdot 10^{11}$
3	15.2	4.1	7800	$2.10 \cdot 10^{11}$
4	6.0	4.1	7800	$2.10 \cdot 10^{11}$
5	7.1	4.1	7800	$2.10 \cdot 10^{11}$
6	9.5	6.0	7800	$2.10 \cdot 10^{11}$
7	12.65	6.0	7800	$2.10 \cdot 10^{11}$
8	16.15	6.0	7800	$2.10 \cdot 10^{11}$
9	3.0	6.0	7800	$2.10 \cdot 10^{11}$
10	11.2	9.9	7800	$2.10 \cdot 10^{11}$
11	6.6	14.2	7800	$2.10 \cdot 10^{11}$
12	9.6	11.0	7800	$2.10 \cdot 10^{11}$
13	3.3	8.0	7800	$2.10 \cdot 10^{11}$

Table C.1. Specification of shaft of model 1.

The parameters of the rigid disks are the following.

	Node number	Mass [kg]	Inertia moment I_d [kgm^2]	Inertia moment I_p [kgm^2]
Impeller	3	$1.3328 \cdot 10^{-2}$	$1.2740 \cdot 10^{-6}$	$2.1560 \cdot 10^{-6}$
Turbine	12	$4.3414 \cdot 10^{-2}$	$3.1360 \cdot 10^{-6}$	$5.8800 \cdot 10^{-6}$

Table C.2. Specification of rigid disk of model 1.

The spring support coefficients of the bearing are given by

	Node number	Stiffness k_{XX}, k_{YY} [N/m]	Damping c_{XX}, c_{YY} [Ns/m]
Bearing 1	7	$1.0 \cdot 10^6$	3
Bearing 2	9	$1.0 \cdot 10^6$	3

Table C.3. Specification of bearing of model 1.

and the unbalance forces $f = \omega^2 u e^{i\Theta}$ in each node, with ω being the rotational speed, are

Node number	Unbalance u [kgm]	Phase Θ [deg]
2	$1.35 \cdot 10^{-7}$	π
4	$1.5 \cdot 10^{-7}$	0
11	$2.01 \cdot 10^{-7}$	0
13	$2.07 \cdot 10^{-7}$	π

Table C.4. Specification of unbalance forces of model 1.

For model 2 (see Figure 7.2) which consists of an inner and outer shaft part with different material properties for some beam elements the specification is as follows.

		Inner Shaft			Outer Shaft		
Element number	Length [mm]	Diameter [mm]	Density [kg/m^3]	Young's modulus [N/m^2]	Diameter [mm]	Density [kg/m^3]	Young's modulus [N/m^2]
1	3.0	6.0	7800	$2.058{\cdot}10^{11}$			
2	5.0	6.0	7800	$2.058{\cdot}10^{11}$	10.2	7800	$2.058{\cdot}10^{10}$
3	6.0	6.0	7800	$2.058{\cdot}10^{11}$	12.0	2646	$7.35{\cdot}10^{9}$
4	6.0	6.0	7800	$2.058{\cdot}10^{11}$	15.2	2646	$7.35{\cdot}10^{9}$
5	6.0	6.0	7800	$2.058{\cdot}10^{11}$	20.0	2646	$7.35{\cdot}10^{9}$
6	6.0	6.0	7800	$2.058{\cdot}10^{11}$	30.0	2646	$7.35{\cdot}10^{9}$
7	5.4	6.0	7800	$2.058{\cdot}10^{11}$	42.0	2646	$7.35{\cdot}10^{9}$
8	5.0	6.0	7800	$2.058{\cdot}10^{11}$	9.0	7800	$2.058{\cdot}10^{10}$
9	31.0	6.0	7800	$2.058{\cdot}10^{11}$	20.0	7800	$0.98{\cdot}10^{10}$
10	3.0	6.0	7800	$2.058{\cdot}10^{11}$	9.0	7800	$2.058{\cdot}10^{10}$
11	5.0	6.0	7800	$2.058{\cdot}10^{11}$	9.0	7800	$2.058{\cdot}10^{10}$
12	6.0	6.0	7800	$2.058{\cdot}10^{11}$	9.0	7800	$2.058{\cdot}10^{10}$
13	4.0	8.5	7800	$2.058{\cdot}10^{11}$			
14	30.2	8.5	7800	$2.058{\cdot}10^{11}$			
15	7.9	8.5	7800	$2.058{\cdot}10^{11}$			
16	13.2	14.7	7800	$2.058{\cdot}10^{11}$			
17	6.4	40.8	7800	$2.058{\cdot}10^{11}$			
18	6.4	26.4	7800	$2.058{\cdot}10^{11}$			
19	6.4	18.0	7800	$2.058{\cdot}10^{11}$			
20	6.4	15.6	7800	$2.058{\cdot}10^{11}$			
21	4.0	13.2	7800	$2.058{\cdot}10^{11}$			

Table C.5. Specification of shaft of model 2.

The bearing configuration is given by

	Node number	Stiffness k_{XX}, k_{YY} [N/m]	Damping c_{XX}, c_{YY} [Ns/m]
Bearing 1	14	98000	39.2
Bearing 2	15	98000	39.2

Table C.6. Specification of bearing of model 2.

and the unbalance forces ($f = \omega^2 u e^{i\Theta}$) are

Node number	Unbalance u [kgm]	Phase Θ [deg]
3	$9.8{\cdot}10^{-7}$	0
8	$9.8{\cdot}10^{-7}$	0
17	$9.8{\cdot}10^{-7}$	0
21	$9.8{\cdot}10^{-7}$	0

Table C.7. Specification of unbalance forces of model 2.

Bibliography

[1] M.A. Akgün. New family of modal methods for calculating eigenvector derivatives. *AIAA journal*, 32(2):379–386, February 1994.

[2] H.W. Alt. *Lineare Funktionalanalysis*. Springer-Verlag, 3.Auflage, 1999.

[3] I. Babuška and J.E. Osborn. Estimates for the errors in eigenvalue and eigenvector approximation by Galerkin methods, with particular attention to the case of multiple eigenvalues. *SIAM J. Numer. Anal.*, 24(6), December 1987.

[4] I. Babuška and J.E. Osborn. Eigenvalue problems. In P.G. Ciarlet and J.L. Lions, editors, *Handbook of Numerical Analysis*, volume 2, chapter Finite Element Methods (Part 1), pages 641–792. Elsevier, 1991.

[5] W. Beitz and K.-H. Küttner, editors. *Dubbel Taschenbuch für den Maschinenbau*. Springer-Verlag, 18.Auflage, 1995.

[6] M.P. Bendsøe and N. Olhoff. A method of design against vibration resonance of beams and shafts. *Optimal Control Applications & Methods*, 6:191–200, 1985.

[7] M.P. Bendsøe and O. Sigmund. *Topology optimization: theory, methods and applications*. Springer-Verlag, 2003.

[8] D. Braess. *Finite Elemente*. Springer-Verlag, 2003.

[9] M. Bruyneel, P. Duysinx, and C. Fleury. A family of MMA approximations for structural optimization. *Structural and Multidisciplinary Optimization*, 24:263–276, 2002.

[10] F. Chatelin. *Spectral approximation of linear operators*. Academic Press, 1983.

[11] D. Childs. *Turbomachinery Rotordynamics*. Wiley, 1993.

[12] P. Duysinx. Solution of topology optimization problems with sequential convex programming. Handout DCAMM course, Topology Optimization - Theory, Methods and Applications, DTU, Kgs. Lyngby, June 2003.

[13] M.S. Eldred, V.B. Venkayya, and W.J. Anderson. Mode tracking issues in structural optimization. *AIAA Journal*, 33(10):1926–1933, October 1995.

[14] A. Ern and J.-L. Guermond. *Theory and practice of finite elements*. Springer-Verlag, 2004.

[15] C. Felippa. Lecture notes: Introduction to Finite Element Methods. http://caswww.colorado.edu/courses.d/IFEM.d/Home.html, 2004.

[16] G. Fichera. Existence theorems in elasticity. In S. Flügge, editor, *Handbuch der Physik*, volume 6a, Part 2, pages 347–389. Springer-Verlag, 1972.

[17] R. Fletcher. *Practical Methods of Optimization*. Wiley, 1987.

[18] C. Fleury. First and second order convex approximation strategies in structural optimization. *Structural Optimization*, (1):3–10, 1989.

[19] C. Fleury and V. Braibant. Structural optimization - a new dual method using mixed variables. *Structural Optimization*, (23):409–428, 1986.

[20] T. Fließbach. *Mechanik*. Spektrum, Akad. Verl., 1996.

[21] R.L. Fox and M.P. Kapoor. Rates of change of eigenvalues and eigenvectors. *AIAA Journal*, 6(12):2426–2429, 1968.

[22] M.I. Friswell. The derivative of repeated eigenvalues and their associated eigenvectors. *Transactions of the ASME*, 118:390–397, July 1996.

[23] R. Gasch and H. Pfützner. *Rotordynamik: Eine Einführung*. Springer, 1975.

[24] C. Geiger and C. Kanzow. *Theorie und Numerik restringierter Optimierungsaufgaben*. Springer-Verlag, 2002.

[25] R. T. Haftka and M. P. Kamat. *Elements of Structural Optimization*. Martinus Nijhoff, 1985.

[26] S.M. Han, H. Benaroya, and T. Wei. Dynamics of transversely vibrating beams using four engineering theories. *Journal of Sound and Vibration*, 225(5):935–988, 1999.

[27] J. Haslinger and R.A.E. Mäkinen. *Introduction to shape optimization : theory, approximation and computation*. SIAM, 2003.

[28] E.J. Haug, K.K. Choi, and V. Komkov. *Design Sensitivity Analysis of Structual Systems*. Academic Press, 1986.

[29] D.G. Hyams and G.M. Fadel. Comparison of various move limit strategies in structural optimization. *AIAA journal*, pages 401–410, 1994.

[30] M. Inagaki. private communication, 2003.

[31] T. Kato. *Perturbation theory for linear operators*. Springer-Verlag, 1966.

[32] N. Kikuchi. *Finite Element Methods in Mechanics*. Cambridge University Press, 1986.

[33] T.S. Kim and Y.Y. Kim. Mac-based mode-tracking in structural topology optimization. *Computers and Structures*, (74):375–383, 2000.

[34] W.G. Kolata. Approximation in variationally posed eigenvalue problems. *Numer. Math.*, 29:159–171, 1978.

[35] M. Kočvara. On the modelling and solving of the truss design problem with global stability constraints. *Structural and Multidisciplinary Optimization*, 23(3):189–203, 2002.

[36] L.D. Landau and E.M. Lifschitz. *Lehrbuch der theoretischen Physik. Band 1. Mechanik*. Akademie-Verlag, Berlin, 1987.

[37] L.D. Landau and E.M. Lifschitz. *Lehrbuch der theoretischen Physik. Band 7. Elastizitätstheorie*. Akademie-Verlag, Berlin, 1991.

[38] O.R. Lang and W. Steinhilper. *Gleitlager*. Springer-Verlag, 1978.

[39] Z.-D. Ma, N. Kikuchi, and H.-C. Cheng. Topological design for vibrating structures. *Computational Methods in Applied Mechanics and Engineering*, 121:259–280, 1995.

[40] Z.D. Ma, N. Kikuchi, and I. Hagiwara. Structural topology and shape optimization for a frequency response problem. *Computational Mechanics*, 13:157–174, 1993.

[41] L. Meirovitch. *Elements of Vibration Analysis*. Wiley, 2nd edition, 1986.

[42] K. Miettinen. *Nonlinear multiobjective optimization*. Kluwer Academic Publishers, 1999.

[43] D.V. Murthy and R.T. Haftka. Derivatives of eigenvalues and eigenvectors of a general complex matrix. *International Journal for Numerical Methods in Engineering*, 26:293–311, 1988.

[44] H.D. Nelson and J.M. McVaugh. The dynamics of rotor-bearing systems using finite elements. *Transactions of the ASME, Journal of Engineering for Industry*, pages 593–600, May 1976.

[45] R.B. Nelson. Simplified calculation of eigenvector derivatives. *AIAA Journal*, 14(9):1201–1205, September 1976.

[46] J. Nocedal and S.J. Wright. *Numerical Optimization*. Springer-Verlag, 1999.

[47] M. Ohsaki, K. Fujisawa, N. Katoh, and Y. Kanno. Semi-definite programming for topology optimization of trusses under multiple eigenvalue constraints. *Comp. Meth. Appl. Mech. Engng.*, 180:203–217, 1999.

[48] N. Olhoff. On optimum design of structures and materials. *Meccanica*, (31):143–161, 1996.

[49] N. Olhoff and E. Lund. Finite element based engineering design sensitivity analysis and optimization. In J. Herskovits, editor, *Advances in Structural Optimization*, pages 1–45. Kluwer Academic Publishers, 1995.

[50] N. Olhoff and R. Parbery. Designing vibrating beams and rotating shafts for maximum difference between adjacent natural frequencies. *Int. J. Solid Structures*, 20(1):63–75, 1984.

[51] J. Rübel. *Modelling and Analysis in Nonlinear Rotordynamics*. PhD thesis, Ruprecht-Karls-Universität Heidelberg, 2005. To be submitted.

[52] A.P. Seyranian, E. Lund, and N. Olhoff. Multiple eigenvalues in structural optimization problems. *Structural Optimization*, (8), 1994.

[53] G. Strang and G.J. Fix. *An analysis of the finite element method*. Prentice-Hall, Englewood Cliffs, 1973.

[54] K. Svanberg. The method of moving asymptotes - a new method for structural optimization. *International Journal for Numerical Methods in Engineering*, 24:359–373, 1987.

[55] K. Svanberg. The method of moving asymptotes - modelling aspects and solution schemes. in: Advanced topics in structural optimization. Technical Report S81, DCAMM, Technical University of Denmark, 1998.

[56] K. Svanberg. A class of globally convergent optimization methods based on conservative convex separable approximations. *SIAM Journal on Optimization*, 12(2):555–573, 2002.

[57] A.Z. Szeri. *Fluid Film Lubrication, Theory and Design*. Cambridge University Press, 1998.

[58] T. Ting. Accelerated subspace iteration for eigenvector derivatives. *AIAA Journal*, 30(8):2114–2118, 1992.

[59] J. M. Vance. *Rotordynamics of Turbomachinery*. Wiley, 1988.

[60] L. Vandenberghe and S. Boyd. Semidefinite programming. *SIAM Review*, 38(1):49–95, March 1996.

[61] B.P. Wang. Improved approximate methods for computing eigenvector derivatives in structural dynamics. *AIAA Journal*, 29(6):1018–1020, June 1991.

[62] D. Werner. *Funktionalanalysis*. Springer-Verlag, 2.Auflage, 1997.

[63] T. Yamamoto and Y. Ishida. *Linear and Nonlinear Rotordynamics*. Wiley, 2001.

[64] K. Yosida. *Functional analysis*. Springer-Verlag, 5th edition, 1978.

[65] C. Zillober. A globally convergent version of the method of moving asymptotes. *Structural Optimization*, (6):166–174, 1993.

[66] C. Zillober. Global convergence of a nonlinear programming method using convex approximations. *Numerical Algorithms*, (27):265–289, 2001.